Characterizing the Chemical and Structural Basis of Animal Coloration from an Evolutionary Perspective

by

Nicholas Matthew Justyn

A dissertation submitted to the Graduate Faculty of
Auburn University
in partial fulfillment of the
requirements for the Degree of
Doctor of Philosophy

Auburn, Alabama
May 6, 2023

Keywords: coloration, carotenoids, nanostructures,
feathers, copepods, UV-vis spectroscopy

Approved by

Geoffrey E. Hill, Chair, Professor of Biological Sciences
Tonia S. Schwartz, Associate Professor of Biological
Jamie R. Oaks, Assistant Professor of Biological Sciences
Matthew E. Wolak, Assistant Professor of Biological Sciences
Ian A. E. Butts, Assistant Professor of Aquaculture, and Aquatic Sciences

Abstract

Many questions regarding how animals produce their striking range of colors remain unanswered, particularly when pigments and structures are combined. In this dissertation, I completed four studies centered around questions involving the mechanisms of color production in different groups of animals. For each of these studies, I present evidence detailing unique color production mechanisms that have been previously unstudied. Chapter 1 examines five birds in the *Manacus* genus to examine color variation in the genus and describes how this new knowledge can inform long standing hypotheses on speciation within their hybrid zones, and the genes involved in feather coloration. Chapter 2 investigates the peculiar case of the persistence of red coloration in the eyespots of *Tigriopus californicus* copepods on carotenoid-restricted diets, and thoroughly details how carotenoids and nanostructures can be combined in a novel manner. Chapter 3 describes the mechanisms that underlie the wide variety of colors present in the Painted Bunting (*Passerina ciris*), including the unique lime green back and pink rump feathers. Painted buntings are one of the most colorful birds in North America, yet surprisingly the mechanisms responsible for their coloration were previously largely unexplored. Chapter 4 examines how vultures produce their black and red head coloration and hypothesizes the potential consequences of each mechanism. I hope that by detailing the mechanisms of color production in these groups of animals, that it will also help inform future research involving signaling and the genetic mechanisms responsible for producing the variation in coloration described.

Acknowledgements

I am thankful to have received so much help and support from so many different people throughout the course of my PhD at Auburn. I would first like to thank my numerous collaborators and coauthors for all of their contributions to each study, and both the Hill and Hood lab groups for helpful discussions about each chapter during lab meetings. In particular, I could not imagine completing these thesis chapters without collaborating closely with Matthew J. Powers, Kyle B. Heine, and Ryan J. Weaver. Without their help, these projects would not have been possible. I would also like to thank Paul Cobine, Mike Miller, and Tony Moss for access to the HPLC, electron microscopy equipment, and UV-microscope, respectively.

A special thanks to my committee Tonia Schwartz, Jamie Oaks, and Matthew Wolak for their helpful insight and suggestions during our committee meetings. I would especially like to thank my advisor Geoffrey Hill for his advice when developing and pursuing research projects, and for never turning down a conversation about feather coloration. Geoff's consistent support through the ups and downs of developing and completing my thesis projects was invaluable.

Most importantly, I would like to thank my wife Ashley Renee Justyn for all of her support throughout my academic career. Her constant encouragement and sense of adventure has inspired all of my research pursuits. Lastly, I would also like to thank my son, Stiles Matthew Justyn, for motivating me to finish my dissertation and continuing to make every day a new learning opportunity.

Table of Contents

List of Figures

Chapter 1

Concentration of lutein and melanization determine feather coloration in the avian genus *Manacus*

Abstract

It is well established that most of the red, orange, and yellow coloration of feathers results from carotenoid pigmentation, but mechanisms determining variation in carotenoid coloration remain unknown for many species of birds. Variation in feather hue among individuals within a species and between species can result from either a change in concentration of a single pigment or the metabolism of a precursor pigment into modified products. Here, I attempt to describe the biochemical differences that underlie variation in plumage coloration among species in the genus *Manacus*. Across this genus, males show striking differences in whether the same patch of ventral plumage is orange, golden yellow, lemon-yellow, or white. I have found that differences in feather hue appear to be due solely to difference in the concentration of lutein in the feathers. Furthermore, gray or olive-green tints to feathers were produced by the deposition of melanin into the barbules of feathers otherwise unpigmented or pigmented with carotenoids, respectively. Thus, a striking range of color phenotypes can be explained entirely by the concentration of a single dietary carotenoid and the presence or absence of melanin in feather barbs.

Introduction

Carotenoids and melanins are the most common pigments used by birds to color feathers (Hill and McGraw 2006). Carotenoids produce the yellow, orange, and red coloration of perching birds (Order Passeriformes) (McGraw 2006b). Birds cannot synthesize carotenoids *de*

novo but must ingest carotenoids that are used to color feathers. The yellow/orange pigments lutein, zeaxanthin, and B-carotene are the three most abundant carotenoids in the diets of most passerine birds, and some birds use these pigments unaltered to color their feathers (Brush and Johnson 1976; McGraw et al. 2003; Mays et al. 2004). These dietary carotenoids can also serve as building blocks that some passerine birds biochemically convert into a variety of new carotenoids (LaFountain et al. 2015; Lopes et al. 2016). These converted carotenoids can result in red, orange, yellow, and even purple feathers (McGraw 2006b; Mendes-Pinto et al. 2012; Hill and Johnson 2012). In contrast to the bright coloration produced by carotenoids, melanins typically produce black, brown, and gray colors in feathers. Melanins can also be combined with carotenoids to alter the appearance of predominantly carotenoid-pigmented feathers (McGraw et al. 2004).

One clade of birds with striking differences in male carotenoid coloration are the four manakin allospecies in the genus *Manacus*. The Orange-collared Manakin (*M. aurantiacus*) has bright orange nape and throat transitioning to yellow on the lower ventral feathers*;* the Golden-collared Manakin (*M. vitellinus*) has a golden nape and throat transitioning to olive green on the lower ventral feathers; the White-collared Manakin (*M. candei*) has a stark white nape and throat with lemon-yellow on lower ventral feathers; and the White-bearded Manakin (*M. manacus*) lacks any orange or yellow coloration having a white nape and throat with lower ventral coloration varying from white to gray (Brumfield and Braun 2001). Females of all four species are olive green and similar to each other. Additionally, Golden- and White-collared Manakins are known to produce viable hybrids (*M. vitellinus x candei*) in well studied zones of hybridization (Parsons et al. 1993; Brumfield and Braun 2001; Brumfield et al. 2001; McDonald et al. 2001; Yuri et al. 2009; Parchman et al. 2013). Male hybrids are variable in the amount of

yellow in their plumage. Some populations are intermediate between the two species, but most resemble *vitellinus* due to unidirectional introgression of *vitellinus* male plumage traits driven by sexual selection (McDonald et al. 2001; Uy and Stein 2006).

The mechanisms by which the *Manacus* genus creates these differences in plumage coloration has not been previously characterized. It has been hypothesized that 4-keto-carotenoids or rhodoxanthin may be the source of orange coloration in the Orange-collared Manakin because rhodoxanthin is present in some species in the closely related genus *Pipra* (Hudon et al. 2012). The feathers of other orange/red species in *Pipra* also contained modified carotenoid pigments including α-doradexanthin, adonirubin, astaxanthin, and canthaxanthin. However, it has previously been shown that mating between the red-rumped and yellow-rumped forms of the Flame-rumped Tanager (*Ramphocelus flammigerus*) result in orange plumage due to a simple concentration difference of the dietary carotenoid lutein between the subspecies (Brush 1970). Previously, the color of *candei* and *vitellinus* were examined, which revealed that these birds exhibit reflectance spectra typical of carotenoid coloration; however, they did not attempt to identify the carotenoids responsible for golden coloration (Brumfield et al 2001; Stein and Uy 2005). I hypothesize that the difference in coloration between the *Manacus* genus is due to a difference in the carotenoids present in each species. Specifically, I expect to find keto-carotenoids in the Orange-collared Manakin, and perhaps converted yellow carotenoids, like canary xanthophylls, in the Golden-collared Manakin.

Here, I examined the collar and belly feathers of the four species in the genus *Manacus*, as well as Golden- x White-collared hybrids, using light microscopy, reflectance spectroscopy, and High Performance Liquid Chromatography (HPLC) to characterize the pigments in feathers and the mechanisms of color production. I sought to determine which carotenoids were present

and their concentrations, as well as to determine if they were dietary or converted. By characterizing plumage coloration differences between closely related species in a genus, and especially between a hybrid and parental species, I aim to provide critical phenotype data for studies of the genetic regulation of plumage pigmentation.

Materials and Methods

Feather collection:

For color quantification and biochemical analysis, I used feathers given to us by Dr. Michael Braun at the Smithsonian Institution. Feathers were plucked from museum specimens of Golden-collared Manakin (*Manacus vitellinus*), White-bearded Manakin (*Manacus manacus*), Orange-collared Manakin (*Manacus aurantiacus*), White-collared Manakin (*Manacus candei*), and hybrids (*Manacus vitellinus x candei*). Approximately 5 feathers were plucked from both the belly and collar region from 6 male specimens of each species and the hybrids. Museum specimens were collected from a variety of locations and from a range of dates (see Supplemental Table 1.1). The hybrid *M. vitellinus x candei* samples came from locality 4 of Brumfield et al. 2001, a population known to show some intermediacy between the parental forms.

Light Microscopy:

Each feather was examined under reflected light before and after pigment extraction. The presence or absence of barbules along the barbs, and the presence of pigmentation in the barbs and barbules was noted for each species. Pictures were taken using an AmScope Microscope Digital Camera at a magnification of 4x.

UV-vis Reflectance spectroscopy:

When performing UV-vis spectroscopy, five feathers were overlapped and taped down flat, ventral side up, onto a black cardboard background. This was done to simulate how the feathers may have been placed on the bird during life, and to eliminate any background noise when sampling the feathers. Three measurements were taken in a dark room at a 90° angle of incidence from each set of feathers using an Ocean Optics USB4000 spectrophotometer and an Ocean Optics PX-2 pulsed xenon light source relative to a white reflectance standard (Labsphere Inc., North Sutton, NH, USA). Spectra were captured using OceanView 1.67. A measurement was taken from the left, center, and right of the distal end of the overlapped group of feathers. Capturing multiple measurements from each plumage patch helps account for any variation in color within or between feathers. The resulting spectral data were analyzed and graphed using the pavo package in R (Maia et al. 2013; 2019).

Carotenoid extraction and HPLC analysis:

A single feather from each location of each bird was cut approximately 1/3 of the way up from the base, removing the bottom portion of the feather that was heavily melanized, and saving the top 2/3 of the feather. The cut feather sections were washed with ethanol and hexane, and then weighed to the nearest 0.1 mg. Each cut feather was then placed in 500 µL acidified pyridine and sealed in a microcentrifuge tube with nitrogen gas to prevent oxidation of any carotenoids (McGraw et al., 2005). The samples were placed on a 95 °C hot plate for 1 hour. Carotenoids were extracted from the pyridine with the addition of 250 µL H_20, 500 µL methyl tert-butyl ether (MTBE), and 250 µL hexane (McGraw 2002). The upper organic phase containing the carotenoids was then was removed. The solvent of the organic phase was evaporated to dryness under vacuum at 30 °C using a centrifugal concentrator. Dried carotenoid samples were resuspended in 80 µL of mobile phase (acetone) for HPLC analysis.

10 µL of suspended carotenoid samples were injected on to a Sonoma C18 column (10 µm, 250 x 4.6 mm, ES Technologies, New Jersey, USA) fitted with a C18 guard cartridge using a Shimadzu Prominence HPLC system. Carotenoids were separated and eluted using mobile phases adapted from Wright (1991) described briefly here. The mobile phases were: A- 80:20 methanol: 0.5M ammonium acetate; B- 90:10 acetonitrile: H_2O; and C- ethyl acetate. A tertiary linear gradient was used that consisted of 100% A to 100% B over 4 min, then 80% C: 20% B over 14 minutes, then 100% B over 3 minutes, ending with 100% A over 11 minutes to re-equilibrate the column (Wright 1991). A flow rate of 1 mL/min was used for a total active run lasting 32 minutes per sample. Multiple samples were run consecutively using an autosampler equipped with an automatic internal and external cleaning port to remove cross-contamination. Carotenoid absorbance was visualized and detected using a Prominence UV/Vis detector set to 450 nm. Carotenoids were identified and quantified by comparison to calibration curves of authentic standards that included: astaxanthin, zeaxanthin, β-carotene, lutein, 3-hydroxy echinenone, and canthaxanthin. Pigment identity was confirmed by comparing the shape and retention time of peaks of feather extracts to carotenoid standards after HPLC and UV-Vis (see Figure 1.3 for representative chromatograms of standards and feather pigments). Carotenoid concentration was normalized by the dry weight of each feather sample and was reported as µg carotenoid/ mg feather dry weight.

The effect of lutein concentration on color

UV-vis spectroscopy results and the HPLC results were compared using linear models and the 'emmeans' package in R to make linear models corrected for multiple comparisons (v.1.4.5, Russel, 2020; R Core Team 2020). First, the concentration of lutein in the belly and collar feathers between the five taxon included in this study were compared. Second, the

concentration of lutein in the belly versus the collar feathers of the three taxon which had lutein in both feather patches (Hybrid, *M. vitellinus*, *M. aurantiacus*) was examined. In a third analysis, the effect of increasing lutein concentration on color components obtained from feathers belonging to each taxon obtained during reflectance spectroscopy was investigated using a mixed effects model that incorporated bird identity to account for non-independence of data among species. The most biologically relevant components that I analyzed were saturation in the yellow wavelengths of light, UV reflectance saturation, carotenoid chroma, mean brightness, and peak wavelength hue (see Pavo manual page 53 for technical details on components). Lastly, the feather brightness (as measured by reflectance spectroscopy) of the collar feathers of each of the five taxa was examined. All figures and graphs were built in R using the 'ggpubr' and 'cowplot' packages (v.0.2.1., Kassambara, 2019; v.1.0.0., Wilke, 2019).

Results

Feather structure and patterning

Variation in pigmentation between feather barbs and barbules produced the variation in plumage coloration observed between the males of each manakin species (see Figure 1.1). Belly feathers of White-bearded Manakins, which in this subspecies appear gray to the eye, had white barbs, and barbules with black oblong dots arranged in stripes running the full length. The black barbule coloration is presumed to be the result of eumelanin. Similarly, belly feathers of Golden-collared Manakins, which appear olive green to the eye, had brightly colored yellow barbs with black stripes of melanization along the entire length of each barbule. The White- and Orange-collared Manakins had "golden yellow" barbs and barbules at the distal portion of their belly feathers, with no melanization. The Golden- x White-collared Manakin hybrid belly feathers also

have “golden yellow” barbules the full length of the “golden yellow” barb. However, in the hybrids, there were some barbules that sporadically had black stripes of melanin in them as well. Belly feathers from all species that had melanized barbules appeared to be uniformly melanized on both sides of the barb.

The three species with yellow or orange coloration in their collar feathers (Golden-, Orange-, and Golden- x White-collared Manakin hybrid) showed the complete loss of barbules towards the distal third of their collar feathers. In addition, the collar feather barbs of these yellow and orange species were wider than the barbs of species lacking carotenoid coloration (White-bearded and White-collared Manakin). The species with white collar feathers did not share the same morphology as the collar feathers possessing carotenoids. White collar feathers had white barbules running the entire length of their feathers, and their barbs were noticeably narrower than barbs of the yellow and orange collar feathers. Melanization was lacking in all collar feathers examined.

Belly

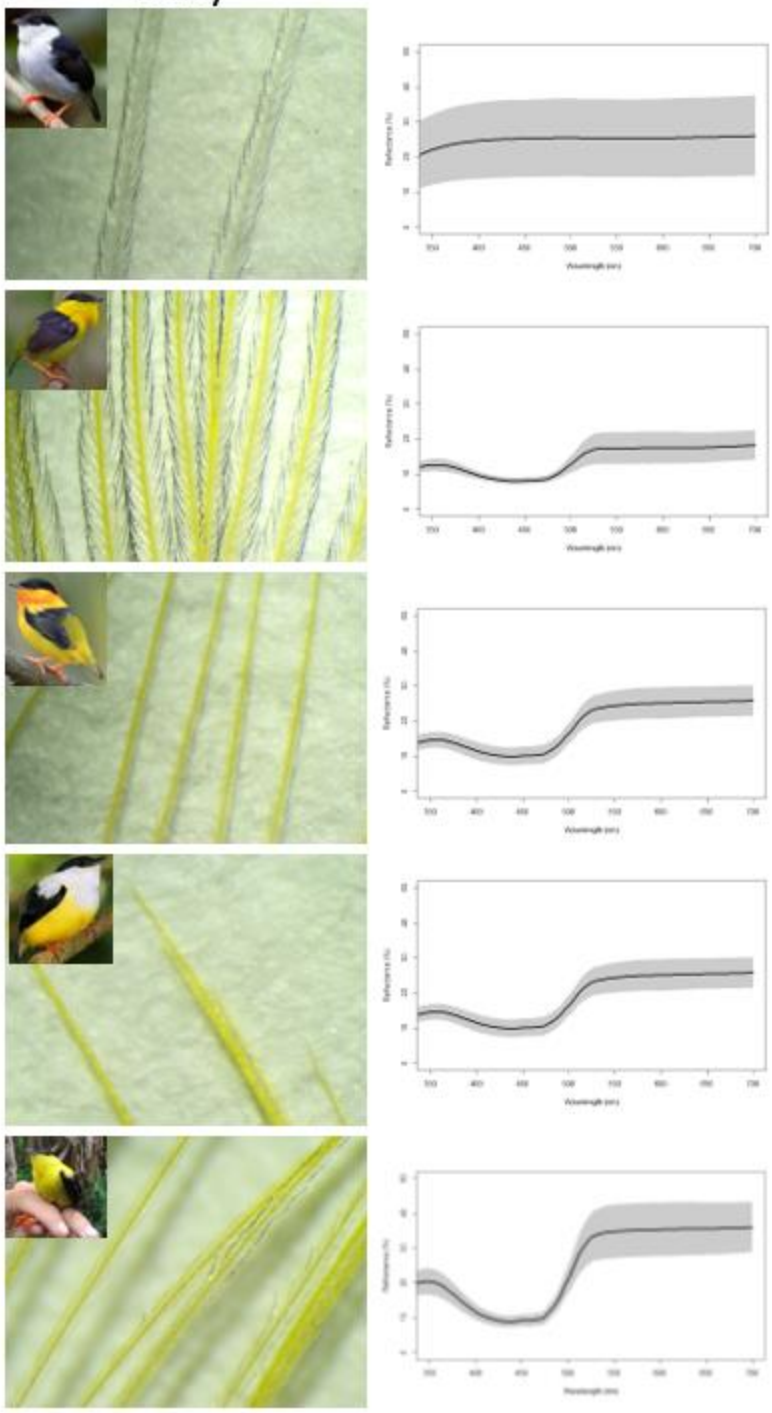

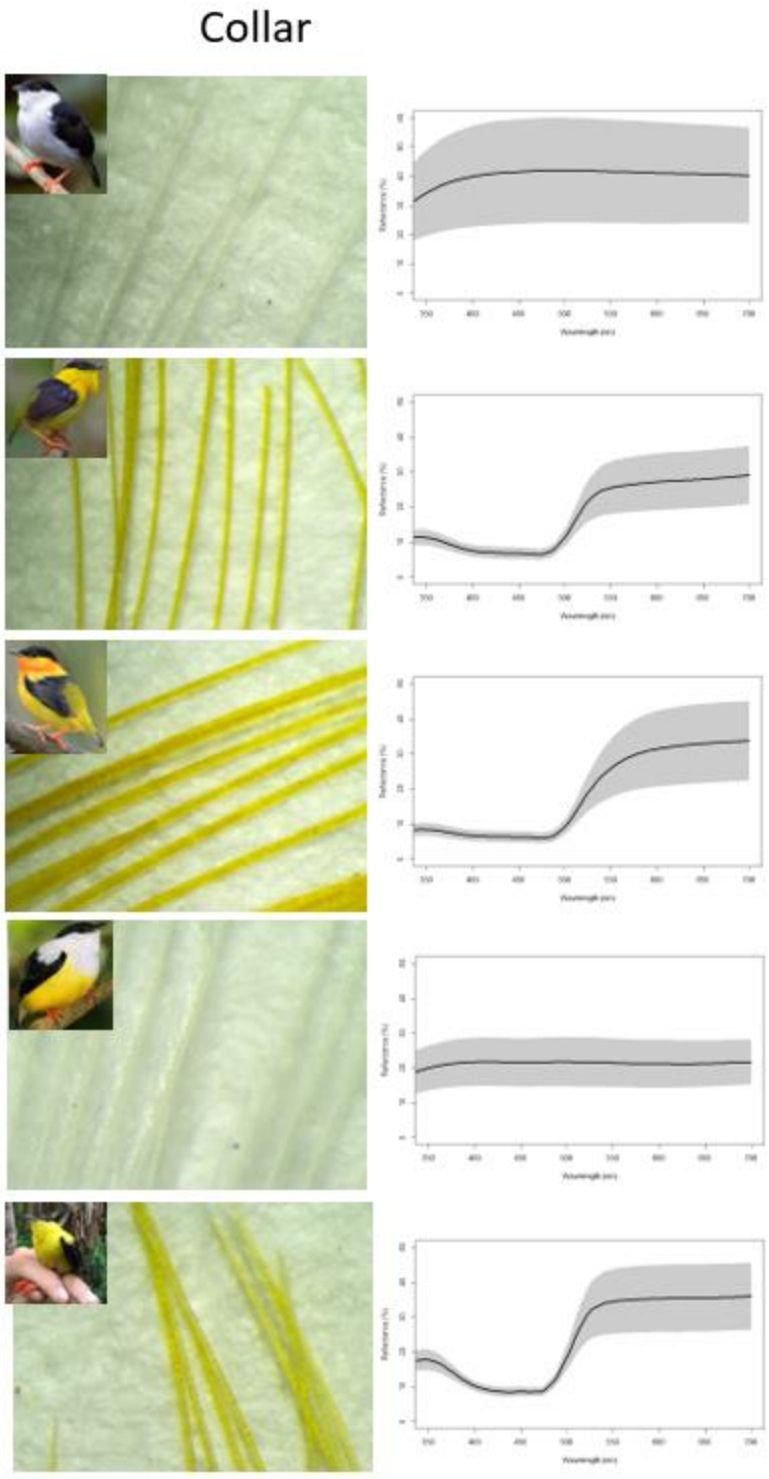

Figure 1.1: Reflectance spectra and light microscope images at 4X magnification of each species' belly and collar feathers.

After pigment extraction from the belly and collar feathers, I confirmed that all orange-yellow parts of the feathers were white, or very pale yellow. This indicates that the carotenoid extraction was successful. This also allowed us to confirm that melanin was not co-deposited in the barbs of the feathers because the orange-yellow feathers were white and not brown or black after extraction (e.g. Red-winged Blackbird; McGraw et al. 2004). The barbules that were black remained black after pigment extraction, which indicates that melanin was not extracted and remained in the feathers.

Feather color quantification

UV-vis reflectance spectroscopy revealed the reflectance spectra of the collar and belly feathers for each taxon (Figure 1.1). Yellow and orange feathers from both belly and collar feathers had spectral curves consistent with the presence of carotenoids (Isaksson et al 2008). Orange-collared Manakins predictably had the highest red and yellow values in their feathers and lowest amount of UV reflectance when compared to the collar feathers of the other species. Interestingly, the Golden- x White-collared Manakin hybrid collar feathers have the lowest spectral purity of the three taxa with carotenoids in their collar feathers. After correcting for multiple comparisons, the mean brightness of *M. manacus* collar feathers was significantly greater than those from *M. vitellinus* (β = 22.32, 95%CI : 7.44 to 36.44, p <0.001), *M. candei* (β = 18.21, 95%CI : 5.24 to 31.18, p <0.01)., *M. aurantiacus* (β = 21.33, 95%CI : 8.36 to 34.30, p <0.001)., and the Hybrid species (β = 15.95, 95%CI : 2.98 to 28.92, p <0.05). All other comparisons of collar feather brightness among taxon were not statistically significant.

Presence and concentration of pigments detected

Based on comparison with analytical standards and carotenoid profiles from the literature, the only carotenoid detectable for each of the species was lutein (Figure 1.2).

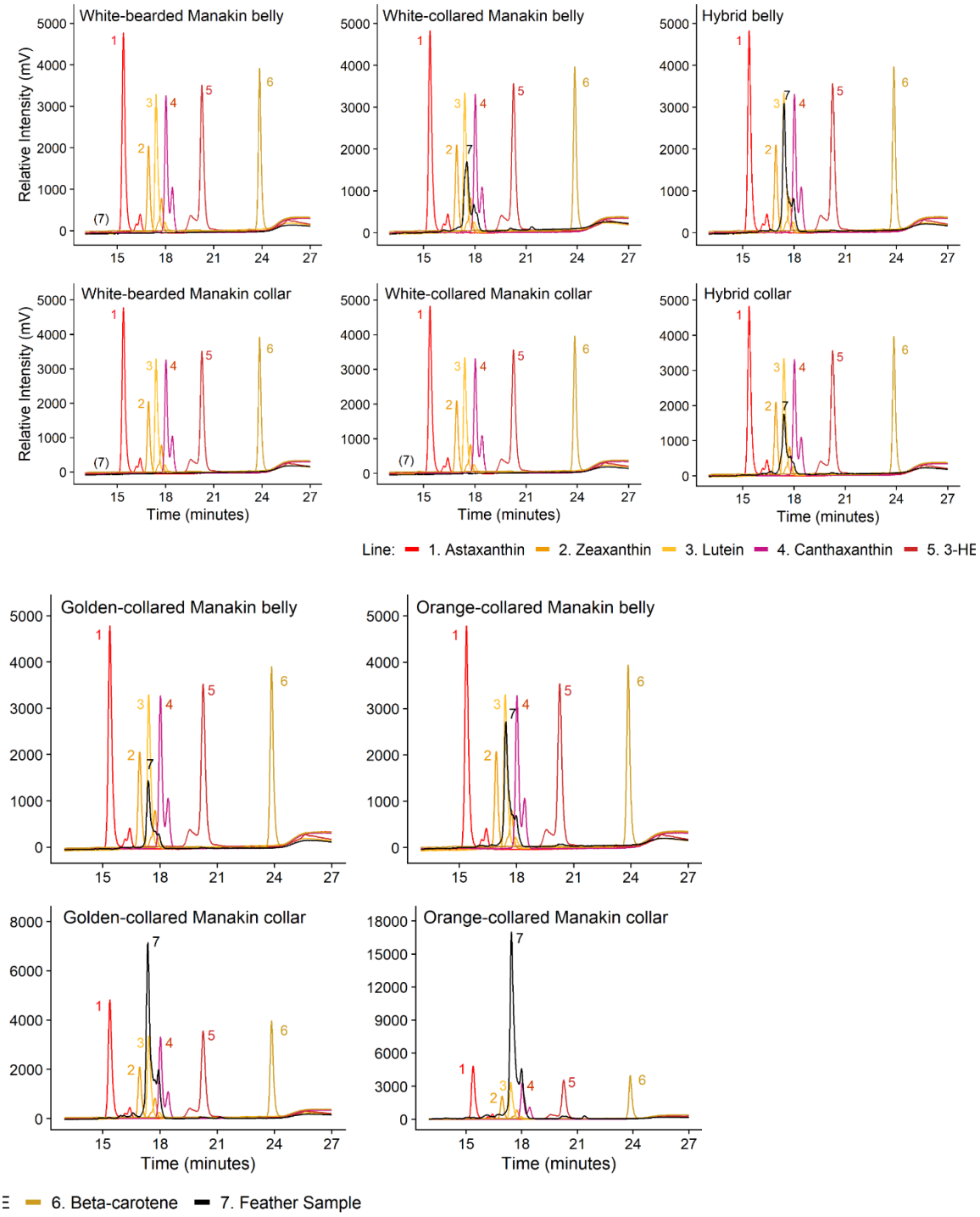

Figure 1.2: Representative HPLC chromatograms for each of the five species of Manakins used in this study. Along the x-axis is time in minutes showing the duration of the 32-minute HPLC/UV-Vis analysis. The y-axis is relative intensity of the signal in millivolts. Peaks are numbered and correspond with the carotenoid standards (1-6) and feathers samples (7). The top row is belly feathers and the bottom row is collar samples.

The list of museum specimens and the date each was collected can be found in Supplemental Table 1.1. The feathers appeared normal at the time of extraction, and the age of the feather samples had no statistically significant effect on lutein concentration (β = 0.0092, 95%CI : -0.05 to 0.07, p = 0.75). It is possible that the two abnormally low lutein measurements were due to inefficient carotenoid extraction.

The average mass-corrected concentration of lutein in collar feathers for each group were: Orange-collared 0.422 µg carotenoid/ mg feather, Golden-collared 0.144 µg/ mg, White x Golden hybrid 0.163 µg/ mg, White-collared 0 µg/ mg, and White-bearded 0 µg/ mg. The adjusted average values for the belly feathers of each bird were: Orange-collared 0.118 µg/ mg, Golden-collared 0.051 µg/ mg, White x Golden hybrid 0.098 µg/ mg, and White-collared 0.108 µg/ mg (see Figure 1.3).

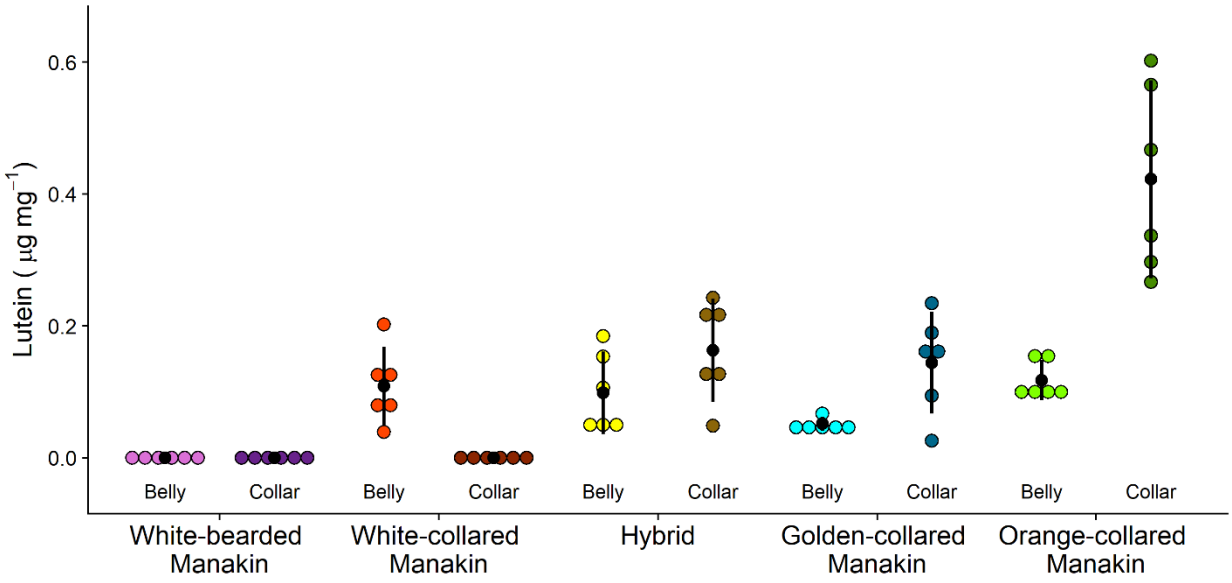

Figure 1.3: Lutein concentrations of individual feather samples. Lutein is shown in micrograms of pigment per milligram of feather tissue. Black dots represent mean lutein concentration and black bars represent 95% confidence intervals. Where black bars (confidence intervals) do not overlap, there is a statistically significant (p < 0.05) difference between groups.

When I compared the lutein concentration in the belly and collar feathers belonging to taxon that have both feather patches pigmented yellow (Hybrid, *M. vitellinus*, *M. aurantiacus*), I found that the lutein concentration in the belly feathers was lower than in the collar feathers. However, this was only statistically significant in *M. vitellinus* (β = -0.09, 95%CI : -0.18 to -0.002, $p < 0.05$) and *M. aurantiacus* (β = -0.31, 95%CI : -0.40 to -0.21, $p < 0.001$). Comparisons of the lutein concentration in belly and/or collar feathers among each of the five taxa in this study can be found in Figure 1.3. In Figure 1.3, statistically significant differences in lutein concentrations between groups are indicated by black bars (confidence intervals) that do not overlap. Notably, the Hybrid species did not significantly differ in the lutein concentration of either its belly nor collar feathers when compared to its yellow pigmented parental species *M. vitellinus* (Belly: β = -0.05, 95%CI : -0.11 to 0.02, $p = 0.27$; Collar: β = -0.02, 95%CI : -0.15 to 0.12, $p = 0.99$). The collar feathers of *M. aurantiacus* contained significantly higher concentrations of lutein than those belonging to any of the other taxa (Supplemental Table 1.2; Figure 1.3).

The effect of lutein concentration on color

The concentration of lutein in each feather was compared to the most biologically relevant color variables obtained from analyzing the reflectance of each plumage patch using pavo. The brightness (β = -2.87, 95%CI : -17.66 to 11.92, $p = 0.69$) and peak wavelength hue (β = -15.60, 95%CI : -44.55 to 13.35, $p = 0.27$) were not significantly affected by the concentration of lutein within the feathers (Figure 1.4). Interestingly, plumage brightness was previously shown to be associated with male mating success in *M. vitellinus* (Stein and Uy 2006). However, an increase in the concentration of lutein in each feather was associated with a statistically significant decrease in UV reflectance saturation (β = -0.11, 95%CI : -0.17 to -0.04, $p < 0.001$,

Figure 1.4). Additionally, an increase in lutein concentration was associated with a statistically significant increase in the carotenoid chroma component provided by pavo (β = 0.14, 95%CI: 0.002 to 0.28, $p < 0.05$) (Figure 1.4; Supplemental Table 1.2).

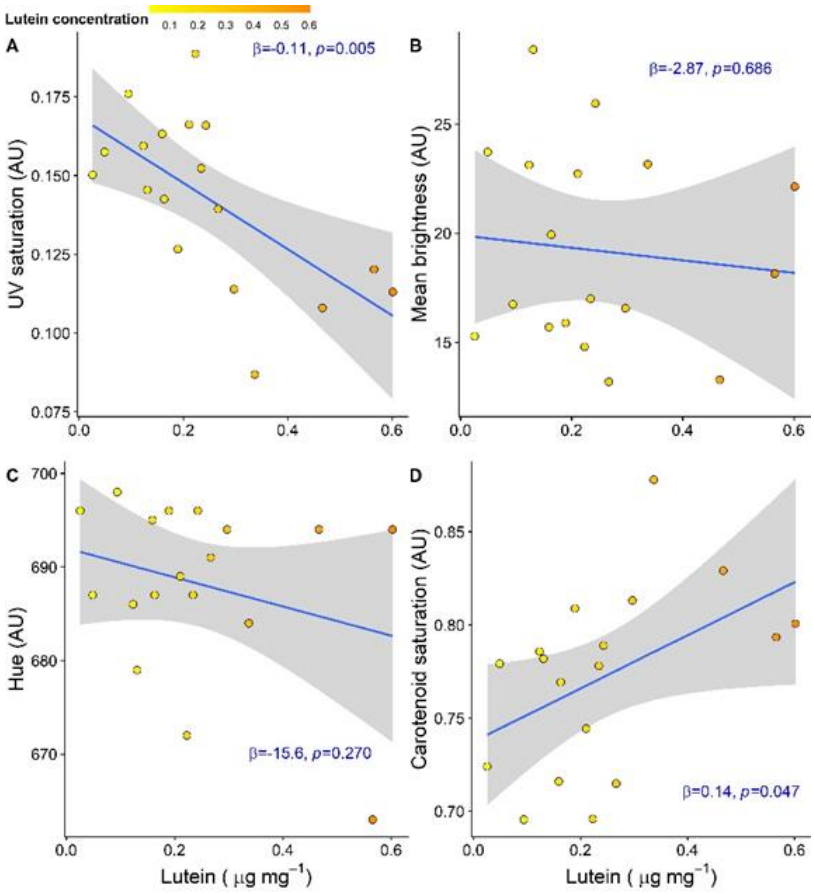

Figure 1.4: The effect of increasing feather lutein concentration (in µg lutein mg-1 feather tissue) on A) UV saturation, B) mean feather brightness, C) mean feather hue, and D) carotenoid chroma. All color variables are expressed in arbitrary units. The blue line shows the slope (β) and the grey shading represents the 95% confidence interval around the slope estimate. Each colored dot represents a single feather sample containing lutein.

Discussion

Deducing the proximate mechanisms that give rise to the color displays of animals is a critical first step in the process of understanding the genes that control species-typical coloration, polymorphisms within species, sexual dichromatism, and ultimately the targets of selection in color evolution (Toews et al. 2016; Andrade et al. 2019; Gazda et al. 2020). Here, I used

reflectance spectroscopy, HPLC, and light microscope observations to investigate the mechanism of color production for manakins in the genus *Manacus*, a species cluster that has been the focus of many speciation and sexual selection studies (Parsons et al. 1993, Brumfield et al. 2001; Brumfield and Braun 2001; McDonald et al. 2001; Stein and Uy 2006; Uy and Stein 2007; Yuri et al. 2009; Concannon et al. 2012; Parchman et al. 2013).

Unexpectedly, I found that the dietary carotenoid lutein was the only pigment within any of the orange, golden, or yellow collar feathers of male *Manacus*. The variation in orange/golden/yellow coloration, which is so striking among males of different species and is the primary phenotypic trait used to diagnose species, is mainly due to differences in the concentration of lutein. One similar previous example exists where the color differences of both the red-rumped and yellow-rumped forms of the Flame-rumped Tanager (*Ramphocelus flammigerus*), and their hybrid with orange plumage, are due to a simple concentration difference in lutein as well (Brush 1970).

Among all collar feathers, the collar feathers of the hybrid manakins are consistently the brightest. Differences in brightness presumably arise from differences in the white microstructural background of yellow feathers (Shawkey and Hill 2005; Shawkey et al. 2006b), but I do not yet have evidence structural variations within these feathers. Differences in brightness could also be simply the result of lower levels of lutein. Among the five taxa, the Orange-collared Manakin had the highest concentration of lutein in the collar feathers, with over twice as much lutein per mg of collar feather compared to the Golden-collared Manakin. The collar feathers of Golden-collared Manakin and those of Golden- x White-collared hybrids had similar amounts of lutein to one another.

It should be noted that collar and belly color vary geographically in hybrid populations of this complex, with many hybrid populations resembling parental Golden-collared populations rather than an intermediate phenotype (Parsons et al. 1993; Brumfield et al. 2001). The hybrids studied here are derived from population 4 of Brumfield et al. (2001), which is expected to be intermediate in both collar and belly color (and therefore in carotenoid concentrations) based on the reflectance data of those authors.

The pigment deposition pattern within individual collar feathers also differed between species. Species with collar feathers containing lutein had a brighter lemon-yellow region along their individual feathers, between the dark melanized base and the more colorful distal portion of the feather. This region of visibly lighter color must be due either to the presence of barbules, a difference in structure along the length of the barbs, and/or a difference in the concentration of lutein, since there was not any variation in the type of carotenoids deposited within the feather. One previous study has shown that barbule presence alone can result in increased reflectance and UV chroma (Laczi et al. 2019).

The impact that barb and barbule morphology might have on feather coloration is often understudied. Wider barbs can enhance the saturation of a feather containing carotenoids (Hill 1994; McCoy et al. 2019). Since the deposition of carotenoids is often associated with morphological modifications, it seems likely that the morphology of the barb and barbules also plays an important role in producing the color variation observed between species (Brush 1990). I observed widening of barbs in the collar feathers of manakins containing lutein, with the Orange-collared Manakins having the widest collar feather barbs. In addition, collar feathers containing lutein did not have barbules attached to the distal third of the feathers. It is unclear if

these feathers develop without barbules, or if the barbules are gradually lost throughout the season, as is the case for some other species of birds (e.g. White-winged Crossbill; Gill 2007).

Birds in this genus expose their feather beard by thrusting it forward during mating displays (Snow 1962). The widening of barbs and absence of barbules in these regions could be important for maximizing this behavioral signaling. Passerines are generally UVS sensitive (Lind et al 2014); however, the White-bearded Manakin has previously been predicted to possess violet-sensitive vision based on the amino acid sequence of its SWS1 opsin gene (Aidala et al. 2012; Ödeen and Håstad 2013). This suggests that the manakins would be unable to see the UV peak produced by lutein in their orange-yellow colored feathers. This may place more importance on the yellow to orange color differences in the collar feathers.

Whether *Manacus* belly feathers had an olive-green tint or not depended on the deposition of melanin pigments. The belly feathers of each species have barbules that span the entire length of the barb, unlike the collar feathers that contain carotenoids. The belly feathers of Golden-collared Manakins, in addition to yellow barbs, have black melanized barbules along the entire length of each barb. This combination of yellow barbs and black barbules produces the dark yellow appearance typically described in the literature as an olive-green color. This coloration is similar to the color seen in *Manacus* females. In addition, the barbs of these belly feathers are relatively thin such that the ratio of black melanized barbule to yellow barb is increased. Similar patterns exist in feathers of other yellow birds, such as the Hooded Warbler (*Wilsonia citrina*) and the White-eyed Vireo (*Vireo griseus*) that also have a dark yellow appearance in some of their plumage patches (Fox and Vevers 1960). The belly feathers of the White-bearded Manakin also have black melanized barbules the full length of the barb, just like the olive-green feathers of the Golden-collared Manakin. This barbule melanization results in the

gray belly feathers of the White-bearded Manakin. The Orange-collared Manakins have some melanized barbules into the middle of the feather, but the barbules become small, lose melanization, and are usually orange towards the distal end of the belly feathers. On average, the pigmented belly feathers had lower concentrations of lutein than the collar feathers. This is likely due to the reduction in width of the barbs in the belly feathers.

In conclusion, the two mechanisms by which the males in genus *Manacus* modify plumage coloration among species is by changing the concentration of lutein that is deposited or by adding melanin to the barbules. It has been previously stated that the reducing or removing carotenoids from a plumage patch would be the simplest way to create differences in color (Brush 1990). In addition to this, I think that adding melanized barbules could be another "simple" mechanism by which birds can change coloration, even though melanism is not associated with dichromatism as often as the deposition of carotenoids (Gray 1996). As seen in these manakins, the addition of melanized barbules can change white to gray, and yellow to olive green. While I have not studied female *Manacus* yet, it is reasonable to suppose that their olive-green plumage arise from similar mechanisms. Thus, melanized barbules likely result in both differences in species-typical plumage pattern and sexual dichromatism in manakins. The genus Manacus achieves a wide range of color variation from white, gray, and green to pale yellow, golden yellow, and orange solely by varying the feather concentration of one dietary carotenoid, lutein, and one location of melanin deposition. These results demonstrate how a relatively simple mechanistic toolkit can result in a striking array of phenotypes. Manacus plumage color differences are likely to have a simple genetic basis because of the simplicity of their color production mechanisms. Future studies on the genetic basis of manakin plumage coloration will

hopefully be informed by these detailed descriptions of their feather color production mechanisms.

Chapter 2

A combination of red structural and pigmentary coloration in the eyespot of a copepod

Manuscript Published in *Journal of the Royal Society Interface* (Justyn et al. 2022)

Abstract

While the specific mechanisms of color production in biological systems are diverse, the mechanics of color production are straightforward and universal. Color is produced through the selective absorption of light by pigments, the scattering of light by nanostructures, or a combination of both. When *Tigriopus californicus* copepods were fed a limited-carotenoid diet of yeast, their orange-red body coloration became faint, but their eyespots remained unexpectedly bright red. Raman spectroscopy indicated a clear signature of the red carotenoid pigment astaxanthin in eyespots; however, refractive index matching experiments showed that eyespot color disappeared when placed in ethyl cinnamate, suggesting a structural origin for the red coloration. We used transmission electron microscopy to identify consecutive nanolayers of spherical air pockets that, when modeled as a single thin film layer, possess the correct periodicity to coherently scatter red light. We then performed microspectrophotometry to quantify eyespot coloration and confirmed a distinct color difference between the eyespot and the body. The observed spectral reflectance from the eyespot matched the reflectance predicted from our models when considering the additional absorbance by astaxanthin. Together, this evidence suggests the persistence of red eyespots in copepods is the result of a combination of structural and pigmentary coloration.

Introduction

Animal coloration is produced by the absorption of light by pigments, the scattering of light by a structure, or a combination of the two mechanisms (Cuthill et al. 2017). Pigmentary and structural coloration are distinct in their ontogeny and mechanisms of color production, but disentangling the relative importance of microstructures versus pigments in the production of a specific color display can be challenging (Shawkey and D'Alba, 2017; Justyn et al. 2022). Such is the case with the brilliant red eyespot coloration of copepods, which has drawn the attention of biologists since the nineteenth century (Elster 1896). Precursor/product feeding experiments documented that *Tigriopus californicus* copepods use a variety of dietary carotenoids to synthesize astaxanthin, and the high concentrations of free and esterified astaxanthin were implicated as the source of orange-red body coloration. In previous studies, when *T. californicus* copepods were fed a carotenoid-restricted diet, their bodies became nearly clear (Weaver et al. 2018). This observation is consistent with the hypothesis that orange-red coloration is a product of carotenoid pigments because, like most animals, copepods are not known to synthesize carotenoids *de novo*. Rather, copepods ingest carotenoids as intact pigments that are then incorporated into their bodies (Powlik 1996). Once carotenoids are ingested, they can be either deposited directly or bioconverted into new carotenoids (Fox 1976). However, even as the bodies of copepods that are deprived of carotenoids faded to be nearly colorless, their eyespots remain a vivid red color (Weaver et al. 2018, Balasubramaniam 2021). Thus, while carotenoids were shown to play an important role in the coloration of copepods, further observations implicate additional mechanisms in the production of red eyespot coloration in copepods.

One explanation for the origin of eyespot coloration is that copepods might endogenously produce other red pigments such as ommochromes (Seligy 1972; McGraw 2006). Alternatively,

the seemingly non-iridescent red color of the eyespot could be produced by nanostructures that coherently scatter red light. There are many examples of structural color in arthropods (Goldstein 2005; Welch and Vigneron 2007; Seago et al. 2009; Fabricant et al. 2013; Kariko et al. 2018) and even in some species of copepods (Gur et al. 2015; Gur et al. 2016). In each of these cases, coloration is produced by fixed structures with high refractive index contrast, typically chitin and air, that possess the correct periodicity to coherently scatter light in the visible spectrum (Land 1972; Noyes et al. 2007). However, non-iridescent red structural color is rarely observed in nature, but iridescent red structural color is common and is sometimes combined with pigments, which reduces the iridescent appearance (Magkiriadou et al. 2014; Hsiung et al 2017; Eliason et al. 2020).

Here, we investigated the mechanisms responsible for the red coloration of the eyespots of *T. californicus* copepods to better understand how color is being maintained in the absence of carotenoids. We first used Raman spectroscopy to detect pigments in the eyespots, and refractive index matching experiments to test for structural coloration in eyespots. We performed transmission electron microscopy (TEM) to visualize and measure any structures capable of producing color. We then modeled the predicted reflectance produced by the nanolayers found within the exoskeleton and used microspectrophotometry to verify our model predictions.

Based on our observations in these procedures, we conclude that *T. californicus* copepods create their red eyespot coloration using a combination of structural color, produced by consecutive nanolayers of spherical air pockets in the exoskeleton, and pigmentary color, by retaining small amounts of astaxanthin. The nanostructures within the exoskeleton effectively act as a single thin film because there is little exoskeleton between each layer, and individually each layer is too small to coherently scatter light in the visible spectrum. Astaxanthin reduces the

iridescence of this thin film and enhances the red coloration of the eyespot. Our findings not only provide evidence of a novel color production mechanism in arthropods but also demonstrates a means to circumvent the apparent biological difficulty of producing brilliant non-iridescent, red coloration using nanostructures. This is accomplished by combining iridescent, red structural coloration with orange-red pigments.

Materials and methods

We took a systematic approach to identify color production mechanisms throughout the body of *T. californicus* copepods. We began by performing light microscopy to determine which regions of the body expressed visible color and which regions were most suitable to evaluate the mechanisms of color production, while avoiding undigested algae in the digestive tract. We then performed Raman spectroscopy on the body and eyespot, and then compared those signals to Raman spectra obtained from carotenoid standards. We chose confocal Raman spectroscopy rather than traditional HPLC because Raman requires a minimal amount of tissue to analyze and can be localized to exceedingly small areas of the body, such as an individual eyespot on a copepod. Next, we used refractive index matching experiments to detect if structural coloration was present, and once confirmed, we used TEM to identify and measure the spacing of any nanostructures that are present. We then modeled the predicted reflectance of the structures using the transfer matrix method (Eliason and Shawkey 2010). Lastly, we measured the reflectance of the body and eyespot of the copepods using microspectrophotometry and compared it to the reflectance predicted by our models.

Copepod husbandry

We collected *Tigriopus californicus* copepods near San Diego, CA, USA in 2014 and have been culturing them in our laboratory at 20-22 ºC, salinity = 32 psu. Copepods were fed ad libitum *Isochrysis galbana* and *Tetraselmis chuii* algae on a natural light cycle, which provide the required precursor carotenoids for red coloration (Weaver et al. 2018). Carotenoid-restricted copepods were fed ad libitum Bragg Nutritional Yeast, which lacks the carotenoids responsible for producing orange-red coloration throughout the body (Weaver et al. 2018). Yeast-fed individuals were raised in the dark and were approximately four months, or four generations, removed from the algae-fed, red-colored population.

Color investigation (light microscopy and refractive index matching)

Copepods were photographed on a glass slide using an AmScope Microscope Digital Camera at 1x and 4x magnifications to capture the appearance of the body and eyespot. Five copepods from both treatment group were then dissected in half using a hypodermic needle, and a drop of ethyl cinnamate, acetone, water, or nothing was placed on each individual in a covered petri dish (n = 10). Pictures were taken after five minutes and 24 hours. Ethyl cinnamate, with a refractive index of 1.558 (Wilcox 1964), was chosen because it approximates the relatively high refractive index of the exoskeleton. Ethyl cinnamate has previously been shown to produce detectable changes in the structural color of spider cuticles that have a refractive index of ~1.60 (Hsiung et al. 2015).

Pigment identification (Raman spectroscopy)

We characterized the carotenoids present in *T. californicus* eyespots and bodies using confocal Raman spectroscopy. Raman spectroscopy is a technique that has been previously

employed to characterize carotenoids present in different animal tissues, including spider silk and bird feathers (Justyn et al. 2022, Hsiung et al. 2017, Thomas et al. 2014). After allowing copepods to visibly air dry, we analyzed whole specimens, including two male and two female algae-fed copepods, as well as two male and three female yeast-fed copepods. To assess changes in carotenoid composition under diet-restriction, both algae- and yeast-fed copepods were sampled in the same anatomic positions, including two eyespot locations,the cephalosome, metasome, urosome, and one caudal ramus (Figure 2.1). We found that the eyespots were completely covered by the exoskeleton. So, to avoid analyzing the exoskeleton rather than the underlying eyespots, we removed the eyespots from one algae- and one yeast-fed copepod using a pin sterilized in 200 proof ethanol. We then bisected the eyespots to expose the center. All copepod samples were attached to a glass slide using clear, double-sided tape. We compared Raman spectra from copepod samples to those of an astaxanthin reference standard (DSM, Heerlen, Netherlands).

We captured Raman spectra using a 532 nm excitation laser through a 50x objective with a numerical aperture of 0.75 and a working distance of 0.37 mm on a LabRam High Resolution Raman microscope (HORIBA Scientific), calibrated with a wafer of pure silicon, at the Surface and Optical Analysis (SOA) Facility at The University of Akron. We used a 100 µm slit aperture, a 400 µm pinhole, an integration time of 5 s x 1 accumulation, and a grating of 1200 lines per mm. We collected spectra from at least two different locations on each copepod eye sample and three different body regions on each whole copepod sample. When analyzing whole copepod samples, we specifically sampled four body regions near the periphery of the animal to avoid the alimentary canal, which appears darkly colored in all samples, and any undigested food within it. Pigmented copepods and eyespot samples were analyzed using a D2 (1%) filter, while

clear samples were analyzed using a D1 (10%) filter to decrease fluorescence and sharpen the Raman peaks, making them more comparable to the red copepod samples. To account for any potential influence from the adhesive, we also took Raman spectra from the double-sided tape using both D1 and D2 filters. Cosmic ray spikes were removed from the spectra, and each sample was checked for burning after each spectrum was collected. No samples were burned. We normalized all of the spectra using Origin Pro v.8.5.1 (OriginLab), then used IgorPro v.6.36 (Wavemetrics) to fit the Raman peaks using a Gaussian distribution and a linear baseline.

Structural characterization and quantification (TEM measurements)

We prepared all copepods for TEM following previously established methods (Heine et al. 2021). First, we placed the copepods into a primary fixative consisting of 12.5 mL of 0.2 M phosphate buffer, 6.25 mL of 10% glutaraldehyde, 5 mL of 10% formaldehyde, and 1.25 mL dH_2O. We then removed the distal portion of the urosome and placed the remaining portion of the copepod into primary fixative overnight at 4 °C to allow the fixative to thoroughly infiltrate the copepod. Next, we washed the sample three times in 0.1 M phosphate buffer for 30 minutes each time before placing it into a secondary fixative of 2% osmium tetroxide in the dark for 90 minutes. We then dehydrated the samples using a seven-step dehydration series and placed the samples into the transitional fluid propylene oxide (PO). We then infiltrated the tissue with a PO:Epon resin ratio of 2:1, 1:1, 1:2, and pure Epon resin over 12 days, for three days per ratio (Hopkins 1978). Samples were cured at 70 °C for 24 hours. Each copepod was embedded longitudinally to consistently section the eyespots. We cut ultra-thin, 80 nm thin cross sections and collected them on 200 mesh copper grids. We stained each of the sections with uranyl

acetate and lead citrate to increase contrast. We completed TEM using a ZEISS EM10 transmission electron microscope in the Auburn University Research Instrumentation Facility.

We measured the thickness of the epicuticle, exocuticle, individual spherical nanostructure layers, and the total thickness of all layers combined, in each of the representative TEM images. Measurements were made at ten random locations and averaged to obtain representative measurements for each of the aforementioned regions. We completed all measurements using ImageJ version 1.53f (Rueden et al. 2017).

Predicted and measured reflectance (thin-film optical modeling and microspectrophotometry)

The predicted peak reflectance of 300 – 700 nm from the structures was calculated using the transfer matrix method (Eliason and Shawkey 2010). We used n = 1 for the refractive index of air and n = 2 for the darker pigmented sclerotin that comprises the epicuticle and exocuticle (Fabricant et al. 2013). The thickness of the single air layer input into the model was adjusted depending on the number of individual spherical nanostructure layers found throughout different regions of the exoskeleton. We also ran the model using various other conditions to account for the possibility of a lower refractive index for chitin, closer to 1.56 (Noyes et al. 2007; Leertouwer et al. 2011), and other alternative conditions that could exist (*see* Supplemental Material).

Using normal specular reflection microspectrophotometry, we measured the reflectance from the eyespot and body of six copepods. We used an AX10 UV-Visible microspectrophotometer (CRAIC Technologies Inc.) to collect the reflectance spectra for each region using a 15x objective (10 x 10 µm area) with black and white standards (Avantes WS-2 and BS-2), following the methods of Hsiung et al. As the images of the 15x objective are of

lower quality, we present the images of the 10x objective in the results section. The results were visualized using the pavo package in R (R Core Team 2020; Maia et al. 2013). Three measurements were obtained from each eyespot and body region of all six copepods. The three measurements from each region of each individual copepod were averaged to create the displayed spectra and shaded variance. The last row of microspec values were adjusted from 699.88 nm to 700 nm to prevent a conflict with calculations made in pavo.

Results

Color investigation (light microscopy and refractive index matching)

Light microscopy revealed the extent of color differences between the copepods raised on an algae diet versus those reared on a carotenoid-restricted, yeast diet (Figure 2.1). The yeast-fed copepods lacked all but a trace of orange-red coloration throughout their body. However, these yeast-fed copepods retained their bright red eyespots, which appeared non-iridescent under both reflected and transmitted light.

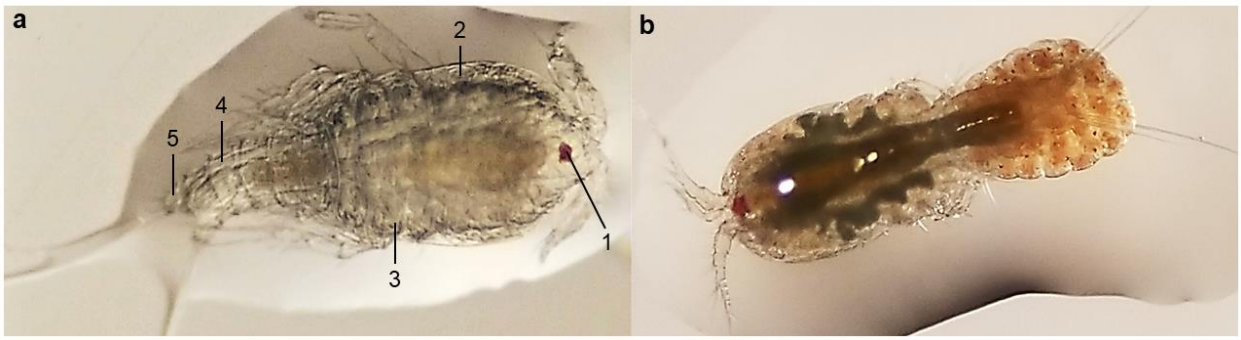

Figure 2.1: Light microscopy indicating Raman sampling locations of both yeast- and algae-fed *Tigriopus californicus* copepods. (a) Male fed a carotenoid-restricted diet of yeast, including the (1) eyespot, (2) cephalosome, (3) metasome, (4) urosome, and (5) caudal ramus. (b) Red, algae-fed female with an egg sac. Both copepods are approximately 1-2mm in size.

Refractive index matching experiments revealed that the copepods completely lost their eyespot color when they were submerged in ethyl cinnamate, while they retained some portion of their color when left in air, water, or acetone for 24 hours (Figure 2.2). The loss of color in ethyl cinnamate is a result of the removal of refractive index contrast that is necessary for producing the structural color. When the structures are filled with ethyl cinnamate, which has a similar refractive index as the exoskeleton, the structural color disappears (Figure 2.2A**)**. Ethyl cinnamate is a highly viscous liquid, so we allowed an extended period of time to allow the ethyl cinnamate to penetrate structures. The orange-red color of the copepod throughout the body persisted in the samples submerged in ethyl cinnamate, indicating that the removal of the red eyespot coloration was not simply the result of carotenoid extraction (Figure 2.2A). In contrast, the orange-red color faded from the body of copepods when submerged in acetone, which is a carotenoid solvent (Figure 2.2B**)**. The eyespot color was also diminished in an acetone solution, indicating that a portion of eyespot coloration was due to carotenoid pigments (Figure 2.2B).

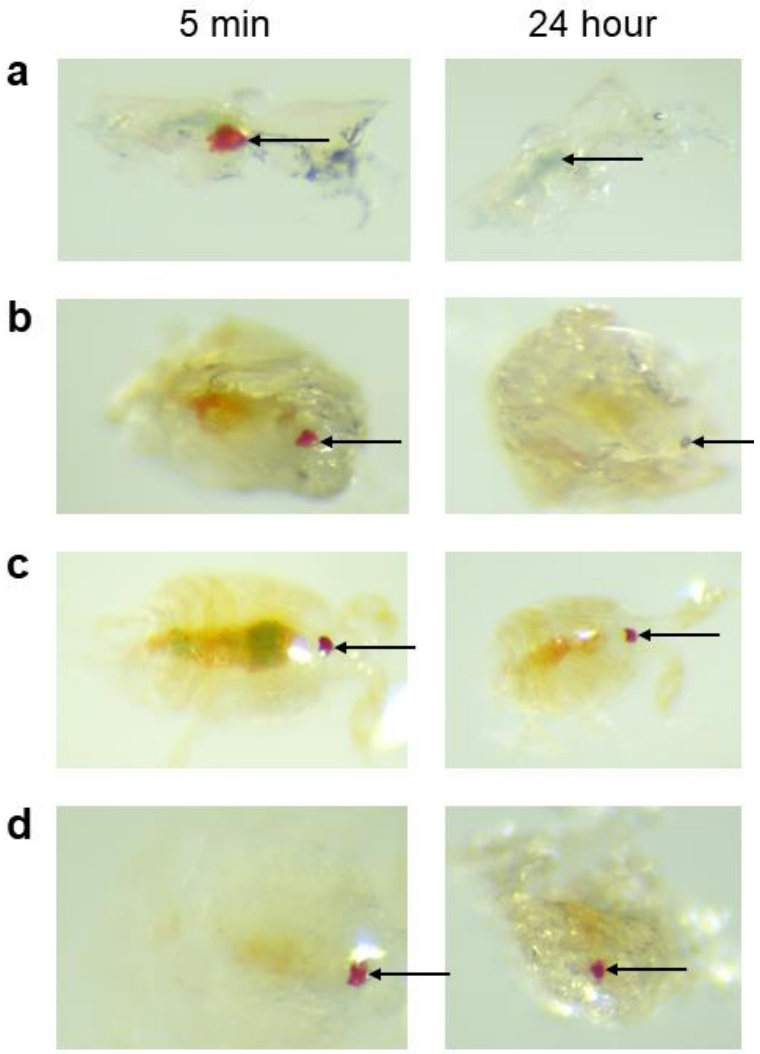

Figure 2.2: Refractive index contrast images. Refractive index matching under reflected light of copepods in (a) ethyl cinnamate where the eyespot coloration completely disappears, (b) acetone where the eyespot coloration is slightly faded, (c) water where the eyespot color is consistent, and (d) air where the eyespot color is consistent after 24 hours. Arrow indicates the eyespot location.

Pigment identification (Raman spectroscopy)

Raman spectra for all samples, including the copepod eyespots of both algae and yeast-fed copepods, body, and carotenoid standards, had three main peaks: one between 1005 cm^{-1} and 1008 cm^{-1}, a second peak between 1151 cm^{-1} and 1159 cm^{-1}, and a third peak between 1507 cm^{-1} and 1525 cm^{-1} (Figure 2.3). These three intense peaks are diagnostic of the presence of a

carotenoid pigment in the sample (Thomas et al. 2014; Arcangeli and Cannistraro 2000). Previously-reported Raman spectra for chitin lack similar peaks (Focher et al. 1992), suggesting that despite our attempts to deprive the yeast-fed copepods of dietary carotenoids—and the clear, color-less appearance of their cuticles—they still deposited detectable amounts of carotenoids in their bodies and eyespots.

The region between the second and third major carotenoid peaks, referred to as the "fingerprint region" (LaFountain et al. 2015) can be used to identify specific carotenoids. The fingerprint region for the red eyespots in both algae- and yeast-fed copepods matched each other, and that of the astaxanthin standard (Figure 2.3). An identical signature was identified for the body (i.e., cephalosome, metasoma, and urosome) of both female and male, red-colored individuals.

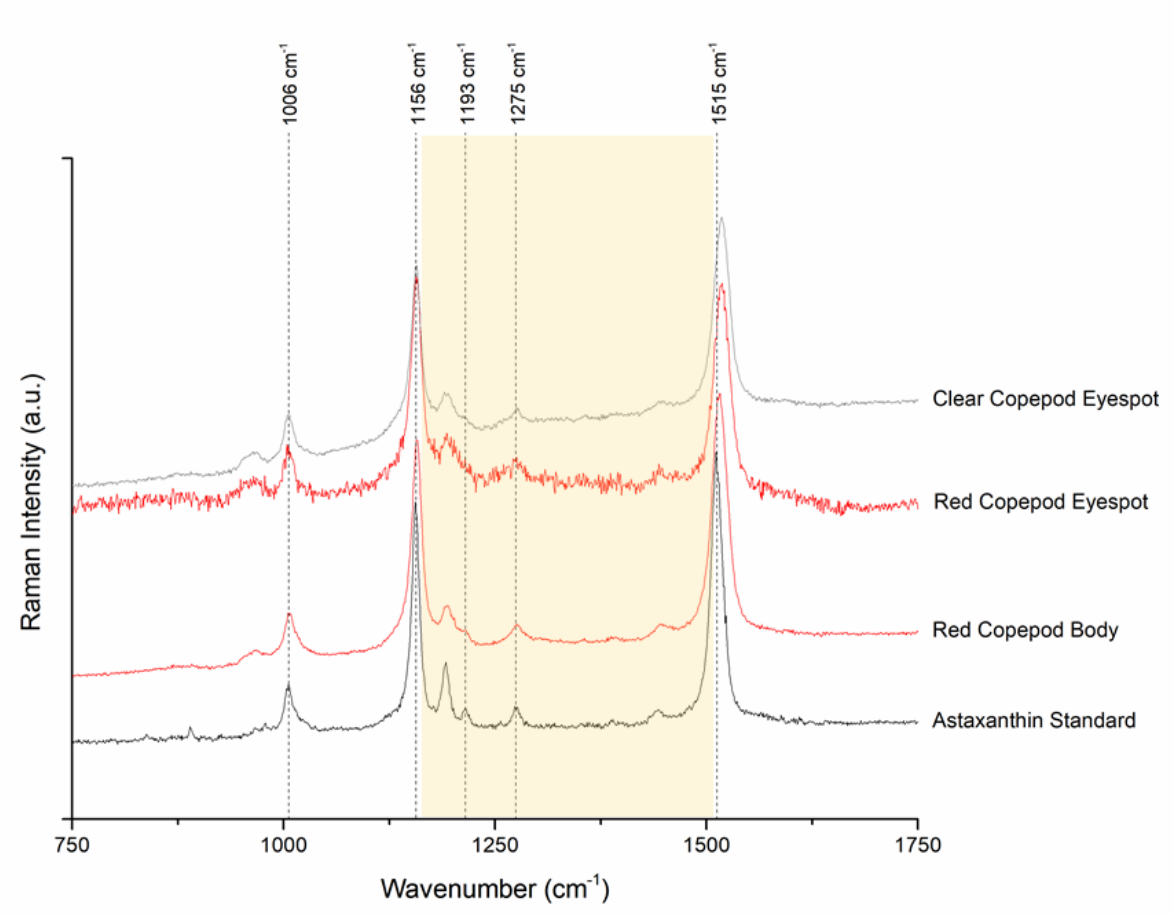

Figure 2.3: Raman spectra for copepods and carotenoid standards including proposed astaxanthin peaks. The black spectra indicate standards, red indicates spectra from red (algae-fed) copepods, and grey indicates spectra from clearer (yeast-fed) copepods. The yellow highlighted region indicates the fingerprint region. "Body" corresponds to sampling locations 2-5 in Figure 1.

Structure characterization and quantification (TEM measurements)

Using TEM and measurements made in ImageJ, we determined the epicuticle was 35.1nm ± 8.6 nm (n = 50 from five images and two copepods) and the exocuticle to be 536.4 nm ± 135.5 nm thick (n = 50 from five images and two copepods). TEM also revealed distinct nanolayers between the epicuticle and exocuticle of the exoskeleton (Figure 2.4). Their shape and low electron density suggested that these structures are likely air spaces. The number of air layers varies throughout the exoskeleton of a copepod, and multiple air layers are seen even

when examining ultrathin sections from the eyespot region of the copepod. With an average spacing of 34.6 nm ± 4.6 nm (n = 50 from five images and two copepods), the individual air layers appear too small to produce structural color by acting as a true multilayer of alternating chitin and air. However, if the width of multiple air layers combined is considered, the layers could act as a single thin-film, with the correct periodicity and refractive index contrast to coherently scatter visible light. A similar phenomenon occurs in feathers where some melanosomes are placed so close together in the barbules that they act as a single layer (McGraw 2006; Shawkey et al. 2006a; Xiao et al. 2014; Eliason et al. 2020). We observed variation in the number of air layers found depending on which region of the copepod was sampled. When the area of the exoskeleton above the eyespot region of the copepod was sampled, three to four air layers were encountered. Throughout the body, variation between one and two air layers were most frequently encountered. The measurements for the thickness of multiple air layers included the thickness of the air layers as well as the small amount of exocuticle between them. We determined the width of two air layers to be 81.5 nm ± 6.4 nm (n = 10 from one image and one copepod), 168.2 nm ± 17.3 nm for three air layers (n = 40 across four images and one copepod), and 220.5 nm ± 33.0 nm for four air layers (n = 30 across three images and one copepod; *see* Supplemental Figure 2.1).

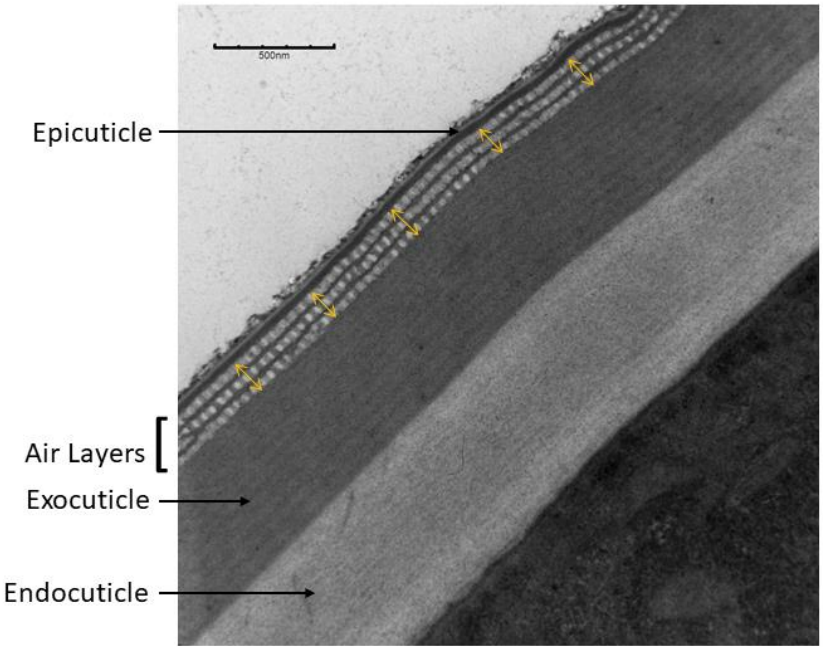

Figure 2.4: Transmission electron micrograph of nanolayers of air spheres found in the exoskeleton of *Tigriopus californicus* copepods. Yellow arrows correspond to random sampling locations. Scale bar = 500 nm.

Predicted and measured reflectance (thin-film optical modeling and microspectrophotometry)

Using the transfer matrix method previously developed by Eliason and Shawkey (2010), we calculated the predicted peak reflectance between 300 - 700 nm. We used the measurements obtained from our TEM images for the thickness of each layer and used previously reported values for the refractive index of air and sclerotized chitin in the model. We estimated the predicted reflectance of an exoskeleton with a single air layer using a refractive index of n = 2 for the epicuticle, n = 1 for one layer of air, and n = 2 for the exocuticle, an air layer thickness of 34.6 nm, and an exoskeleton thickness of 536.4 nm. This resulted in a low amount of reflectance without a peak in the visible wavelengths of light, and some reflectance in the ultraviolet wavelengths of light (Figure 2.5A). We used these same parameters, only varying the thickness of the air layer, to determine the predicted reflectance for each number of air layers observed in the exoskeleton. When two air layers are combined, with a thickness of 81.5 nm, they are

predicted to produce a discrete peak at 326 nm in the UV-A range, and an overall higher amount of reflectance than one layer (Figure 2.5B). Three air layers combined have an average thickness of 168.2 nm, and four air layers combined have an average thickness of 220.5 nm. Both three and four air layers present in the exoskeleton are predicted to maximally reflect long wavelengths of light in the orange-red region of the visible spectrum (Figure 2.5C and 2.5D). On each figure, we also shaded the typical range (400-550nm) that astaxanthin absorbs light, which peaks around 476 nm - 481 nm (Ilagan et al. 2005; Elde et al. 2012). Since astaxanthin is co-deposited throughout the copepod body and eyespot, it should absorb a significant amount of the light in this region of the visible spectrum. Although rare, we saw more than four layers of air spaces in small regions throughout the copepod exoskeleton. We estimated the thickness of any additional layer by increasing the thickness by 80 nm for each additional layer past four layers. These estimates from five to eight layers varied in the amount of reflectance produced, but seven and eight layers, with a spacing of 460 nm and 540 nm respectively, notably also produced a high amount of reflectance in the orange-red region of the visible spectrum (*see* Supplemental Figure 2.2).

In addition to these calculations, we also changed each value in the model to alternative values to determine how, if at all, the predicted peak reflectance is impacted. While we chose to use an estimate of 2.0 for the refractive index of chitin based on previous work, changing the refractive index of chitin to a more conservative estimate of 1.56 does not change the hue of the predicted reflectance, however, it does lower the brightness by approximately half (*see* Supplemental Figure 2.3). These refractive indices used encompass the range of values potentially attributed to sclerotinized chitin. While the TEM images suggest that the spaces we observe are air layers, it is also possible that they are filled with water. To simulate this, we

changed the refractive index of the air layers to 1.333 for water and ran additional models. This again significantly reduces the refractive index contrast between layers, and therefore decreases the brightness, while the hue once again remains unchanged (*see* Supplemental Figure 2.4). Actual reflectance spectra obtained by microspectrophotometry mostly matched the reflectance spectra predicted by our models with three or four air layers (Figure 2.5C-D**;** see Supplemental Figure 2.5). However, reflectance in UV wavelengths was lower than predicted if four air layers are present, and the reflection of visible wavelengths began to increase at ~550, rather than ~500nm (Figure 2.5D). Both of these differences are likely due to the absorbance of astaxanthin present in the eyespot This also suggests that three or four air layers are most common above the eyespot, since the predicted reflectance of three and four layers most closely matches the observed reflectance. Importantly, these data confirmed the distinct color difference between the red eyespot and the orange body (Figure 2.6; Figure S4): reflectance in the body began to rise at shorter wavelengths than in the eyespot, presumably due to spherical, air-filled nanostructures above the eyespot.

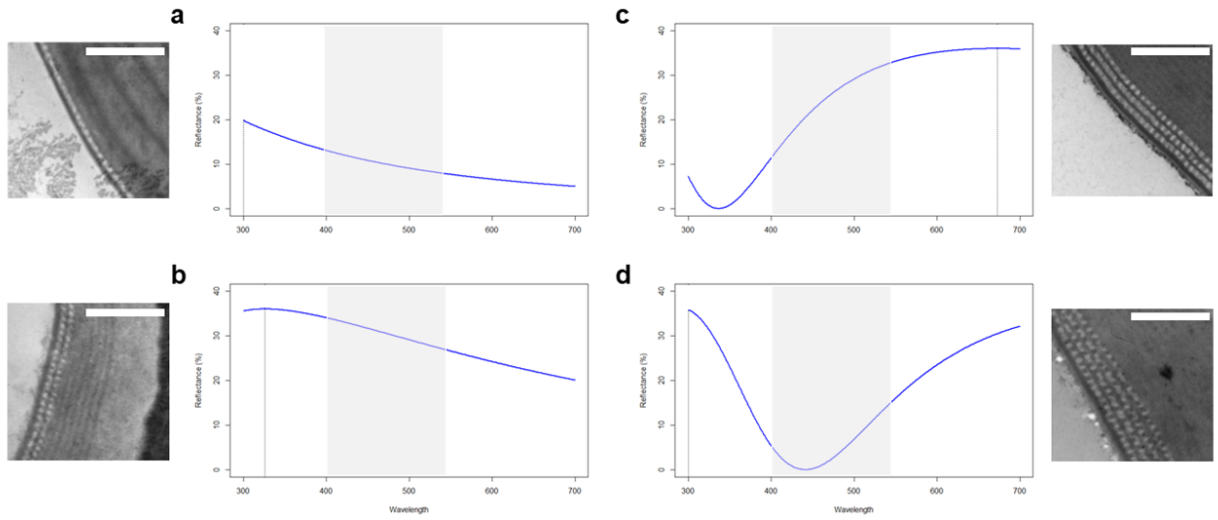

Figure 2.5: Periodicity of nanolayers of air spheres in the exoskeleton and predicted structural color peak reflectance. (a) One air layer found throughout the body, (b) two air layers found throughout the body, (c) three air layers found in the eyespot region, and (d) four air layers found in the eyespot region. The shaded region from 400-550 nm represents the typical absorption range for carotenoids. Scale bars = 500 nm.

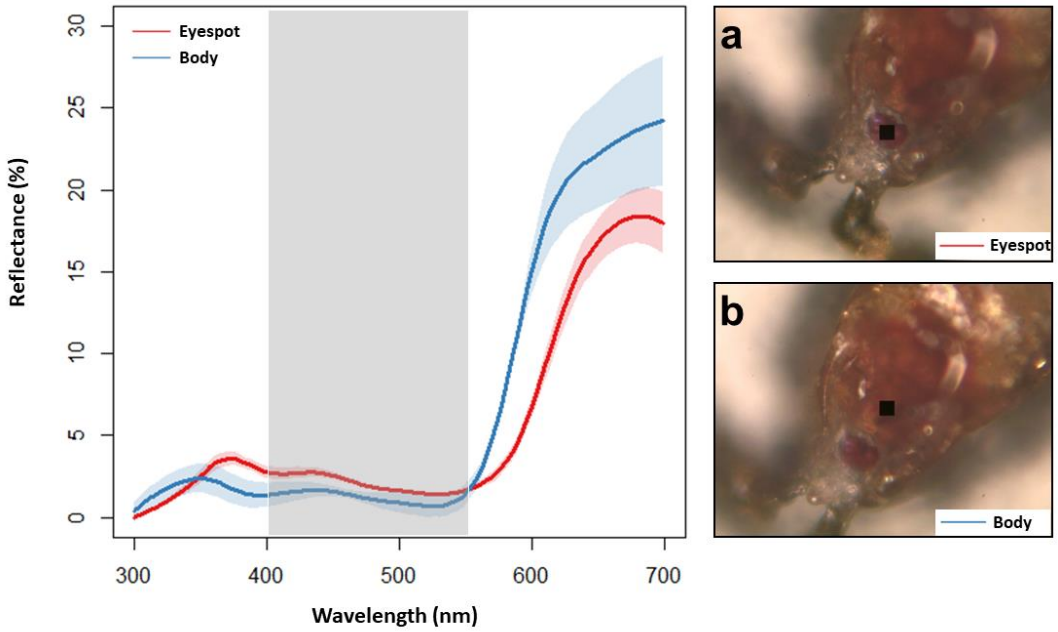

Figure 2.6: Reflectance spectra of astaxanthin and structural color combined, measured using microspectrophotometry (15x objective) from a copepod eyespot (bottom red line) and body (top blue line). Three measurements from each region were averaged to create the displayed spectra and shaded variance. The grey shaded region from 400-550 nm represents the typical absorption range for carotenoids. Representative images of the (a) eyespot and (b) body were taken during microspectrophotometry using the 10x objective. The black square in each

image represents the sampling location of the microspectrophotometer. See supplemental Figure 2.5 for the microspec of all six individual copepod eyespots and bodies.

Discussion

When *Tigriopus californicus* copepods are maintained through multiple generations on a yeast diet that provides limited access to carotenoids, their bodies lose almost all orange-red coloration. However, the eyespots of these same yeast-fed copepods remain bright red. To investigate the source of this red eyespot coloration, we employed a combination of chemical and microscopy techniques, which revealed that the red eyespot coloration is the result of a combination of astaxanthin and structural coloration.

Using Raman spectroscopy, we found that copepods on a carotenoid-restricted diet continue to incorporate astaxanthin into their eyespots. The source of the carotenoids used by these animals is unclear, but sufficient carotenoids must remain in their environment to maintain red eyespots even as red body coloration fades. Saturating a copepod section in ethyl cinnamate resulted in the loss of all red eyespot coloration. On the other hand, when we removed carotenoid pigments with the solvent acetone, a brown-red eyespot remained. The opposite was true for the orange body, which remained orange in ethyl cinnamate (Figure 2.2A**)**, but became transparent in acetone (Figure 2.2B**)**. This transition in eyespot coloration from scarlet to a more reddish brown is likely caused by the loss of light absorption in the middle of the visible spectrum by astaxanthin. By contrast, the body (i.e., not surrounding the eyespot) likely relies solely on pigments for coloration, so it becomes transparent following carotenoid removal via acetone. Additionally, a violet or purple color is noticeable around the edge of the eyespot in the higher magnification images included in Figure 2.6A and 2.6B. This further suggests a structural origin

for the eyespot color and matches our predicted reflectance for four layers of nanostructures (Figure 2.5D).

To further investigate the hypothesis that nanostructures are involved in the red color production of copepods, we studied the nano-scale components of sectioned copepods using TEM. These images revealed stacked nanolayers comprised of spherical pockets (which appear to be filled with air) in the exoskeleton throughout the body and above the eyespot region of the copepod. We repeatedly observed a pattern of three or four layers stacked together above the eyespots of copepods, and the total thickness of these stacked layers was 168.2 nm and 220.5 nm, respectively. The individual spherical nanostructures comprising the air layers appear to be relatively spherical in cross-sectional micrographs, suggesting that anisotropy in the form of elongated air spaces is not present. This is significant because it suggests that the structure is unlikely to interact with polarized light in a transformative way (Lindon et al. 2016). If these are not spheres, for instance if they are continuous tubes, we would expect some amount of variation in the cross sections, which we did not observe. The presence of one or two air layers throughout the exoskeleton could be advantageous to copepods by reflecting UV light and aiding in protection against UV radiation that is known to significantly influence survival and reproductive success in copepods that live in shallow splash pool habitats (Heine et al. 2019; Hylander et al. 2014; Heine and Hood 2020). Carotenoids in both the body and eyespot additionally contribute to UV light absorption and, thereby, aid in UV protection.

Using the measurements obtained from TEM, we used the transfer matrix method to demonstrate that, when combined together, three and four layers of nanostructures possess the correct periodicity to coherently scattering orange-red light (590 - 700 nm). Microspectrophotometry from individual copepod eyespots confirmed high reflectance in these

wavelengths, but with a somewhat later onset of increased reflectance (~550 rather than the predicted 500nm), and reduced UV reflectance compared to the model with four air layers, which are both likely caused by absorption of astaxanthin (Figure 2.5C-D; *see also* Figure 2.1; 45, 46). Microspectrophotometry also revealed similar levels of UV reflectance from both the eyespot and body regions of the copepods sampled; however, the location of the peak in the UV varied slightly, which is likely due to the presence of the nanostructures as well.

Taken together, these observations suggest that structural elements produce a base color that is modified by astaxanthin via absorption of light in the middle of the visible light spectrum and UV. The presence of astaxanthin results in the redder hue, increased saturation, and reduced iridescence and UV reflectance of the eyespot coloration (Figure 2.7).

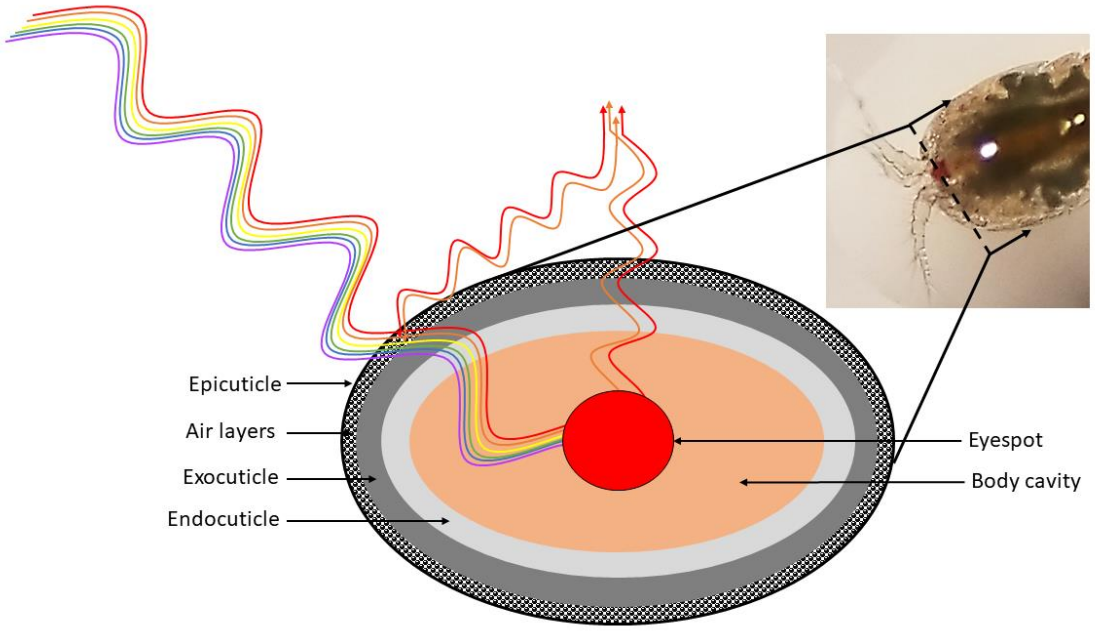

Figure 2.7: Proposed cross section schematic for how light interacts with nanolayers of spheres deposited in the exoskeleton and astaxanthin deposited within the eyespot. Incident light first is coherently scattered by the three or four nanolayers of air spheres, and light is absorbed by the darker sclerotized exocuticle. Finally, any remaining light is absorbed by astaxanthin in the eyespot, and remaining orange-red wavelengths of light are reflected. The darker red color of the eyespot is likely due to the presence of three or four layers of spheres

deposited in the exoskeleton surrounding the eyespot which reflects orange-red light, as opposed to the one or two layers found in the exoskeleton throughout the rest of the body which reflects small amounts of UV light. Astaxanthin is deposited in the eyespot.

A combination of red structural color and pigmentary color is rare in animals, but the idea has been hypothesized previously. For instance, jumping spiders (*Maratus volans*) also combine red-orange ommochromes and red structural color to create a non-iridescent, saturated, bright red color (Hsiung et al. 2017). We hypothesize that copepods combine both astaxanthin and structures in a similar manner to jumping spiders, which is why their eyespots appear non-iridescent under light microscopy. Jumping spiders and other bright red animals like House Finches (*Haemorhous mexicanus*) produce red color for display, but the red eyespot of a copepod is unlikely involved in sexual signaling (Hsiung et al. 2017, Hill et al. 2019, Powers et al. 2020). Instead, the bright red eyespot color, that is present in many other organisms as well, may have a functional role. Given the apparent maintenance of astaxanthin in the eyespot of *T. californicus,* we suspect there is a need to maintain red coloration in the eyespot. Unlike the more complex eyes of some other arthropods, the eyespots of copepods likely do not form cohesive images; rather, copepod eyespots detect changes in light versus dark and polarized light (Martin et al. 2000; Werth 2012; Buskey et al. 1966; Busy and Hartline 2003; Cohen and Forward 2002; Cohen and Forward 2005; Yoshida et al. 2004). Because *T. californicus* resides primarily in shallow rock pools and cannot migrate to avoid UV light, the maintenance of astaxanthin in the eyespots may also play a protective role against UV light, similar to that in more complex eyes (Stahl et al. 2000). Carotenoids responsible for protection and light absorption are located in the retina of some animal eyes and are known for absorbing blue light and protecting photoreceptive cells, as well as quenching reactive oxygen species (Krinsky et al. 2004; Feldman et al. 2010; Abdel-Aal et al. 2013). Alternatively, red coloration may allow

individuals to preferentially absorb blue wavelengths of light more efficiently at night and during crepuscular hours in shallow waters. As such, we speculate that such strict color maintenance could be a result of conserving an endogenous feeding rhythm similar to that observed in *Acartia tonsa* (Stearns 1986).

Cumulatively, our findings document a rare example of red structural color in nature and is one of the few examples of multiple subwavelength nanostructures that combine to produce a single thin film capable of coherently scattering visible wavelengths of light. This novel color production mechanism in arthropods illustrates a mechanism to produce and maintain brilliant red coloration with limited access to dietary pigments like carotenoids. Additionally, examining how nanolayers of air pockets incorporated into the exoskeleton could impact their vision, could be an interesting avenue of research in the future when studying copepods or other arthropods with similar bright red eyespots.

Chapter 3

Painting the Bunting: Carotenoids and structural elements combine to produce the feather coloration of the male Painted Bunting (Passerina ciris)

Manuscript Published in *Ornithology* (Justyn et al. 2023)

Abstract

Male Painted Buntings (*Passerina ciris*) display at least six distinct plumage colors that encapsulate much of the visible light spectrum, yet the specific mechanisms responsible for generating this diversity of color have not been identified. Here, we show that metabolically derived carotenoids and nanostructures capable of producing structural color were ubiquitous across feather patches. We used digital photography, light microscopy, spectrophotometry, carotenoid extraction, and high-performance liquid chromatography to show that the resulting color of each feather patch depended on the concentration of carotenoids, melanins, and underlying feather nanostructures. For example, we found that the blue-violet head feathers contained low concentrations of ketolated carotenoids, which is not typical of blue-violet structurally colored feathers. Additionally, the red breast and orange belly feathers contained a green tuned structural color visible after carotenoid extraction, which is not typical of feathers that contain ketolated carotenoids. Although, none of these abnormal combinations of carotenoids and structural coloration appeared to significantly impact feather color. Conversely, we found the purple rump, dark green greater coverts, and bright yellow-green mantle feather coloration resulted from the combination of high concentrations of carotenoids and the presence of structural color. For the first time, we identify the combination of red ketolated carotenoids and blue structural color as a mechanism to produce purple feather coloration. Identifying the specific mechanisms that give rise to the diversity of colors within this species will facilitate the

study of the –to date– unknown signaling functions of colors produced through the combination of carotenoids and nanostructures in Painted Buntings and other songbirds.

Introduction

Birds display a range of feather colors that completely encapsulate the human visible spectrum and extends into ultra-violet wavelengths (Stoddard and Prum 2011) (Stoddard and Prum 2011). The color gamut displayed by birds results from two discrete, yet complementary mechanisms: absorption and reflection of specific wavelengths of light from pigments, or coherent scattering of light by feather nanostructures (i.e, structural coloration; for a review see McGraw 2006a; 2006b; Prum 2006). Decades of research have provided great detail on these coloration mechanisms in theory yet identifying how those mechanisms interact and give rise to coloration of specific species has been limited to a relatively small subset of birds.

Carotenoids are one of the main types of pigments birds incorporate into their plumage when displaying conspicuous non-iridescent yellow, orange, or red hues (McGraw 2006). Yellow feather coloration in songbirds most often arises from the deposition of yellow xanthophyll carotenoids obtained from the diet (Brush and Johnson 1976; McGraw et al. 2003; Mays et al. 2004). In some species, such as the American Goldfinch (*Carduelis tristis*) and Common Canary (*Serinus canaria*), yellow coloration is derived from canary xanthophyll carotenoids, which are produced by the dehydrogenation of the dietary lutein and zeaxanthin (McGraw and Gregory 2004; Koch et al. 2016). Songbirds that display red to orange coloration often bioconvert yellow carotenoids obtained from their diet to ketocarotenoids through oxidative metabolism (Brush 1990; Lopes et al 2016; Mundy et al 2016; Toomey et al. 2022).

Common red ketocarotenoids in bird plumage include canthaxanthin, adonirubin, and α-doradexanthin (LaFountain et al. 2015).

Non-iridescent structural feather coloration arises from coherent scattering of incident light by specialized cells within feather barbs that form a 'spongy' layer of keratin and air (Prum 2006). The specific wavelengths of light reflected, and thus the color produced, depends on the spacing intervals of the spongy layer (D'Alba et al. 2012.). For example, when the spongy layer possesses the correct periodicity to coherently scatter visible wavelengths of light, non-iridescent short wavelength colors in the blue to violet range are most commonly produced (Dufresne et al. 2009; Saranathan et al. 2012). An important additional component of non-iridescent structural feather coloration is the presence of melanin pigments within the feather barbs (Shawkey and Hill 2006). Melanin pigments are synthesized *de novo* from tyrosine and cysteine amino acids and produce black and brown colors (eumelanins) or earthy yellow to rufous colors (phaeomelanins; McGraw et al. 2005). In structurally colored feathers, layers of melanosomes–melanin containing organelles–are typically deposited beneath the spongy layer at the center of the barbs, which helps to absorb incoherently scattered light and allows the structural color produced by the spongy layer to be seen (Shawkey and Hill 2006).

Carotenoids can also be deposited into structurally colored feather barbs to produce green or purple feather coloration (D'Alba et al. 2012; Prum et al. 2014; Justyn et al. 2022b). However, the resulting color is not always as simple as adding together the two colors produced by each mechanism independently (Shawkey and D'Alba 2017). For example, when yellow pigments are deposited in developing feathers the air spaces within the spongy layer that would otherwise produce a blue color are commonly increased–or tuned–to coherently scatter longer, green wavelengths of light (D'Alba et al. 2012; Prum et al. 2014). Moreover, carotenoids themselves

can alter the resulting color of the feathers by acting as a filter that limits the wavelengths of light that reach the spongy layer below (Justyn et al. 2022b).

Male Painted buntings (*Passerina ciris)* are perhaps the most brilliantly colored breeding bird in North America and display a patchwork of red, orange, purple, yellow-green, green, and blue-violet feathers. Despite the eye-catching combination of colors displayed by these birds, the specific mechanisms responsible for creating their wide array of colors has not yet been fully described. Here, we identify the color production mechanisms of the six distinct feather colors of male Painted Buntings. We describe a unique combination of carotenoids and nanostructures in all color patches examined. These discoveries reveal how birds can produce a variety of colors by adjusting the carotenoids and melanins deposited in the feather and the spongy layer within the barbs.

Materials and Methods

Feather Collection

We sampled feathers from six plumage patches representing six distinct colors (Figure 3.1) from two male Painted Bunting specimens in the Auburn University Museum of Natural History (AUM 1517; 2098): 1) red upper breast 2) orange belly 3) purple rump 4) dark green greater coverts 5) bright yellow-green mantle 6) blue-violet nape. We also sampled blue head feathers from male Indigo Bunting (*Passerina cyanea;* AUM 1509) and red breast feathers from male Northern Cardinal (*Cardinalis cardinalis;* AUM 1468). Blue Indigo Bunting and red Northern Cardinal feathers were selected because they are closely related to Painted Buntings and possess either blue or red feathers, respectively. For all birds, we removed five feathers from

each plumage patch using tweezers and stored them in opaque envelopes until they were analyzed.

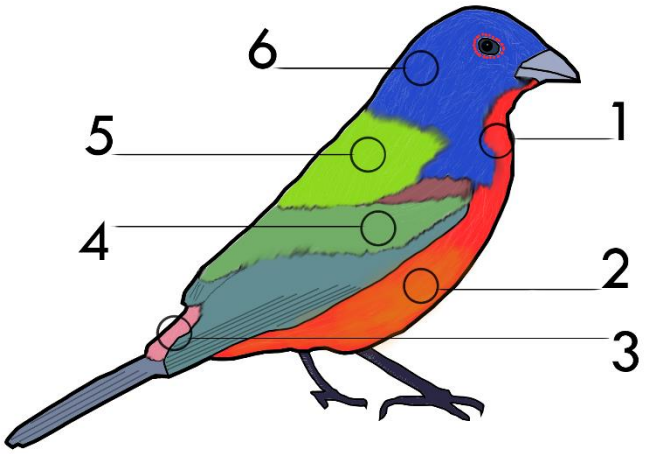

Figure 3.1: Feather collection regions of male Painted Buntings used in this study. 1) red upper breast 2) orange belly 3) purple rump 4) dark green greater coverts 5) bright yellow-green mantle 6) blue-violet nape.

Color Characterization

We took high-resolution macro photographs of each feather with a Nikkor 55-300mm lens set to an aperture of *f*/18, shutter speed 1/200 s, fit with extension tubes mounted on a Nikon D3300 camera body that was secured to a tripod. Photographs were taken in a dark room from a fixed distance and the only light source was a speedlight flash set to full power and fit with a custom diffuser. This photography method and setup results in an image that captures only light reflected from the feathers and produces an essentially completely black background. We took photos of feathers both before and after carotenoid extraction (see below). For photos taken after pigment extraction, we washed feathers in 100% ethanol to remove residual pyridine and dried them under a stream of nitrogen gas. RAW image files were imported to RawTherapee and subjected to identical image processing parameters and saved in .jpeg format. We also used light

microscopy to putatively identify the distribution of melanin within feathers from each plumage patch of Painted Buntings using an AmScope microscope digital camera at 4x magnification under reflected light.

To quantify feather coloration, we measured each of the six Painted Bunting plumage patches using UV-vis reflectance spectroscopy. For each plumage patch, five feathers were overlapped and taped down flat, ventral side up, onto a black cardboard background. We measured feather reflectance before and after carotenoid extraction (see below). Three measurements were then taken from each set of feathers in a dark room at a 90° angle of incidence using an Ocean Optics USB4000 spectrophotometer and an Ocean Optics PX-2 pulsed xenon light calibrated by a white reflectance standard (Labsphere Inc., North Sutton, NH, USA). We measured the left, center, and right of the distal end of the overlapped group of feathers. Taking multiple measurements from each plumage patch helps account for any variation in color within or between feathers. The resulting spectral data were captured using OceanView 1.67 and analyzed and graphed using the *pavo* package in R (Maia et al. 2013; 2019).

Carotenoid Extraction

We extracted carotenoids from feathers following the methods of McGraw et al. (2001). Briefly, we cut the distal colored barbs of each feather, weighed them to the nearest 0.1 mg, and then placed them in microcentrifuge tubes. We sequentially washed feathers in hexane and ethanol, then incubated them in 1 mL of acidified pyridine at 95 °C for 5 h. We transferred the pyridine containing the carotenoids to a new tube, performed a secondary extraction of feathers for 1 h, then pooled both extractions together. The carotenoid extracts were transferred from pyridine to a 2:1 mixture of methyl tert-butyl ether (MTBE): hexane by the addition of distilled

water, and followed by vigorous shaking for 30 sec. We evaporated the MTBE:hexane phase to dryness under vacuum at 30 °C, resuspended the samples in 100 % HPLC-grade acetone, then capped the tubes with nitrogen gas and stored them at -80 °C until further analysis. We also extracted carotenoids from whole feathers following the same procedure and reserved the carotenoid-extracted feather for photography and spectrophotometry.

Carotenoid Identification via HPLC

We separated carotenoids from feather extracts by injecting the solution on a C18 column (10 µm, 250 x 4.6 mm, ES Technologies, New Jersey, USA), connected to a Shimadzu HPLC, and using a mobile phase gradient and conditions following Weaver et al (2018b). We identified carotenoids by comparison of retention times to authentic standards analyzed under the same conditions as the samples, or when unavailable, by comparison of sample carotenoid retention times to known carotenoids extracted from other species (*e.g.* Canary xanthophyll from Common Canary. We calculated the carotenoid concentration as µg carotenoid mg feather mass $^{-1}$.

Results

Color Characterization

Before pigment extraction, we found that the originally red breast and orange belly feathers produced reflectance spectra that are typical of red ketolated carotenoid-based feathers; relatively high levels of reflectance in the 550–700 nm range of the visible spectrum and maximum absorbance in the 475–550 nm range (Figure 3.2A; 3.2B). After carotenoid extraction, the feathers appeared white under light microscopy which indicates that the majority of carotenoids were successfully extracted, and that the feathers did not contain significant amounts

of melanin (Supplemental Figure 3.1A; 3.1B). However, when placed on a black background, the post extraction breast and belly feathers appeared blue-green and produced reflectance spectra with maximum reflectance in the 500–575 nm range (Figure 3.2A;3.2B). Red breast feathers from a male Northern Cardinal, known to be colored solely by ketolated carotenoids (Hill and McGraw 2006), appeared white after carotenoid extraction, even on a black background (Supplemental Figure 3.2).

The orange base of the purple-colored rump feathers also appeared green-blue after carotenoid extraction. However, there was a substantial blue shift near the distal end of the feather where the purple coloration was previously present. The reflectance curve of the distal tip of the purple feathers shows a shift of maximum reflectance of 350 and 600-700 nm before extraction, to a single reflectance peak near 450 nm in the blue region of the visible spectrum after extraction (Figure 3.2C;3.2D). Additionally, a small amount of spotting was visible along the barbs of the feather after carotenoid extraction without the addition of a black background (Supplemental Figure 3.1C. These individual spots likely represent small amounts of melanin present in each individual sponge cell within the barbs (Stavenga et al. 2011).

The observed color of blue-violet head feathers remained the same before and after carotenoid extraction (Figure 3.2E) and the peak of the reflectance curve near 400 nm was unchanged (Figure 3.2F). Light microscopy revealed a dark black coloration in both the barbs and barbules, indicating a substantial amount of what is likely eumelanin (Supplemental Figure 3.1E). Carotenoid-free blue Indigo Bunting feathers also appeared the same color pre- and post-carotenoid extraction (Supplemental Figure 3.3).

Before pigment extraction, we found that the originally green greater coverts and yellow-green mantle feathers produced reflectance spectra with relatively high levels of reflectance in

the 550 nm range and maximum absorbance in the 450 nm range (Figure 3.2E;3.2F). After carotenoid extraction the greater covert and mantle feathers appeared visually more blue-green, although they retained a reflectance spectrum pattern with a maximum reflectance in the 550 nm range (Figure 3.2E;3.2F). Light microscopy of the yellow-green mantle feathers revealed a spotted pattern, similar to that of the purple feathers, indicating small amounts of melanin deposited within each sponge cell within the barb (Supplemental Figure 3.1F). However, unlike any other Painted Bunting plumage patch, the darker green covert feathers appeared very brown under light microscopy, which indicates a substantial presence of pheomelanin (Supplemental Figure 3.1D).

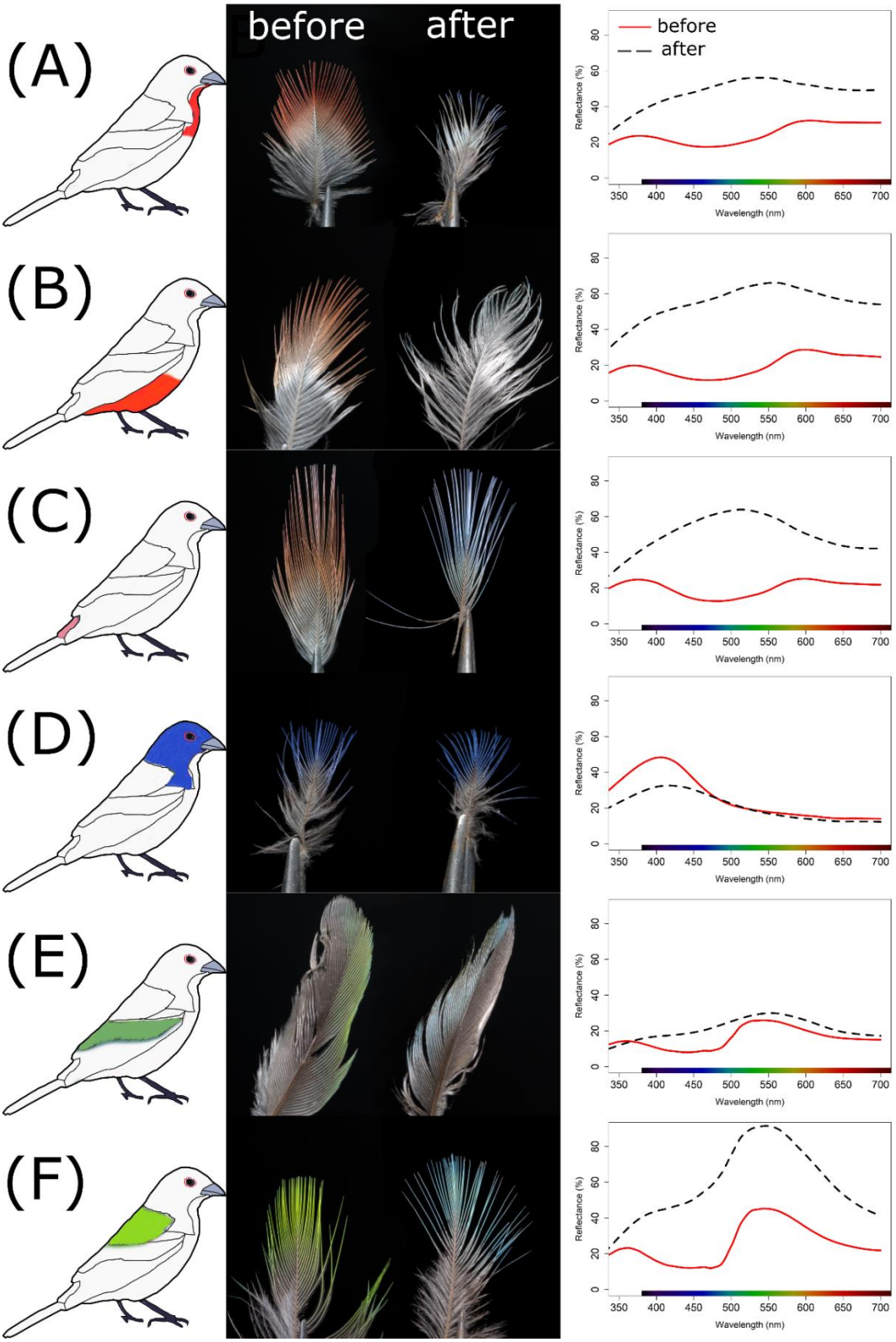

Figure 3.2: Photographic and spectrophotometric characterization of male Painted Bunting feathers from each of the six plumage patches before and after carotenoid extraction.

Carotenoid Identification via HPLC

We found the same four ketolated carotenoids in red, orange, and purple feathers of the male Painted Bunting: astaxanthin, α-doradexanthin, adonirubin, and canthaxanthin– although red feathers had qualitatively higher concentrations than orange or purple feathers (Figure 3.3A). The blue-violet Painted Bunting feathers shared a similar carotenoid profile, however, the signal for astaxanthin was below the threshold and therefore too low to be accurately attributed to the feathers. The other three carotenoids were also present in the blue feathers in lower, yet detectable, amounts compared to the red, orange, and purple feathers (Figure 3.3A). The green wing feathers and yellow-green back feathers contained high amounts of canary xanthophylls, with the yellow back feathers containing about twice as much per sample (Figure 3.3B). Notably, there were no dietary carotenoids, such as lutein or zeaxanthin, detected in any of the feather samples, and canary xanthophylls and ketocarotenoids did not occur in the same plumage patches.

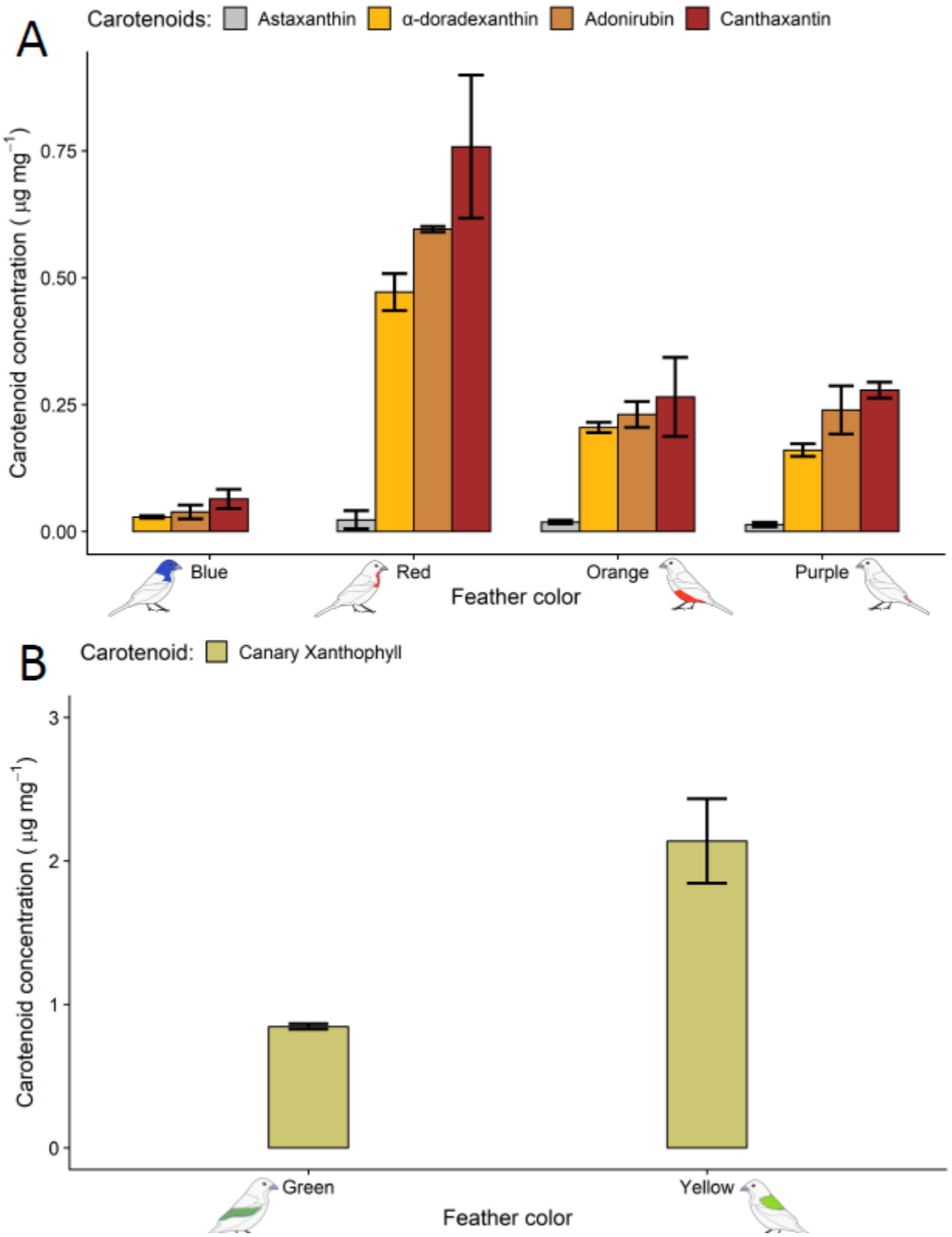

Figure 3.3: Carotenoid profiles of feathers from the six plumage patches of male Painted Bunting. Bars show mean carotenoid content ± s.d. (µg carotenoid mg feather mass $^{-1}$) of A) red, orange, purple, and blue feathers and B) yellow-green and green feathers (n = 2).

Discussion

Here, we show that the six distinct plumage patches of the male Painted Bunting all contain combinations of carotenoid pigments and color-producing nanostructures that co-exist in each of the plumage patches. We found that the concentrations of carotenoids deposited, and the tuning of the spongy layer within the barbs of the feathers, is responsible for the color differences between similarly colored plumage patches. These discoveries outline how pigments and nanostructures can be combined to achieve a wide array of non-iridescent feather colors in a single species.

The Mechanism for Purple Plumage Coloration in Painted Bunting

Purple-pink plumage coloration is rare among birds; eloquently described as an island among continents of more common hues within the color gamut of bird feathers (Stoddard and Prum 2011). To-date, identification of the mechanisms that are capable of producing this color are similarly scarce. When documented, previous studies have shown that purple feathers results from the presence of specific carotenoids (Prum et al. 2014; Mendes-Pinto et al. 2012; Berg et al. 2013; LaFountain et al. 2010). We know of only one previous study that demonstrated that structural color enhances purple coloration of Purple-breasted Cotinga (*Cotinga cotinga*) feathers that already contain purple carotenoids (Justyn et al. 2022b). The combination of red ketocarotenoids and blue structural color has previously been hypothesized to produce the purple color of the Red-bearded Bee-eater (*Nyctiornis amictus*; Stoddard and Prum 2011) and the Pompadour Cotinga (*Xipholena punicea*; Brush 1969), *however* this combination of mechanisms to create purple feather coloration has never been empirically tested. Here, for the first time, we show that the purple feather coloration of male Painted Bunting results from the combination of feather nanostructures that reflect violet wavelengths of light (425 nm) and red ketocarotenoids.

We found evidence for a limited amount of melanin deposited within each sponge cell within the barbs (Supplemental Figure 3.1F). Importantly, our results also indicate that the presence and tuning of structural coloration is independent from the presence of pigments in feathers, since orange and purple feathers contained similar types and concentrations of carotenoids (Figure 3.3A).

Ubiquitous Deposition of Carotenoid in Feathers with Spongy Keratin Layers that Confer Structural Coloration

We found that the red, orange, and purple feathers contained the same four ketolated carotenoids: astaxanthin, adonirubin, α-doradexanthin, and canthaxanthin. Yet, the red feathers had qualitatively higher concentrations than the orange and purple feathers, which had similar concentrations to one another. These ketocarotenoids are typically associated with red coloration in Cardinalidae and absorb wavelengths between 400 – 550 nm (Hill and McGraw 2006; Justyn et al. 2022a). Unexpectedly, we found that all red and orange feathers appeared green-blue after carotenoid extraction when placed on a black background, which indicates that the barbs contain a spongy layer capable of producing structural color (Figure 3.2A, 3.2B). Since red ketocarotenoids absorb light in the green region of the visible spectrum, and the underlying structural color produced in these feathers' peaks around 550 nm, it is not visible in the presence of ketocarotenoids. For comparison, Northern Cardinal feathers were placed on a black background and examined after pigment extraction. We did not find any evidence of structural coloration, indicating that underlying nanostructures capable of producing structural color were not present (Supplemental Figure 3.2). Light microscopy indicated an absence of melanin in the barbs and barbules of the red and orange Painted Bunting feathers, which further explains why

the structural color does not seem to influence feather color and is not visible after pigment extraction unless the feathers are placed on a dark background (see Supplemental Figure 3.1A; 3.1B).

The blue-violet head feathers also contained three of the ketocarotenoids in low concentrations, which is not typical of blue feathers in other species, such as the Indigo Bunting (Supplemental Figure 3.3). However, the observed color of blue-violet head feathers remained the same before and after carotenoid extraction and the peak of the reflectance curve near 400 nm was unchanged (Figure 3.2D). This indicates that the low ketocarotenoid concentration in these feathers does not significantly contribute to the feather color. The noticeably high concentration of melanin in these feathers likely contributes to the persistence of structural color as well. Comparable reflectance curves before and after pigment extraction also demonstrates that the extraction process does not significantly damage or alter the nanostructures or melanin content within the feather, and that the reflectance measurements taken after extraction accurately reflect the structural coloration of the feathers.

The yellow-green and green plumage patches contained varying concentrations of canary xanthophylls with an absorption range from 400 – 500 nm and with an underlying spongy layer that reflects light in the blue-green region of the visible spectrum (MacDougall and Montgomerie 2003). The combination of a green tuned structural color with yellow canary xanthophylls that don't absorb as far into the visible spectrum as ketocarotenoids, enables the combination of the two to produce these unique yellow-green and green colors. The difference between the bright yellow-green back and the dark green wing feathers appears to be primarily due to the yellow-green feathers having approximately twice the concentration of canary xanthophylls (Figure 3.3B). Additionally, the darker green plumage patches had a visibly higher concentration of

melanin (Supplemental Figure 3.1C; 3.1D) because the structural color of both feathers after pigment extraction was nearly identical (Figure 3.2E, 3.2F). This evidence suggests that the concentration of carotenoids and melanins can be independently modified without impacting the structural color of a feather.

In total, we found three different structural colors produced by nanostructures throughout Painted Bunting feathers. The structural color produced by the spongy layer in red and orange feather barbules have a broad reflectance peak shifted into the green wavelengths (~550 nm), compared to the typical narrower peak (~400 nm) produced in the blue-violet head feathers. Interestingly, after pigment extraction, purple rump feathers revealed a third more blue (~450 nm) structural color in the distal half of the feather, and a lighter blue-green color (similar to orange and red feathers) toward the base (Figure 3.2C). This reflectance shift corresponds with the shift in color from purple in the distal part of the feather, to orange toward the base before pigment extraction. This difference between a blue-green, blue, and violet structural color is likely due to a difference in spongy layer spacing along the length of the barb, with the smallest spacing producing the shortest wavelength color near the distal tip of the feather (D'Alba et al. 2012). However, the color could also be influenced by the difference in the concentration of melanin or ratio of eumelanin to pheomelanin within the basal melanin layer of the feather (Shawkey and Hill 2006). For example, the dark green feathers appeared brown after carotenoid extraction, indicating a higher concentration of pheomelanin, and the blue-violet colored feathers appeared dark black, indicating a higher concentration of eumelanin (McGraw and Hill 2006; Supplemental Figure 3.1D; 3.1E).

We demonstrate that male Painted Buntings use a combination of carotenoid pigments and feather nanostructures to produce coloration across the six plumage patches investigated

here. We demonstrate how purple feather coloration can be produced through the combination of red pigments and blue structural color. We also provide evidence that suggests the concentration of carotenoids, melanins, and structural coloration spacing can be modified independently of one another.

One interesting question raised by these findings is that if ketocarotenoids and structural coloration are costly to produce and serve as honest indicators of individual quality (Weaver et al 2017; Weaver et al. 2018a; Hill et al. 2019; White 2020) what evolutionary processes lead to using them in a seemingly wasteful way? In blue-violet Painted Bunting feathers, limited ketocarotenoids are deposited, and in red and orange feathers, nanostructures capable of producing structural color are formed, even though neither of these seemingly contribute to the color or function of the feather in any way. Perhaps this is telling about the genetic underpinnings of these mechanisms and a bird's ability to regulate these processes to specific plumage patches. To test this, future studies could sample other species known to combine pigments and structural colors in different feather patches, like the red feathers of parrots, to determine if red feathers contain structural coloration in their red barbs, or red pigments in their structurally colored feathers, like the male Painted Bunting. Uncovering the mechanisms for coloration of multiple ornaments in other taxa may prove useful for further testing hypotheses about the signaling functions of colorful integuments and the evolutionary history of ornamentation.

Chapter 4

The mechanisms of color production in black skin versus red skin on the heads of New World vultures

Manuscript Published in *Avian Research (Justyn et al. 2023)*

Abstract

A determination of how the color of animal integument is produced is a starting point for investigations into the function and evolution of coloration. The mechanisms that give rise to the color of bare skin of New World vultures are largely unexplored. Here, we investigate the source of color production in the bare skin of Turkey Vultures (*Cathartes aura*) and Black Vultures (*Coragyps atratus*). Using UV-vis reflectance spectroscopy, we found evidence that hemoglobin is the primary pigment responsible for the red coloration of the bare skin on the heads of Turkey Vultures, and that eumelanin is responsible for the black coloration of the bare skin on the heads of Black Vultures. Light microscopy of incisional skin samples further supported these mechanisms of color production by revealing the presence of numerous blood vessels near the surface of the Turkey Vulture skin, and a high concentration of melanosomes in the skin of Black Vultures. Using high performance liquid chromatography (HPLC), we detected carotenoids within the skin of both species with significantly higher total concentrations of carotenoids in the skin of Turkey Vultures compared to the skin of Black Vultures. The carotenoids detected were dietary carotenoids that typically produce yellow coloration when accumulated in integument and were present in low concentrations. We hypothesize that the dietary carotenoids present do not contribute to the color of the skin, but rather help to compensate for the lack of melanosomes found in Turkey Vulture skin. The presence of additional carotenoids may act as an antioxidant to minimize UV damage when the bare Turkey

Vulture head skin is exposed to direct sunlight for prolonged periods of time when soaring and scavenging for food.

Introduction

The mechanisms that produce feather coloration have received substantial research attention, but far fewer studies have examined the mechanisms that give rise to the coloration of bare skin in birds (Hill and McGraw 2006; Davis and Clarke 2022). The color production mechanisms promoting the color of the bare heads of carrion-eating birds is a prime example of the limits of current knowledge regarding skin coloration. In both Old World Vultures (Order Accipitriformes) and New World Vultures (Order Cathartiformes), many species lack feathers on their heads and necks as an adaptation to feeding on carcasses and for thermoregulation (Ward et al. 2008). The bare heads of these birds are most commonly black, red, orange, or yellow (Del Hoyo et al. 1992). A common assumption is that black head coloration results from eumelanin deposited in the skin, but the source of red coloration in the heads of many vultures is unknown (Nicolaï et al. 2020). With multiple potential mechanism for the production of skin coloration such as red or black, visual assessment is not adequate for determining how a particular visual display is achieved—analysis of pigments and nanostructures is required (McGraw et al. 2004). Even mechanisms that produce similar colors can be the result of completely different biological processes and evolutionary forces (Iverson and Karubian 2017; Orteu and Jiggins 2020). For example, while ketolated carotenoids are the most common source of red coloration in bird integument, birds can also achieve red skin coloration by using hemoglobin as the primary chromatophore (Toral et al. 2008). By passing highly oxygenated blood near the surface of the

skin, birds can flush and turn their skin red, sometimes in combination with carotenoids (Negro et al. 2006).

Here, we examined the skin and blood of two New World Vultures, the Turkey Vulture (*Cathartes aura*) and the Black Vulture (*Coragyps atratus*), 1) to determine the mechanisms that produce the red head coloration of mature adults of the former and the black head coloration of the latter, and 2) to hypothesize the functional consequences for these differences. A prior study of the yellow skin on the heads of Egyptian Vultures confirmed that vultures are capable of using carotenoids to color their skin (Negro et al. 2002). However, the mechanisms used by other vultures to create their skin color are unknown. We quantified the color of the skin using UV-vis reflectance spectroscopy, examined the structure of the skin using light microscopy, and quantified the concentration of carotenoids present in the skin and blood of each species.

Materials and Methods

Skin and blood sample collection

All work involving live birds for this study was carried out under federal (USGS #23835) and state (Mississippi permit for SAR) permits, as well as an IACUC protocol (18-551). Black Vultures (n = 7) and Turkey Vultures (n = 7) were captured using baited walk-in traps (Wildlife Dominion Management LLC) set at two locations in Mississippi (33.5256° N, -88.6721° W; 32.3757° N, -88.6133° W). Trap sites are within solid waste management facilities and are separated by 130 km. Traps were baited with deer collected from local roadways after vehicular-related mortalities.

Trapping was carried out on November 22 – 23, 2022. Birds were captured and transferred to a holding container prior to processing. The age of each Turkey Vulture (HY =

Hatching Year [birds < 1 year old), SY = Second Year, ASY = After Second Year) was determined by a combination of head and beak color as described by Henckel (1981). Black Vultures were aged by the amount of feathering on their head, as well as beak color (see Pyle 2008). Approximately 2 mL of blood was sampled from the right basilic vein. Blood was collected from the basilic vein using a 25 G, 1.6 cm needle affixed to a 2 mL syringe (BD Integra) and transferred to a 3 mL non-heparinized phlebotomy tube. A small sample of blood was transferred to blotting paper for use in assigning the sex to each bird genetically, an assessment carried out by Animal Genetics (Tallahassee, Florida).

We applied a small (~ ½ cm strip) of capsaicin cream (0.1% Capsaicin; Capzasin HP) to the skin of the nape of each bird, a location distal to the parietal bone, approximately ~2 cm anterior to the top of the bird's eye. After the cream was allowed to absorb into the skin, a time of approximately 2 minutes, sterile forceps were used to grasp the skin, gently pulling back posterior to the head. Sterile, surgical scissors were then used to excise a small 1 – 2 cm^2 of skin that included the epidermis and dermis. Once excised, this skin sample was transferred to a 20 mL, sterile, glass scintillation vial. Styptic powder (Dogswell; Whitebridge Pet Brands) was then spread into the incision on the bird and the area treated with a thin covering of NewSkin (0.2 % Benzethonium chloride; Advantice Health LLC). The bird was then held for 2 minutes to ensure that the bleeding had been staunched and there was no obvious changes in the bird's behavior. If the bird did not show abnormal behavior and there was no bleeding noted from the wound, each bird was released.

Blood and skin samples were immediately transferred to a cooler and stored on ice until additional processing away from the field site. Upon returning to the lab (Mississippi State

University), containers of blood and skin biopsies were purged using gaseous nitrogen then stored in a -80°C freezer until shipment to Auburn University.

UV-vis reflectance spectroscopy

We used UV-vis reflectance spectroscopy to quantify the color of Turkey (n = 5) and Black Vulture (n = 5) skin samples, prior to carotenoid extraction. Each skin sample was placed on a black cardboard background, ventral side up, and gently pressed flat with tweezers. We obtained three measurements from each skin sample at a 90° angle of incidence in a dark room. We used an Ocean Optics USB4000 spectrophotometer connected to an Ocean Optics PX-2 pulsed xenon light source to obtain all of the measurements reported. Prior to capturing reflectance spectra, we calibrated our measurements using a white reflectance standard (Labsphere Inc., North Sutton, NH, USA). We captured multiple measurements from each skin sample to account for any variation in color within samples. The spectral data obtained were acquired using OceanView 1.67, and then analyzed and visualized using the pavo package in R (Maia et al. 2013; 2019; R Core Team 2020).

Skin Analysis

We took a single representative incisional skin sample from a Turkey (n = 1) and Black Vulture (n = 1) and placed them in 10% neutral buffered formalin for at least 48 hours prior to processing at Mississippi State University College of Veterinary Medicine histology laboratory. Samples were either bisected longitudinally or placed whole into a tissue cassette. Each section was routinely processed, paraffin embedded, sectioned at 5 μm, and stained with hematoxylin and eosin (H&E) for light microscopy.

Carotenoid extraction and HPLC

We performed carotenoid extractions from 100 µL of Turkey (n = 5) and Black Vulture (n = 5) plasma in 500 µL acetone. We first added acetone to the plasma, vortexed for 10s, and then sonicated at 10W for 10s. We used centrifugation to pellet and remove cellular debris, saving the carotenoid extract suspended in acetone. The carotenoid extract from the blood plasma was evaporated to dryness, resuspended in 60 µL acetone, and capped with nitrogen for immediate HPLC analysis. Prior to extracting carotenoids from the Turkey (n = 5) and Black Vulture (n = 6) skin, we cut a small segment of skin and thoroughly washed it with water and ethanol. We then dried and weighed the sample to standardize the extracted carotenoid concentrations (conc) by tissue mass. The final mass of the skin tissue in grams used from each bird can be found in the supplemental data file, but summary statistics are reported here for convenience (all values in grams: avg mass = 0.046; median mass = 0.043; min = 0.031; max = 0.073; st.dev = 0.014). Skin samples were homogenized in 500 µL acetone first by grinding with a pestle and mortar and then by sonication at 10W for 10s. While uncommon in plasma carotenoids, some avian species add fatty acid esters to carotenoids in their soft tissue like skin. To remove potential fatty esters from the skin carotenoids, we performed a saponification (Toomey and McGraw 2007). We dried our carotenoid extract and resuspended in 250 µL ethanol. We then added 100 µL 0.02M KOH dissolved in methanol and vortexed for 10s. We then added 250 µL water, 500 µL methyl-tert-butyl-ether, and 250 µL hexane and vortexed for 30s. Finally, we added 100 µL of saturated saltwater and shook the tubes vigorously for 1 minute to transfer the carotenoids to the organic layer. This process was repeated twice to minimize

carotenoid loss. The organic phase containing carotenoids was transferred to a new tube, dried down, resuspended in 70 µL acetone, and capped with nitrogen for immediate HPLC analysis.

We separated and quantified carotenoids using HPLC following the methods of Weaver et al. (2018) and Wright et al. (1991). We injected 10 µL of carotenoid extract in acetone on to a Sonoma C18 column (10 µm, 250 x 4.6 mm, ES Technologies, New Jersey, USA) fitted with a C18 guard cartridge. Carotenoids were separated using a Shimadzu Prominence HPLC system with mobile phases A 80:20 methanol: 0.5M ammonium acetate, B 90:10 acetonitrile: water, and C ethyl acetate in a tertiary gradient of 100%A to 100%B over 4 min, then to 80% C: 20% B over 14 min, back to 100% B over 3 min, and returning to 100% A over 5 min and held for 6 min [9, 52]. We visualized and detected carotenoid absorbance using a Prominence UV/Vis detector set to a wavelength of 450 nm. We identified and quantified carotenoids by comparison to authentic standards that included: astaxanthin, zeaxanthin, β-carotene, lutein, 3-hydroxyechinenone, and canthaxanthin. We normalized carotenoid concentration by the dry weight or plasma volume of each skin and blood sample, respectively (reported as µg carotenoid per g tissue). For carotenoids in the tissue samples for which we had no pure standard for quantification (echinenone, α-cryptoxanthin, β-cryptoxanthin), we used the quantification curve for 3-hydroxyechinenone to calculate their mass standardized concentrations, as is required practice when lacking a matching pure standard (Blanco et al. 2013, Richins et al. 2014).

Statistical Analysis

All statistical analyses were performed in R (R Core Team 2020) using the following packages: ‘lme4’ (Bates et al. 2014), ‘Hmisc’ (Harrell Jr and Dupont 2021), ‘lmerTest’ (Kuznetsova et al. 2017), ‘agricolae’ (De Mendiburu 2014), ‘MASS’ (Venables and Ripley

2013), ‘emmeans’ (Lenth et al. 2018), ‘car’ (Fox and Weisberg 2018), ‘sf’ (Pebesma 2018), ‘rstatix’ (Kassambara, 2021), and ‘MuMIn’ (Barton 2009). Data wrangling was performed in R with the help of the follow packages: ‘tidyverse’ (Wickham 2017), ‘dplyr’ (Wickham et al. 2015), ‘reshape2’ (Wickham 2007), ‘plotrix’ (Lemon 2006), and ‘HH’ (Heiberger et al. 2015). Figures were produced using the following packages: ‘ggpubr’ (Kassambara 2018), ‘cowplot’ (Wilke 2016), ‘RColorBrewer’ (Neuwirth 2014), and ‘ggjoy’ (Wilke 2017). For a full review of our statistical analyses, please refer to the annotated R-code included in the supplemental material; we provide below a brief description of each analysis and the type of modeling used.

We normalized all carotenoid concentration data by the mass of tissue from which we extracted the pigment. We transformed carotenoid concentrations to fit model assumptions of normality using a $\log_{10}$ transformation. To examine the overall effects on carotenoid concentrations among individuals in our dataset, we first performed a two-way ANOVA on the following categorical variables and their pairwise interactions: sex (male vs female), age [ASY] after second year vs [SY] second year or younger), species (Black vs Turkey Vulture), and tissue type (skin vs blood). Only one individual bird was a SY bird (ID#: R59). So, we combined data from that bird with the hatch year individuals to make the two broad age groupings ASY and SY. All other birds besides R59 in the SY group were hatch year individuals. We also tested for pairwise interactions between each of these four variables. We performed this analysis for total carotenoid concentrations, zeaxanthin concentration, β-carotene concentration, lutein concentration, and the concentration of the “minor” carotenoids detected in low abundance (echinenone, α-cryptoxanthin, and β-cryptoxanthin). Due to a repeatedly observed interaction between tissue and species (see results below), we blocked data by tissue and species together for linear modeling.

To examine the differences in carotenoid concentrations between Black Vultures and Turkey Vultures, we fit linear mixed effects model with individual age group as a random effect to account for potential non-independence of data obtained from birds of the same age group. As noted above, tissue type and species were blocked as a single variable in the analysis because of a significant interaction between the two separate variables. Pairwise differences between each tissue and species were estimated from this model using the 'emmeans' package, after applying a Tukey's correction for Type 1 error due to repeated pairwise comparisons.

To examine differences in carotenoid concentrations between after second year (ASY) and hatch/second year birds (SY), we fit a linear mixed model with tissue type as a random effect to control for non-independence of carotenoid concentration data from skin and blood within each age group. The age and species group variables were blocked together, to account for any potential interactions between the two variables (we detected this effect with minor carotenoid concentrations). However, pairwise differences between each age group and species were estimated from this model also using 'emmeans'.

We analyzed differences due to sex using a linear mixed model in a similar manner as described above. Even though we detected no interaction between species and sex, to control for the overwhelming effect of species on the data, we blocked the variables by species and sex. We included a random effect of tissue type, as we did with the linear model fit to examine differences between the age groups. Pairwise differences between each sex and species were estimated from this linear model using 'emmeans'. All statistical tests were deemed to be significant at $a = 0.05$.

Results

UV-vis reflectance spectroscopy

We found that the reflectance spectra obtained from the Turkey Vulture skin samples (Figure 4.1) did not match any of the spectra for other pigments commonly deposited within red colored integument (Toral et al. 2008). The high amount of reflectance in the middle of the spectrum from 450 – 550 nm is not characteristic of carotenoids, which typically absorb these wavelengths of light, even if combined with structures (Justyn et al. 2022a; 2022b). Instead, the reflectance spectra closely resembles that of hemoglobin (Bender et al. 2009; Kim et al. 2014; Negro et al. 2006). The reflectance spectra of the Black Vulture skin (Figure 4.1) closely resembles that of eumelanin (Toral et al. 2008). While all skin samples visibly maintained coloration when sampled, it is possible that the skin samples may have faded since the time of collection. This could have resulted in less bright reflectance spectra when compared to reflectance spectra obtained directly from living vulture skin.

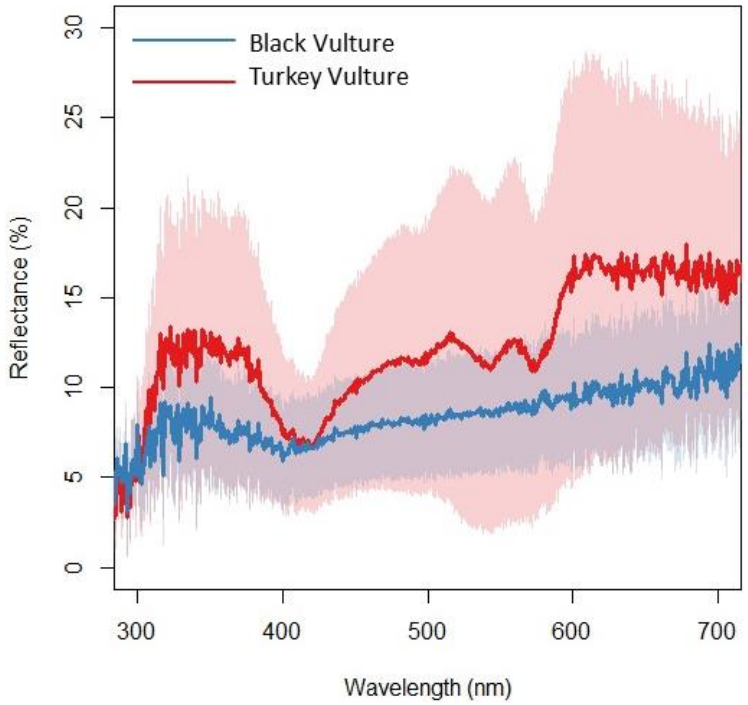

Figure 4.1: UV-vis reflectance spectra of A) Turkey and B) Black Vulture skin samples.

Skin Analysis

We found very few melanosomes scattered across the skin sample of the Turkey Vulture (Figure 4.2A), and a much denser presence of melanosomes in the Black Vulture skin sample (Figure 4.2B). There was also an absence of lipid filled vacuoles present in either sample, suggesting that carotenoids are not deposited in significant concentrations in the skin of either species. When observing the histological structures present in the skin samples, there are numerous blood vessels near the surface of the Turkey Vulture skin. The layer of collagen in the Turkey Vultures appears thicker than the layer in the Black Vultures, although both are likely too thin to produce structural color (Prum and Torres 2003).

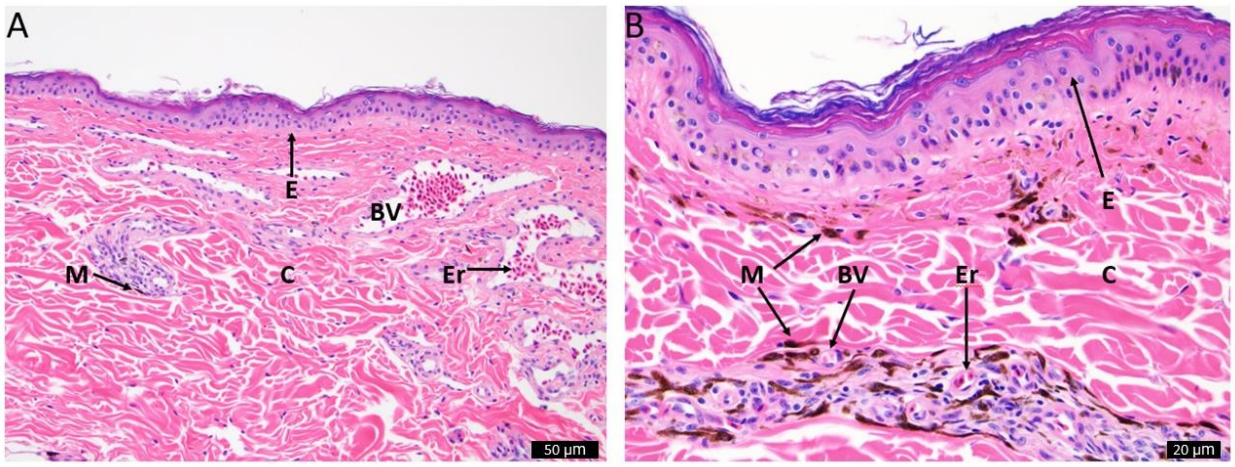

Figure 4.2: Images of skin section from A) Turkey and B) Black Vulture showing the absence of melanosomes in the Turkey Vulture skin and the presence in Black Vulture skin. E – epidermis, Er – erythrocyte, C – collagen, BV – blood vessel, M – melanocyte. Scale bar = 50µm and 20µm, respectively.

Carotenoid extraction and HPLC.

We detected six primary carotenoids in the skin and blood of Turkey and Black Vultures (Supplemental Figure 4.1). These included lutein, zeaxanthin, α-cryptoxanthin, β-cryptoxanthin, echinenone, and β-carotene (Supplemental Figure 4.1). These carotenoids were detectable in all

samples from both species (Supplemental Figure 4.2). We observed that the three most abundant carotenoids across all samples were lutein, zeaxanthin, and β-carotene (Figure 4.3). The other three carotenoids detected, α-cryptoxanthin, β-cryptoxanthin, echinenone were present in much lower concentrations - we refer to these three as "minor carotenoids" in these species here forward. Across the two species, the skin and blood, the two sexes, and the two age groups analyzed, we observed similar proportions of these carotenoids (Figure 4.3).

We observed a statistically significant effect of species on the carotenoid concentrations measured across all samples (Species – dfn = 1, dfd = 7, f = 7.11, p = 0.0322). We also observed a marginal interaction between species and tissue type (Species:Tissue – dfn = 1, dfd = 7, f = 4.01, p = 0.0854). There was a significant effect of species and marginal effect of age on zeaxanthin concentration (Species – dfn = 1, dfd = 6, f = 14.45, p = 0.0090; Age – dfn = 1, dfd = 6, f = 4.53, p = 0.0774). For the concentration of β-carotene across our sample data, we detected a marginal interaction between tissue type and species (Species:Tissue – dfn = 1, dfd = 7, f = 3.95, p = 0.0873). We detected no clear effect of any of our variables on lutein concentrations across the sample data. However, we did detect a significant effect of tissue type and species on the concentrations of the minor carotenoids echinenone, α-cryptoxanthin, and β-cryptoxanthin (Species – dfn = 1, dfd = 7, f = 12.16, p = 0.0102; Tissue Type – dfn = 1, dfd = 7, f = 7.24, p = 0.0311). For the minor carotenoids, we observed a significant interaction between species and tissue type (Species:Tissue – dfn = 1, dfd = 7, f = 11.17, p = 0.0124) .

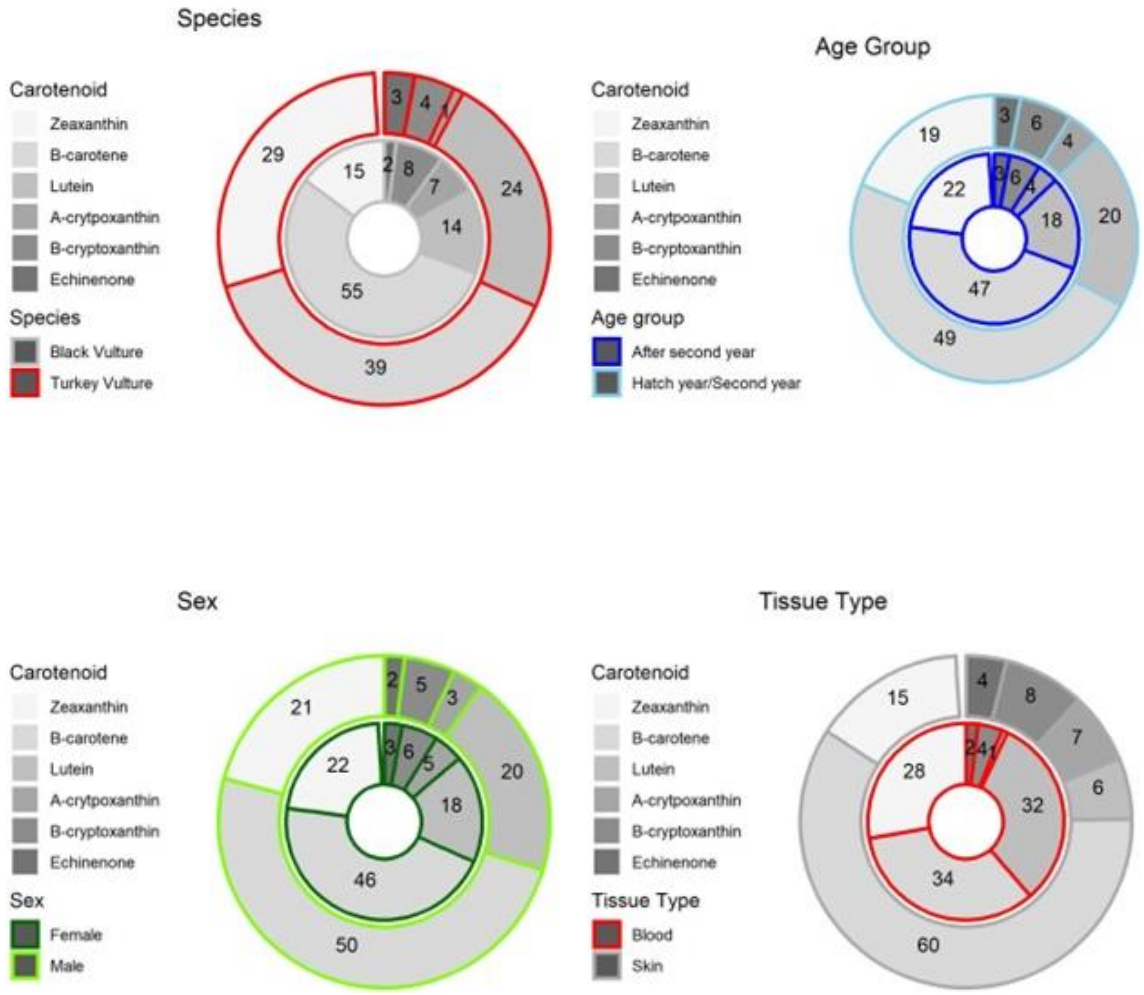

Figure 4.3: Relative proportions of each carotenoid in each vulture species, age group, sex, and tissue type. Proportions are displayed as a percent of the total signal measured by the UV-vis detector during HPLC. Where a section does not add up to 100%, the missing fraction represents any noise detected during the HPLC run that was not part of the carotenoid peaks.

When tissue concentrations were evaluated between species, we found that Turkey Vultures (Mean conc in μg g^{-1} ± SE; 0.62 ± 0.12) accumulated significantly more carotenoids than Black Vultures (Mean conc in μg g^{-1} ± SE; 0.19 ± 0.11; β = 1.40; t = 3.01 p = 0.0079). We found that Turkey Vulture skin (Mean conc in μg g^{-1} ± SE; 0.89 ± 0.15) had, on average, significantly greater concentrations of carotenoids than Black Vulture skin (Mean conc in μg g^{-1} ± SE; 0.10 ± 0.14; β = 2.30; t = -4.06; p = 0.0045) (Figure 4.4). This appeared to be driven by

zeaxanthin, β-carotene, and minor carotenoid concentrations (Figure 4.4). While not significantly different, Black Vulture blood was observed to hold higher concentrations of carotenoids (Mean conc in μg g^{-1}±SE; 0.33 ± 0.16) than Black Vulture skin (Mean conc in μg g^{-1} ± SE; 0.10 ± 0.14; β = 1.10; t = 1.90; p = 0.2649), on average (Figure 4.4).

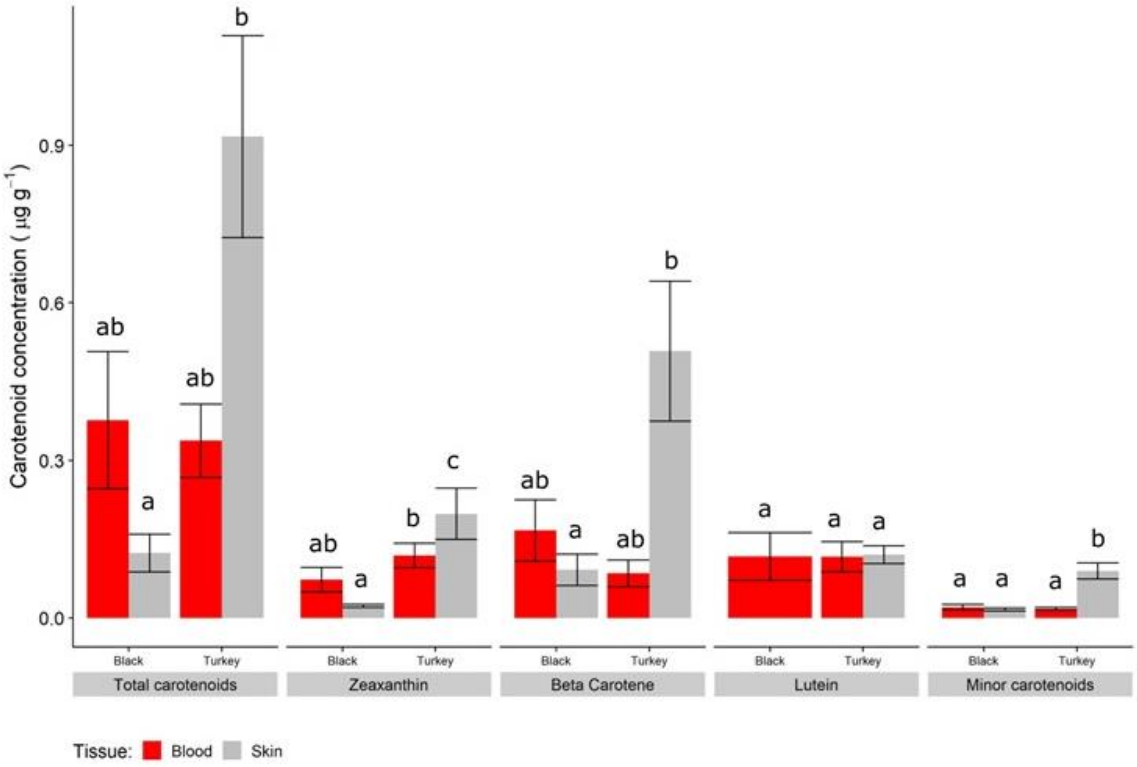

Figure 4.4: Carotenoid concentrations per vulture species, standardized by tissue mass.

We found that, on average, ASY individuals (Mean conc in μg g^{-1} ± SE; 0.54 ± 0.10) sequestered higher concentrations of carotenoids in their tissues compared to SY (Mean concentration in μg g^{-1} ± SE; 0.27 ± 0.13). Although, this difference was not statistically significant (β = 0.58; t = -1.17; p = 0.2603). However, when making pairwise comparisons between the two species and age groups, we found only marginal statistical differences in a single comparison. We found that ASY Turkey Vultures (Mean conc in μg g^{-1} ± SE; 0.74 ± 0.14) had, on average, higher concentrations of carotenoids than ASY Black Vultures (Mean conc in

μg g^{-1} ± SE; 0.28 ± 0.12; β = 1.47; t= -2.57; p = 0.0862 (Supplemental Figure 4.3). This was broadly visible across the separate carotenoid concentrations as well (Supplemental Figure 4.3). However, we only observed a statistically significant difference between the zeaxanthin concentrations of ASY Turkey Vultures (Mean conc in μg g^{-1} ± SE; 0.21 ± 0.02) and younger Black Vultures (Mean conc in μg g^{-1} ± SE; 0.02 ± 0.04; β = 2.26; t = 4.01; p = 0.0055) or ASY Black Vultures (Mean conc in μg g^{-1} ± SE; 0.06 ± 0.03; β = 1.53; t = -4.02; p = 0.0061) (Supplemental Figure 4.3). For minor carotenoids, ASY Turkey Vultures (Mean conc in μg g^{-1} ± SE; 0.06 ± 0.02) did have marginally greater concentrations than ASY Black Vultures (Mean conc in μg g^{-1} ± SE; 0.02 ± 0.02; β = 0.96; t = -2.52; p = 0.0946) (Supplemental Figure 4.3).

We found that the two sexes had similar concentrations of carotenoids in their tissues, with no significant differences detected between male (Mean conc in μg g^{-1} ± SE; 0.45 ± 0.13) and female birds (Mean conc in μg g^{-1} ± SE; 0.36 ± 0.10; β = 0.33; t =-0.67; p = 0.5107) (Supplemental Figure 4.4). This same pattern was observed when looking at the specific carotenoid concentrations as well (Supplemental Figure 4.4).

Discussion

The mechanisms that produce the various colors of bare skin that are displayed by different species of birds are poorly understood. Here, we analyzed blood as well as skin collected from the bare heads of two differently colored New World vulture species, the Turkey Vulture and Black Vulture, to characterize the mechanisms of color production and physiological differences between the two species. Using UV-vis reflectance spectroscopy and light microscopy, we found evidence that hemoglobin is the primary pigment responsible for the red

coloration of the Turkey Vulture head skin, while eumelanin is responsible for the black coloration of the Black Vulture head skin.

To characterize the color production mechanisms present in the skin of both vulture species, we first performed UV-vis spectroscopy to examine the spectral reflectance patterns. UV-vis spectroscopy initially indicated that hemoglobin is primarily responsible for the red coloration of the Turkey Vulture skin and that eumelanin is responsible for the black coloration of the Black Vulture skin (Figure 4.1). High reflectance between 450-550 nm indicated that red ketolated carotenoids, like astaxanthin, were not present in sufficient quantities to impact the skin color because ketolated carotenoids absorb light heavily within this range (Ilagan et al. 2005; Elde et al. 2012). We also observed that the skin from both species had a moderate levels of UV refection, with the Turkey Vulture skin being the most UV reflective. The moderate UV peak present is not typical for integument that contains melanin, which highly absorbs UV light. This could perhaps indicate that the structural organization of the collagen is slightly reflecting UV light in both species (Jourdie et al. 2004; Prum and Torres 2003).

In an effort to search for possible structural differences between the two species, we performed light microscope histology. We observed a high number of melanosomes within the Black Vulture compared to the skin of the Turkey Vulture, further indicating that the black skin color is due to the presence of eumelanin (Figure 4.2). We did not observe any lipid vacuoles containing carotenoids deposited in either of the skin samples, but we did observe numerous blood vessels near the surface of the Turkey Vulture's skin. The presence of an abundance of blood vessels further suggests that hemoglobin is the primary source of coloration for the red skin, and that Turkey Vultures also likely possess the ability for facial flushing (Negro et al 2006).

In comparison to the Black Vulture skin sample, the Turkey Vulture skin also has a thicker layer of collagen, which could result in the increased UV reflection observed. Alternatively, this layer of collagen might play no role in the head coloration of Turkey Vultures and the increased UV reflectance could be due simply to the increased concentrations of hemoglobin near the surface of the skin (Kim et al. 2014; Bender et al. 2009; Prum and Torres 2003). Additionally, vultures are thought to be sensitive to and capable of perceiving UV light (Ödeen & Håstad 2013). The significant amount of UV reflectance seen in the Turkey Vulture skin would be visible by other vultures, and could play a role in signaling, regardless of the method of production.

We conclude that the red coloration of the bare heads of Turkey Vultures is a product of hemoglobin, but we did observe detectable levels of dietary carotenoids in the skin and blood from both species (Figure 4.3). The detected carotenoid profiles we observed (lutein, zeaxanthin, α-cryptoxanthin, β-cryptoxanthin, echinenone, and β-carotene) matched those previously reported for the dark heads of Black Vultures and Andean Condors (*Vultur gryphus*) (Blanco et al. 2013). Blanco et al. (2013) observed these same carotenoids in similar proportions in the plasma of Black Vultures, but found much higher levels of lutein relative to β-carotene in the Andean Condor, citing dietary differences due to increased vegetal consumption in the condors as the probable explanation for the disparity between those two species. We found significantly higher concentrations of lutein and β-carotene in the skin of Turkey Vulture compared to the skin of the Black Vulture (Figure 4.4). Moreover, we observed that the skin of Turkey Vultures contained significantly more total carotenoids than the skin of Black Vultures. The difference in carotenoid concentrations between skin samples could be the result of more blood being trapped in the Turkey Vulture skin because of the abundance of blood vessels in this tissue, irrespective

of the similar concentration of carotenoids in the blood (standardized by plasma volume) in both species (Figure 4.4). We are confident, however, that the concentrations of yellow dietary carotenoids in the skin of Turkey Vultures were too low to significantly contribute to head coloration. Indeed, the concentrations detected were much lower than typically seen in the integument of other species confirmed to utilize carotenoids as the primary source of visible coloration (McGraw & Toomey 2010; Negro et al. 2002).

If carotenoids are not contributing to coloration, why does the red-headed vulture species have higher concentrations of skin carotenoids compared with the black-headed species? Higher concentration of carotenoids in the heads of Turkey Vultures compared to the Black Vultures may help to compensate for the lack of melanin in their skin and serve as an antioxidant to minimize UV damage that Turkey Vultures receive while soaring in direct sunlight for long periods of time (Darvin et al. 2011; Lademann et al. 2011; Zerres & Stahl 2020). Increased levels of carotenoids may not be necessary in the skin of Black Vultures, since the high levels of melanin present already protect skin from UV radiation (Nicolaï et al. 2020). Although, a meta-analysis of songbird studies and an experimental study of canaries presented evidence that carotenoids do not serve as important antioxidants in birds (Koch et al. 2018; Weaver et al. 2018b), these studies focused on fully feathered bird species that were protected from UV radiation by their feathers. Vultures are exposed to full sunlight for hours per day and the production of free radicals may be substantially higher in the exposed skin of vultures compared with the feathered bodies of songbirds. An increased concentration of carotenoids in the Turkey Vulture skin, combined with the UV reflection observed, may help the Turkey Vulture reduce the negative effects of high levels of UV radiation.

References

Abdel-Aal, E. S. M., Akhtar, H., Zaheer, K., Ali, R. (2013). Dietary sources of lutein and zeaxanthin carotenoids and their role in eye health. *Nutrients* 5, 1169-1185.

Aidala, Z., Huynen, L., Brennan, P. L., Musser, J., Fidler, A., Chong, N., ... & Hauber, M. E. (2012). Ultraviolet visual sensitivity in three avian lineages: paleognaths, parrots, and passerines. *Journal of Comparative Physiology A*, *198*(7), 495-510.

Alboukadel Kassambara (2019). ggpubr: 'ggplot2' Based Publication Ready Plots. R package version 0.2.1. https://CRAN.R-project.org/package=ggpubr

Alboukadel Kassambara (2021). rstatix: Pipe-Friendly Framework for Basic Statistical Tests. R package version 0.7.0. https://CRAN.R-project.org/package=rstatix

Andrade, P., Pinho, C., i de Lanuza, G. P., Afonso, S., Brejcha, J., Rubin, C. J., ... & Pellitteri-Rosa, D. (2019). Regulatory changes in pterin and carotenoid genes underlie balanced color polymorphisms in the wall lizard. *Proceedings of the National Academy of Sciences*, *116*(12), 5633-5642.

Arcangeli, C. & Cannistraro, S. (2000). In situ Raman microspectroscopic identification and localization of carotenoids: Approach to monitoring of UV-B irradiation stress on antarctic fungus. *Biopolymers: Original Research on Biomolecules* 57, 179-186.

Balasubramaniam, A. (2021). A Bioinformatic Analysis of the Biosynthesis of Carotenoids in the Copepod Tigriopus californicus. (Master's Thesis, Wilfrid Laurier University)

Barton, K. (2009). MuMIn: multi-model inference. http://r-forge.r-project. org/projects/mumin/.

Bates, D., Mächler, M., Bolker, B. & Walker, S. (2014). Fitting linear mixed-effects models using lme4. arXiv preprint arXiv:1406.5823.

Bender, J. E., Shang, A. B., Moretti, E. W., Yu, B., Richards, L. M., & Ramanujam, N. (2009). Noninvasive monitoring of tissue hemoglobin using UV-VIS diffuse reflectance spectroscopy: a pilot study. *Optics Express*, *17*(26), 23396-23409.

Berg, C. J., A. M. LaFountain, R. O. Prum, H. A. Frank, and M. J. Tauber (2013). Vibrational and electronic spectroscopy of the retro-carotenoid rhodoxanthin in avian plumage, solid-state films, and solution. *Archives of biochemistry and biophysics 539*:142–155.

Blanco, G., Hornero-Méndez, D., Lambertucci, S. A., Bautista, L. M., Wiemeyer, G., Sanchez-Zapata, J. A., Garrido-Fernandez, J., Hiraldo, F. & Donázar, J. A. (2013). Need and seek for dietary micronutrients: Endogenous regulation, external signalling and food sources of carotenoids in New World vultures. *PLoS One*, *8*: e65562.

Bleiweiss, R. (2005). Variation in ultraviolet reflectance by carotenoid-bearing feathers of tanagers (Thraupini: Emberizinae: Passeriformes). *Biol. J. Linn. Soc.*, *84*(2), 243-257.

Brumfield, R. T., & Braun, M. J. (2001). Phylogenetic relationships in bearded manakins (Pipridae: Manacus) indicate that male plumage color is a misleading taxonomic marker. *The Condor*, *103*(2), 248-258.

Brumfield, R. T., Jernigan, R. W., McDonald, D. B., & Braun, M. J. (2001). Evolutionary implications of divergent clines in an avian (Manacus: Aves) hybrid zone. *Evolution*, *55*(10), 2070-2087.

Brush, A. H. (1963). Astaxanthin in the Cedar Waxwing. *Science* 142, 47-48.

Brush A. H. (1969). On the nature of "cotingin". *The Condor* 71:431–433.

Brush, A. H. (1970). Pigments in hybrid, variant and melanic tanagers (birds). *Comparative Biochemistry and Physiology*, *36*(4), 785-793.

Brush, A. H. (1990). Metabolism of carotenoid pigments in birds. *The FASEB Journal*, *4*(12), 2969-2977.

Brush, A. H., & Johnson, N. K. (1976). The evolution of color differences between Nashville and Virginia's warblers. *The Condor*, *78*(3), 412-414.

Buskey, E. J., Hartline, D. K. (2003). High-speed video analysis of the escape responses of the copepod Acartia tonsa to shadows. *Biol. Bull*. 204, 28-37.

Buskey, E. J., Mann, C. G., Swift, E. (1986). The shadow response of the estuarine copepod Acartia tonsa (Dana). *J. Exp. Mar. Biol. Ecol*. 103, 65-75.

Claus O. Wilke (2019). cowplot: Streamlined Plot Theme and Plot Annotations for 'ggplot2'. R package version 1.0.0. https://CRAN.R-project.org/package=cowplot

Cobbs, C., Heath, J., Stireman III, J. O., Abbot, P. (2013). Carotenoids in unexpected places: gall midges, lateral gene transfer, and carotenoid biosynthesis in animals. *Mol. Phylogenet. Evol.* 68, 221-228.

Cohen, J. H., Forward, R. B. (2002). Spectral sensitivity of vertically migrating marine copepods. *Biol. Bull.* 203, 307-314.

Cohen, J. H., Forward, R. B. (2005). Diel vertical migration of the marine copepod Calanopia americana. II. Proximate role of exogenous light cues and endogenous rhythms. *Mar. Biol.* 147, 399-410.

Costantini, D., & Møller, A. P. (2008). Carotenoids are minor antioxidants for birds. *Functional Ecology*, *22*(2), 367-370.

Cuthill, I. C., Allen, W. L., Arbuckle, K., Caspers, B., Chaplin, G., Hauber, M. E., ... & Caro, T. (2017). The biology of color. *Science*, *357*(6350), eaan0221.

D'Alba, L., Kieffer, L., & Shawkey, M. D. (2012). Relative contributions of pigments and biophotonic nanostructures to natural color production: a case study in budgerigar (Melopsittacus undulatus) feathers. *Journal of Experimental Biology, 215*(8), 1272-1277.

Darvin, M. E., Sterry, W., Lademann, J., & Vergou, T. (2011). The role of carotenoids in human skin. Molecules, 16(12), 10491-10506.

Davis, S. N., & Clarke, J. A. (2022). Estimating the distribution of carotenoid coloration in skin and integumentary structures of birds and extinct dinosaurs. Evolution, 76(1), 42-57.

De Mendiburu, F. (2014). Agricolae: statistical procedures for agricultural research. R package version, 1.

Del Hoyo, J., Del Hoyo, J., Elliott, A., & Sargatal, J. (1992). Handbook of the birds of the world (Vol. 2). Barcelona: Lynx edicions.

Dufresne, E. R., H. Noh, V. Saranathan, S. G. Mochrie, H. Cao, and R. O. Prum (2009). Self-assembly of amorphous biophotonic nanostructures by phase separation. *Soft Matter 5*:1792–1795.

Dyck, J. (1992). Reflectance spectra of plumage areas colored by green feather pigments. *The Auk*, *109*(2), 293-301.

Elde, A. C., Pettersen, R., Bruheim, P., Järnegren, J., & Johnsen, G. (2012). Pigmentation and spectral absorbance signatures in deep-water corals from the Trondheimsfjord, Norway. *Marine Drugs*, *10*(6), 1400-1411.

Elster, A. (1896). Über einen Fundort von Diaptomus superbus, nebst einigen Bemerkungen über Farben der Copepoden. *Zool. Anz.* 31.

Eliason, C. M., Maia, R., Parra, J. L., Shawkey, M. D. (2020). Signal evolution and morphological complexity in hummingbirds (Aves: Trochilidae). *Evolution* 74, 447-458.

Eliason, C. M., & Shawkey, M. D. (2010). Rapid, reversible response of iridescent feather color to ambient humidity. *Opt. Express* 18, 21284-21292.

Elster, A. (1896). Über einen Fundort von Diaptomus superbus, nebst einigen Bemerkungen über Farben der Copepoden. *Zool. Anz.* 31.

Fabricant, S. A., Kemp, D. J., Krajíček, J., Bosakova, Z., Herberstein, M. E. (2013). Mechanisms of color production in a highly variable shield-back stinkbug, Tectocoris diopthalmus (Heteroptera: Scutelleridae), and why it matters. *PLoS One* 8.

Feldman, T., Yakovleva, M., Lindström, M., Donner, K., Ostrovsky, M. (2010). Eye adaptation to different light environments in two populations of Mysis relicta: a comparative study of carotenoids and retinoids. *J. Crust. Biol.* 30, 636-642.

Focher, B., Naggi, A., Torri, G., Cosani, A., Terbojevich, M. (1992). Structural differences between chitin polymorphs and their precipitates from solutions—evidence from CP-MAS 13C-NMR, FT-IR and FT-Raman spectroscopy. *Carbohydr. Polym.* 17, 97-102.

Fox, D. L. (1976). Animal biochromes and structural colours: physical, chemical, distributional & physiological features of coloured bodies in the animal world.

Fox, J. & Weisberg, S. (2018). *An R companion to applied regression*, Sage publications.

Fox, H. M., & Vevers, G. (1960). Nature of animal colours.

Gazda, M. A., Araújo, P. M., Lopes, R. J., Toomey, M. B., Andrade, P., Afonso, S., ... & Hill, G. E. (2020). A genetic mechanism for sexual dichromatism in birds. *Science*, *368*(6496), 1270-1274.Gill, F. B. (2007). *Ornithology*. Macmillan.

Goldstein, D. H. (2005). Reflection properties of Scarabaeidae. *Polarization Science and Remote Sensing II*, *5888*, 58880T.

Goodwin, T. W., Srisukh, S. (1949). Some observations on astaxanthin distribution in marine Crustacea. *Biochem. J.* 45, 268.

Gray, D. A. (1996). Carotenoids and sexual dichromatism in North American passerine birds. *The American Naturalist*, *148*(3), 453-480.

Gur, D., Leshem, B., Pierantoni, M., Farstey, V., Oron, D., Weiner, S., Addadi, L. (2015). Structural basis for the brilliant colors of the sapphirinid copepods. *J. Am. Chem. Soc.* 137, 8408-8411.

Gur, D., Leshem, B., Farstey, V., Oron, D., Addadi, L., Weiner, S. (2016). Light-Induced Color Change in the Sapphirinid Copepods: Tunable Photonic Crystals. *Adv. Funct. Mater.* 26, 1393-1399.

Harrell Jr, F. E. & Dupont, C. (2021). Hmisc: Harrell Miscelleneous.

Heath, J. J., Cipollini, D. F., Stireman III, J. O. (2013). The role of carotenoids and their derivatives in mediating interactions between insects and their environment. *Arthropod-Plant Inte.* 7, 1-20.

Henckel, R. E. 1981. Ageing the Turkey Vulture HY to ASY. North American Bird Bander 6(3), 106-107.

Heiberger, R. M., Heiberger, R. M. & Burt Holland, B. H. (2015). Statistical Analysis and Data Display An Intermediate Course with Examples in R, Springer.

Heine, K. B., & Hood, W. R. (2020). Mitochondrial behaviour, morphology, and animal performance. *Biological Reviews*, *95*(3), 730-737.

Heine, K. B., Justyn, N. M., Hill, G. E., Hood, W. R. (2021). Ultraviolet irradiation alters the density of inner mitochondrial membrane and proportion of inter-mitochondrial junctions in copepod myocytes. *Mitochondrion* 56, 82-90.

Heine, K. B., Powers, M. J., Kallenberg, C., Tucker, V. L., Hood, W. R. (2019). Ultraviolet irradiation increases size of the first clutch but decreases longevity in a marine copepod. *Ecol. Evol.* 9, 9759-9767.

Hill, G. E. (1994). Trait elaboration via adaptive mate choice: sexual conflict in the evolution of signals of male quality. *Ethology Ecology & Evolution*, *6*(3), 351-370.

Hill, G. E., Hood, W. R., Ge, Z., Grinter, R., Greening, C., Johnson, J. D., Park, N. R., Taylor, H. A., Andreasen, V. A., Powers, M. J., Justyn, N. M., Parry, H. A., Kavazis, A. N.,& Zhang, Y. (2019). Plumage redness signals mitochondrial function in the house finch. *Proceedings of the Royal Society B*, *286*(1911), 20191354.

Hill, G. E., & Johnson, J. D. (2012). The vitamin A–redox hypothesis: a biochemical basis for honest signaling via carotenoid pigmentation. *The American Naturalist*, *180*(5), E127-E150.

Hill, G. E. & McGraw, K. J. (Eds.). (2006). *Bird coloration: mechanisms and measurements* (Vol. 1). Harvard University Press.

Hopkins, C. C. E. (1978). The male genital system, and spermatophore production and function in *Euchaeta norvegica* Boeck (Copepoda: Calanoida). *J. Exp. Mar. Biol. Ecol.* 35, 197-231.

Hsiung, B. K., Blackledge, T. A., Shawkey, M. D. (2014). Structural color and its interaction with other color-producing elements: perspectives from spiders. In *The Nature of Light: Light in Nature V* (Vol. 9187, p. 91870B). International Society for Optics and Photonics.

Hsiung, B. K., Deheyn, D. D., Shawkey, M. D., Blackledge, T. A. (2015). Blue reflectance in tarantulas is evolutionarily conserved despite nanostructural diversity. *Sci. Adv.* 1, e1500709.

Hsiung, B. K., Justyn, N. M., Blackledge, T. A., Shawkey, M. D. (2017). Spiders have rich pigmentary and structural color palettes. *J. Exp. Biol.* 220, 1975-1983.

Hudon, J., Storni, A., Pini, E., Anciães, M., & Stradi, R. (2012). Rhodoxanthin as a characteristic keto-carotenoid of manakins (Pipridae). *The Auk*, *129*(3), 491-499.

Hylander, S., Grenvald, J. C., Kiørboe, T. (2014). Fitness costs and benefits of ultraviolet radiation exposure in marine pelagic copepods. *Fun. Ecol.* 28, 149-158.

Ilagan, R. P., Christensen, R. L., Chapp, T. W., Gibson, G. N., Pascher, T., Polívka, T., & Frank, H. A. (2005). Femtosecond time-resolved absorption spectroscopy of astaxanthin in solution and in α-crustacyanin. *The Journal of Physical Chemistry A*, *109*(14), 3120-3127.

Isaksson, C., Ornborg, J., Prager, M., & Andersson, S. (2008). Sex and age differences in reflectance and biochemistry of carotenoid-based colour variation in the great tit Parus major. *Biological Journal of the Linnean Society*, *95*(4), 758-765.

Iverson, E. N., & Karubian, J. (2017). The role of bare parts in avian signaling. *The Auk: Ornithological Advances*, *134*(3), 587-611.

Jourdie, V., Moureau, B., Bennett, A. T., & Heeb, P. (2004). Ultraviolet reflectance by the skin of nestlings. *Nature*, *431*(7006), 262-262.

Justyn, N. M., Heine, K. B., Hood, W. R, Peteya, J. A., Vanthournout, B., Debruyn, G., Shawkey, M. D., Weaver, R. J., and Hill, G. E. (2022a). A combination of red structural and pigmentary coloration in the eyespot of a copepod. *Journal of the Royal Society Interface*, *19*(190), 20220169.

Justyn, N. M., Nallapaneni, A., Parnell, A. J., Karim, A., & Shawkey, M. D. (2022b). A synergistic combination of structural and pigmentary colour produces non-spectral colour

in the purple-breasted cotinga, *Cotinga cotinga* (Passeriformes: Cotingidae). *Biological Journal of the Linnean Society*, *135*(1), 62-70.

Kariko, S., Timonen, J. V., Weaver, J. C., Gur, D., Marks, C., Leiserowitz, L., ... & Li, L. (2018). Structural origins of coloration in the spider *Phoroncidia rubroargentea* Berland, 1913 (Araneae: Theridiidae) from Madagascar. *J. R. Soc. Interface*, *15*(139), 20170930.

Kassambara, A. (2018). ggpubr:"ggplot2" based publication ready plots. *-R package version 0.1*, 7.

Kim, O., McMurdy, J., Jay, G., Lines, C., Crawford, G., & Alber, M. (2014). Combined reflectance spectroscopy and stochastic modeling approach for noninvasive hemoglobin determination via palpebral conjunctiva. *Physiological Reports*, *2*(1), e00192.

Koch, R. E., Kavazis, A. N., Hasselquist, D., Hood, W. R., Zhang, Y., Toomey, M. B., & Hill, G. E. (2018). No evidence that carotenoid pigments boost either immune or antioxidant defenses in a songbird. *Nature Communications*, 9(1), 1-7.

Koch, R. E., McGraw, K. J., & Hill, G. E. (2016). Effects of diet on plumage coloration and carotenoid deposition in red and yellow domestic canaries (Serinus canaria). The Wilson Journal of Ornithology, 128(2), 328-333.

Krinsky, N. I., Landrum, J. T., Bone, R. A. (2003). Biologic mechanisms of the protective role of lutein and zeaxanthin in the eye. *Ann. Rev. Nutr.* 23, 171-201.

Kuznetsova, A., Brockhoff, P. B. & Christensen, R. H. (2017). lmerTest package: tests in linear mixed effects models. *Journal of Statistical Software, 82*, 1-26.

Laczi, M., Hegyi, G., Kötél, D., Csizmadia, T., Lőw, P., & Török, J. (2019). Reflectance in relation to macro-and nanostructure in the crown feathers of the great tit (Parus major). *Biological Journal of the Linnean Society*, *127*(1), 113-124.

Lademann, J., Meinke, M. C., Sterry, W., & Darvin, M. E. (2011). Carotenoids in human skin. *Experimental Dermatology*, *20*(5), 377-382.

Lademann, J., Meinke, M. C., Sterry, W., & Darvin, M. E. (2011). Carotenoids in human skin. *Experimental Dermatology*, *20*(5), 377-382.

LaFountain, A. M., S. Kaligotla, S. Cawley, K. M. Riedl, S. J. Schwartz, H. A. Frank, and R. O. Prum (2010). Novel methoxy-carotenoids from the burgundy-colored plumage of the Pompadour Cotinga *Xipholena punicea*. *Archives of Biochemistry and Biophysics* 504: 142–153.

LaFountain, A. M., Prum, R. O., Frank, H. A. (2015). Diversity, physiology, and evolution of avian plumage carotenoids and the role of carotenoid–protein interactions in plumage color appearance. *Arch. Biochem. Biophys.* 572, 201-212.

Land, M. F. (1972). The physics and biology of animal reflectors. *Prog. Biophys. and Mol. Biol.* 24, 75-106.

Leertouwer, H. L., Wilts, B. D., & Stavenga, D. G. (2011). Refractive index and dispersion of butterfly chitin and bird keratin measured by polarizing interference microscopy. *Optics Express*, *19*(24), 24061-24066.

Lemon, J. (2006). Plotrix: a package in the red light district of R. *R-News*, *6*, 8–12.

Lenth, R., Singmann, H., Love, J., Buerkner, P. & Herve, M. (2018). Emmeans: Estimated marginal means, aka least-squares means. *R package version,* 1, 3.

Lind, O., Mitkus, M., Olsson, P., & Kelber, A. (2014). Ultraviolet vision in birds: the importance of transparent eye media. *Proceedings of the Royal Society B: Biological Sciences*, *281*(1774), 20132209.

Lindon, J. C., Tranter, G. E., & Koppenaal, D. (2016). *Encyclopedia of spectroscopy and spectrometry*. Academic Press.

Lopes, R. J., J. D. Johnson, M. B. Toomey, M. S. Ferreira, P. M. Araujo, J. Melo-Ferreira L. Andersson, G. E. Hill, J. C. Corbo, and M. Carneiro (2016). Genetic basis for red coloration in birds. *Current Biology* 26:1427–1434.

MacDougall, A. K., and R. Montgomerie (2003). Assortative mating by carotenoid-based plumage colour: a quality indicator in American goldfinches, *Carduelis tristis*. *Naturwissenschaften* 90:464–467.

Magkiriadou, S., Park, J. G., Kim, Y. S., Manoharan, V. N. (2014). Absence of red structural color in photonic glasses, bird feathers, and certain beetles. *Phys. Rev. E* 90, 062302.

Maia, R., Eliason, C. M., Bitton, P. P., Doucet, S. M., & Shawkey, M. D. (2013). pavo: an R package for the analysis, visualization and organization of spectral data. *Methods in Ecology and Evolution*, *4*(10), 906-913.

Maia, R., Gruson, H., Endler, J. A., & White, T. E. (2019). pavo 2: new tools for the spectral and spatial analysis of colour in R. *Methods in Ecology and Evolution*.

Martin, G. G., Speekmann, C., Beidler, S. (2000). Photobehavior of the harpacticoid copepod *Tigriopus californicus* and the fine structure of its nauplius eye. *Invert. Biol.* 119, 110-124.

Mays Jr, H. L., McGraw, K. J., Ritchison, G., Cooper, S., Rush, V., & Parker, R. S. (2004). Sexual dichromatism in the yellow-breasted chat Icteria virens: spectrophotometric analysis and biochemical basis. *Journal of Avian Biology*, *35*(2), 125-134.

McCoy, D. E., Shultz, A. J., Vidoudez, C., van der Heide, E., Trauger, S. A., & Haig, D. (2019). Microstructures amplify seemingly honest signals in carotenoid-colored tanagers. *bioRxiv*, 799783.

McDonald, D. B., R. P. Clay, R. T. Brumfield, and M. J. Braun. 2001. Sexual selection on plumage and behavior in an avian hybrid zone: experimental tests of male-male interactions. Evolution 55:1443-1451.

McGraw, K. J. (2006a). Pterins, Porphyrins, and Psittacofulvins. *Bird Coloration: Mechanisms and Measurements* (G.E. Hill and K.J. McGraw, Editors). Harvard Press, Cambridge MA, USA, 354-398.

McGraw, K. J. (2006b). Mechanics of carotenoid-based coloration. In, *Bird Coloration: Mechanisms and Measurements, Volume 1* (Hill, G. E., and McGraw, K. J.). pp. 177-242.

McGraw, K. J., Adkins-Regan, E., & Parker, R. S. (2002). Anhydrolutein in the zebra finch: a new, metabolically derived carotenoid in birds. *Comparative Biochemistry and Physiology Part B: Biochemistry and Molecular Biology*, *132*(4), 811-818.

McGraw, K. J., Beebee, M. D., Hill, G. E., & Parker, R. S. (2003). Lutein-based plumage coloration in songbirds is a consequence of selective pigment incorporation into feathers. *Comparative Biochemistry and Physiology Part B: Biochemistry and Molecular Biology*, *135*(4), 689-696.

McGraw, K. J., and A. J. Gregory (2004). Carotenoid pigments in male American goldfinches: what is the optimal biochemical strategy for becoming colourful? *Biological Journal of the Linnean Society* 83:273–280.

McGraw, K. J., G. E. Hill, R. Stradi, and R. S. Parker (2001). The influence of carotenoid acquisition and utilization on the maintenance of species-typical plumage pigmentation in

male American goldfinches (*Carduelis tristis*) and northern cardinals (*Cardinalis cardinalis*). *Physiological and Biochemical Zoology* 74:843–852.

McGraw, K. J., Hudon, J., Hill, G. E., & Parker, R. S. (2005). A simple and inexpensive chemical test for behavioral ecologists to determine the presence of carotenoid pigments in animal tissues. *Behavioral Ecology and Sociobiology*, *57*(4), 391-397.

McGraw, K. J., R. J. Safran, and K. Wakamatsu (2005). How feather colour reflects its melanin content. *Functional Ecology* 19:816–821.

McGraw, K. J. & Toomey, M. B. (2010). Carotenoid accumulation in the tissues of zebra finches: predictors of integumentary pigmentation and implications for carotenoid allocation strategies. *Physiological and Biochemical Zoology*, *83*(1), 97-109.

McGraw, K. J., Wakamatsu, K., Clark, A. B., & Yasukawa, K. (2004). Red-winged blackbirds Agelaius phoeniceus use carotenoid and melanin pigments to color their epaulets. *Journal of Avian Biology*, *35*(6), 543-550.

Mendes-Pinto, M. M., LaFountain, A. M., Stoddard, M. C., Prum, R. O., Frank, H. A., & Robert, B. (2012). Variation in carotenoid–protein interaction in bird feathers produces novel plumage coloration. *Journal of the Royal Society Interface*, *9*(77), 3338-3350.

Moran, N. A., Jarvik, T. (2010). Lateral transfer of genes from fungi underlies carotenoid production in aphids. *Science* 328, 624-627.

Mundy, N. I., J. Stapley, C. Bennison, R. Tucker, H. Twyman, K. W. Kim, T. Burke, T. R. Birkhead, S. Andersson, and Slate, J. (2016). Red carotenoid coloration in the zebra finch is controlled by a cytochrome P450 gene cluster. *Current Biology* 26:1435–1440.

Negro, J. J., Grande, J. M., Tella, J. L., Garrido, J., Hornero, D., Donázar, J. A., Sanchez-Zapata, J. A., BenÍtez, J. R., & Barcell, M. (2002). An unusual source of essential carotenoids. *Nature*, *416*(6883), 807-808.

Negro, J. J., Sarasola, J. H., Fariñas, F., & Zorrilla, I. (2006). Function and occurrence of facial flushing in birds. *Comparative Biochemistry and Physiology Part A: Molecular & Integrative Physiology*, *143*(1), 78-84.

Neuwirth, E. (2014). RColorBrewer: ColorBrewer palettes. R package version 1.1-2.

Nicolaï, M. P., Shawkey, M. D., Porchetta, S., Claus, R., & D'Alba, L. (2020). Exposure to UV radiance predicts repeated evolution of concealed black skin in birds. *Nature Communications*, *11*(1), 1-8.

Noyes, J. A., Vukusic, P., Hooper, I. R. (2007). Experimental method for reliably establishing the refractive index of buprestid beetle exocuticle. *Opt. Express* 15, 4351-4358.

Ödeen, A., & Håstad, O. (2013). The phylogenetic distribution of ultraviolet sensitivity in birds. *BMC evolutionary biology*, *13*(1), 36.

Orteu, A., & Jiggins, C. D. (2020). The genomics of coloration provides insights into adaptive evolution. *Nature Reviews Genetics*, *21*(8), 461-475.

Parchman, T. L., Gompert, Z., Braun, M. J., Brumfield, R. T., McDonald, D. B., Uy, J. A. C., ... & Buerkle, C. A. (2013). The genomic consequences of adaptive divergence and reproductive isolation between species of manakins. *Molecular ecology*, *22*(12), 3304-3317.

Parsons, T. J., Olson, S. L., & Braun, M. J. (1993). Unidirectional spread of secondary sexual plumage traits across an avian hybrid zone. *Science*, *260*(5114), 1643-1646.

Pebesma, E. J. (2018). Simple features for R: standardized support for spatial vector data. *The R Journal*, 10, 439.

Potticary, A. L., Morrison, E. S., & Badyaev, A. V. (2020). Turning induced plasticity into refined adaptations during range expansion. *Nature communications*, *11*(1), 1-13.

Powers, M. J., Hill, G. E., & Weaver, R. J. (2020). An experimental test of mate choice for red carotenoid coloration in the marine copepod Tigriopus californicus. *Ethology*, *126*(3), 344-352.

Powlik, J. J. (1996). *Ecology of Tigriopus californicus (Copepoda, Harpacticoida) in Barkley Sound, British Columbia* (Doctoral dissertation, University of British Columbia).

Prum R. O. (2006). Anatomy, physics, and evolution of structural colors. In *Bird Coloration, vol. 1 Mechanisms and Measurements* (G. E. Hill and K. J. McGraw, Editors) 295–355 (Harvard University Press, Cambridge).

Prum, R. O., LaFountain, A. M., Berg, C. J., Tauber, M. J., & Frank, H. A. (2014). Mechanism of carotenoid coloration in the brightly colored plumages of broadbills (Eurylaimidae). *Journal of Comparative Physiology B*, *184*(5), 651-672.

Prum, R. O., & Torres, R. (2003). Structural colouration of avian skin: convergent evolution of coherently scattering dermal collagen arrays. *Journal of Experimental Biology*, *206*(14), 2409-2429.

Pyle, P. 2008. Identification Guide to North American Birds. Part II: Anatidae to Alcidae. Slate Creek Press, Point Reyes Station, California. xi + 836 pp.

R Core Team. (2020). R: a language and environment for statistical computing. Vienna, Austria: R Foundation for Statistical Computing. See https://www.R-project.org/.

Richins, R. D., Kilcrease, J., Rodgriguez-Uribe, L. & O'connell, M. A. (2014). Carotenoid extraction and quantification from *Capsicum annuum*. *Bio-Protocol*, 4.

Ringelberg, J. (1980). Aspects of red pigmentation in zooplankton, especially copepods. *Am. Sot. Limnol. Oceanogr. Spec. Symp* 3, 91-97.

Rueden, C. T., Schindelin J., Hiner M. C., DeZonia B. E., Walter A. E., Arena E. T., Eliceiri K. W. (2017). ImageJ2: ImageJ for the next generation of scientific image data. *BMC Bioinformatics* 18, 529.

Russell Lenth (2020). emmeans: Estimated Marginal Means, aka Least-Squares Means. R package version 1.4.5. https://CRAN.R-project.org/package=emmeans

Salvato, B., Libertini, A., Lazzaretto, I. (1990). Evidence of chemical signalling in *Tigriopus fulvus* (Copepoda, Harpacticoida). *Crustaceana* 59, 171-179.

Saranathan, V., Forster, J. D., Noh, H., Liew, S. F., Mochrie, S. G., Cao, H., ... & Prum, R. O. (2012). Structure and optical function of amorphous photonic nanostructures from avian feather barbs: a comparative small angle X-ray scattering (SAXS) analysis of 230 bird species. *Journal of The Royal Society Interface*, *9*(75), 2563-2580.

Seago, A. E., Brady, P., Vigneron, J. P., Schultz, T. D. (2009). Gold bugs and beyond: a review of iridescence and structural colour mechanisms in beetles (Coleoptera). *J. R. Soc. Interface* 6, S165-S184.

Seligy, V. L. (1972). Ommochrome pigments of spiders. *Comp. Biochem. Physiol*. 42, 699-709.

Shawkey, M. D., & Hill, G. E. (2005). Carotenoids need structural colours to shine. *Biology Letters*, *1*(2), 121-124.

Shawkey, M. D. & D'Alba, L. (2017). Interactions between colour-producing mechanisms and their effects on the integumentary colour palette. *Philos. T. R. Soc. B* 372, 20160536.

Shawkey, M. D., & Hill, G. E. (2006). Significance of a basal melanin layer to production of non-iridescent structural plumage color: evidence from an amelanotic Steller's jay (Cyanocitta stelleri). *Journal of Experimental Biology*, *209*(7), 1245-1250.

Shawkey, M. D., Estes, A. M., Siefferman, L. M., & Hill, G. E. (2003). Nanostructure predicts intraspecific variation in ultraviolet–blue plumage colour. *Proceedings of the Royal Society of London B: Biological Sciences*,*270*(1523), 1455-1460.

Shawkey, M. D., Hauber, M. E., Estep, L. K., & Hill, G. E. (2006a). Evolutionary transitions and mechanisms of matte and iridescent plumage coloration in grackles and allies (Icteridae). *Journal of the Royal Society Interface*, *3*(11), 777-786.

Shawkey, M. D., Hill, G. E., McGraw, K. J., Hood, W. R., & Huggins, K. (2006b). An experimental test of the contributions and condition dependence of microstructure and carotenoids in yellow plumage coloration. *Proceedings of the Royal Society B: Biological Sciences*, *273*(1604), 2985-2991.

Snow, D. W. (1962). A field study of the Black and White Manakin, Manacus manacus, in Trinidad. *WI Zoologica*, *47*, 67-104.

Stahl, W., Heinrich, U., Jungmann, H., Sies, H., Tronnier, H. (2000). Carotenoids and carotenoids plus vitamin E protect against ultraviolet light–induced erythema in humans. *Am. J. of Clin. Nutr.* 71, 795-798.

Stavenga, D. G., J. Tinbergen, H. L. Leertouwer, and B. D. Wilts (2011). Kingfisher feathers–colouration by pigments, spongy nanostructures and thin films. *Journal of Experimental Biology* 214:3960–3967.

Stearns, D. E. (1986). Copepod grazing behavior in simulated natural light and its relation to nocturnal feeding. *Mar. Ecol. Prog.* 30, 65-76.

Stein, A. C., & Uy, J. A. C. (2005). Plumage brightness predicts male mating success in the lekking golden-collared manakin, Manacus vitellinus. *Behavioral Ecology*, *17*(1), 41-47.

Stoddard, M. C., & Prum, R. O. (2008). Evolution of avian plumage color in a tetrahedral color space: a phylogenetic analysis of new world buntings. *The American Naturalist*, *171*(6), 755-776.

Stoddard, M. C., & Prum, R. O. (2011). How colorful are birds? Evolution of the avian plumage color gamut. *Behavioral Ecology*, *22*(5), 1042-1052.

Thomas, D. B., McGoverin, C. M., McGraw, K. J., James, H. F., & Madden, O. (2013). Vibrational spectroscopic analyses of unique yellow feather pigments (spheniscins) in penguins. *Journal of the Royal Society Interface*, *10*(83), 20121065.

Thomas, D. B., McGraw, K. J., James, H. F., & Madden, O. (2014). Non-destructive descriptions of carotenoids in feathers using Raman spectroscopy. *Analytical Methods*, *6*(5), 1301-1308.

Toews, D. P., Taylor, S. A., Vallender, R., Brelsford, A., Butcher, B. G., Messer, P. W., & Lovette, I. J. (2016). Plumage genes and little else distinguish the genomes of hybridizing warblers. *Current Biology*, *26*(17), 2313-2318.

Toomey, M. B., C. I. Marques, P. M. Araújo, D. Huang, S. Zhong, Y. Liu, G. D. Schreiner, C. A. Myers, P. Pereira, S. Afonso, P. Andrade, M. A. Gazda, R. J Lopes, I. Viegas, R. E. Koch, M. E. Haynes, D. J. Smith, Y. Ogawa, D. Murphy, R. E. Kopec, D. M. Parichy, M. Carneiro, and J. C. Corbo (2022). A mechanism for red coloration in vertebrates. *Current Biology* in press.

Toomey, M. B., & McGraw, K. J. (2007). Modified saponification and HPLC methods for analyzing carotenoids from the retina of quail: implications for its use as a nonprimate model species. *Investigative Ophthalmology & Visual Science*, *48*(9), 3976-3982.

Toral, G. M., Figuerola, J., & Negro, J. J. (2008). Multiple ways to become red: pigment identification in red feathers using spectrometry. *Comparative Biochemistry and Physiology Part B: Biochemistry and Molecular Biology*, *150*(2), 147-152.

Venables, W. N. & Ripley, B. D. (2013). *Modern applied statistics with S-PLUS*, Springer Science & Business Media.

Ward, J., McCafferty, D. J., Houston, D. C., & Ruxton, G. D. (2008). Why do vultures have bald heads? The role of postural adjustment and bare skin areas in thermoregulation. *Journal of Thermal Biology*, *33*(3), 168-173.

Weaver, R. J., Cobine, P. A. & Hill, G. E. (2018a). On the bioconversion of dietary carotenoids to astaxanthin in the marine copepod, *Tigriopus californicus*. *Journal of Plankton Research, 40,* 142-150.

Weaver, R. J., R.E. Koch, and G. E. Hill (2017). What maintains signal honesty in animal colour displays used in mate choice. *Philosophical Transactions of the Royal Society, B* 372:20160343.

Weaver, R. J., P. Wang, G. E. Hill, and P. A. Cobine (2018b). An in vivo test of the biologically relevant roles of carotenoids as antioxidants in animals. *Journal of Experimental Biology* 221:jeb183665.

Welch, V. L., Vigneron, J. P. (2007). Beyond butterflies—the diversity of biological photonic crystals. *Opt. Quant. Electron.* 39, 295-303.

Werth, A. J. (2012). Hydrodynamic and sensory factors governing response of copepods to simulated predation by Balaenid Whales. *Int. J. Ecol*. 2012, 1-13.

Wilcox, R. E. (1964). Immersion liquids of relatively strong dispersion in the low refractive index range (1.46 to 1.52). *American Mineralogist: Journal of Earth and Planetary Materials*, *49*(5-6), 683-688.

White, T. E. (2020). Structural colours reflect individual quality: a meta-analysis. *Biology Letters* 16:20200001.

Xiao, M., Dhinojwala, A., & Shawkey, M. (2014). Nanostructural basis of rainbow-like iridescence in common bronzewing Phaps chalcoptera feathers. *Optics express*, *22*(12), 14625-14636.

Yoshida, T., Toda, T., Kuwahara, V., Taguchi, S., Othman, B. H. R. (2004). Rapid response to changing light environments of the calanoid copepod *Calanus sinicus*. *Mar. Biol.* 145, 505-513.

Appendix 1: Supplemental Tables and Figures

Chapter 1: *Manacus* coloration

Supplemental Information Table 1.1: Summary of museum specimens sampled to perform feather analyses. *M. vitellinus* x *M. candei* refers to the hybrid also referred to as the yellow-collared *M. candei* in main text.

Species	USNM	Locality	Year collected
M. vitellinus	608987	Gamboa, Panama	1994
M. vitellinus	608136	Gamboa, Panama	1991
M. vitellinus	608135	Gamboa, Panama	1991
M. vitellinus	608985	Gamboa, Panama	1994
M. vitellinus	534054	Gamboa, Panama	1963
M. vitellinus	470154	Gamboa, Panama	1959
M. candei	608194	N bank Rio Teribe 3 km SW Charagre, Quebrada Carbon, Panama	1991
M. candei	608195	N bank Rio Teribe 3 km SW Charagre, Quebrada Carbon, Panama	1991
M. candei	614059	N bank Rio Teribe 3 km SW Charagre, Quebrada Carbon, Panama	1991
M. candei	608197	N bank Rio Teribe 3 km SW Charagre, Quebrada Carbon, Panama	1991
M. candei	614061	N bank Rio Teribe 3 km SW Charagre, Quebrada Carbon, Panama	1991
M. candei	614062	N bank Rio Teribe 3 km SW Charagre, Quebrada Carbon, Panama	1991
M. vitellinus x candei	608161	3/5 km SE RR bridge E (=S) bank Changuinola River, Panama	1991
M. vitellinus x candei	608159	3/5 km SE RR bridge E (=S) bank Changuinola River, Panama	1991
M. vitellinus x candei	614037	3/5 km SE RR bridge E (=S) bank Changuinola River, Panama	1991
M. vitellinus x candei	614038	3/5 km SE RR bridge E (=S) bank Changuinola River, Panama	1991
M. vitellinus x candei	608167	3/5 km SE RR bridge E (=S) bank Changuinola River, Panama	1991
M. vitellinus x candei	608168	3/5 km SE RR bridge E (=S) bank Changuinola River, Panama	1991
M. aurantiacus	448955	Soná, Rio San Pablo, La Isleta, Veraguas, Panama	1953
M. aurantiacus	448952	Soná, Rio San Pablo, La Isleta, Veraguas, Panama	1953
M. aurantiacus	448945	Soná, Rio San Pablo, La Isleta, Veraguas, Panama	1953

M. aurantiacus	448939	Soná, Rio San Pablo, La Isleta, Veraguas, Panama	1953
M. aurantiacus	448944	Soná, Rio San Pablo, La Isleta, Veraguas, Panama	1953
M. aurantiacus	448942	Soná, Rio San Pablo, La Isleta, Veraguas, Panama	1953
M. manacus	384069	Los Gorros, Colombia	1945
M. manacus	384068	Los Gorros, Colombia	1945
M. manacus	384066	Los Gorros, Colombia	1945
M. manacus	384067	Los Gorros, Colombia	1945
M. manacus	411825	Coloso, Colombia	1948
M. manacus	411826	Coloso, Colombia	1948

Supplemental Information Table 1.2: Results from statistical models comparing lutein concentration among species' belly feathers (A), lutein concentration among species' collar feathers (B), feather brightness among species (C), lutein concentrations in species with yellow bellies and collars (D), and models estimating the relationship between lutein concentration and reflectance measurements estimated using the 'pavo' R package (E). Columns are as follows left to right: estimate of effect, standard error, degrees of freedom, t-value, p-value, confidence intervals.

A. Lutein Comparison - BELLY

contrast	estimate	SE	df	t.ratio	p.value	lower.CI	upper.CI
M. vitellinus - Hybrid	-0.04697	0.0227	25	-2.0671	0.2651	-0.11371	0.019762
M. vitellinus - M. aurantiacus	-0.0662	0.0227	25	-2.9134	0.0525	-0.13294	0.000533
M. vitellinus - M. manacus	0.051485	0.0227	25	2.2657	0.1893	-0.01525	0.11822
M. vitellinus - M. candei	-0.05686	0.0227	25	-2.5021	0.1222	-0.12359	0.009879
Hybrid - M. aurantiacus	-0.01923	0.0227	25	-0.8462	0.9133	-0.08596	0.047505
Hybrid - M. manacus	0.098458	0.0227	25	4.3329	0.0017	0.031723	0.165193
Hybrid - M. candei	-0.00988	0.0227	25	-0.4349	0.9920	-0.07662	0.056852
M. aurantiacus - M. manacus	0.117688	0.0227	25	5.1792	0.0002	0.050953	0.184422
M. aurantiacus - M. candei	0.009346	0.0227	25	0.4113	0.9936	-0.05739	0.076081
M. manacus - M. candei	-0.10834	0.0227	25	-4.7679	0.0005	-0.17508	-0.04161

B. Lutein Comparison - COLLAR

contrast	estimate	SE	df	t.ratio	p.value	lower.CI	upper.CI
M. vitellinus - Hybrid	-0.01889	0.0457	25	-0.41282	0.993513	-0.15331	0.115523
M. vitellinus - M. aurantiacus	-0.27818	0.0457	25	-6.07791	2.19E-05	-0.4126	-0.14376
M. vitellinus - M. manacus	0.144237	0.0457	25	3.151437	0.031103	0.00982	0.278654
M. vitellinus - M. candei	0.144237	0.0457	25	3.151437	0.031103	0.00982	0.278654
Hybrid - M. aurantiacus	-0.25928	0.0457	25	-5.66509	6.16E-05	-0.3937	-0.12487
Hybrid - M. manacus	0.163132	0.0457	25	3.564255	0.011911	0.028715	0.297548
Hybrid - M. candei	0.163132	0.0457	25	3.564255	0.011911	0.028715	0.297548

M. aurantiacus - M. manacus	0.422416	0.0457	25	9.229347	1.51E-08	0.287999	0.556833
M. aurantiacus - M. candei	0.422416	0.0457	25	9.2293	1.51E-08	0.287999	0.556833
M. manacus - M. candei	1.11E-16	0.045769	25	2.43E-15	1	-0.13442	0.134417

C. Brightness Comparison - COLLAR

contrast	**estimate**	**SE**	**df**	**t.ratio**	**p.value**	**lower.CI**	**upper.CI**
M. vitellinus - Hybrid	-6.36668	4.2127	25	-1.51131	0.565017	-20.4933	8.507488
M. vitellinus - M. aurantiacus	-0.99005	4.2127	25	-0.23502	0.999275	-15.1167	13.88412
M. vitellinus - M. manacus	-22.3175	4.2127	25	-5.29768	0.000156	-36.4442	-7.44335
M. vitellinus - M. candei	-4.10449	4.2127	25	-0.97431	0.864138	-18.2311	10.76967
Hybrid - M. aurantiacus	5.37663	4.2127	25	1.276291	0.707597	-7.59292	18.34618
Hybrid - M. manacus	-15.9508	4.2127	25	-3.78637	0.006971	-28.9204	-2.98129
Hybrid - M. candei	2.262186	4.2127	25	0.536992	0.982545	-10.7074	15.23174
M. aurantiacus - M. manacus	-21.3275	4.2127	25	-5.06266	0.000283	-34.297	-8.35792
M. aurantiacus - M. candei	-3.11444	4.2127	25	-0.7393	0.945077	-16.084	9.855108
M. manacus - M. candei	18.21303	4.2127	25	4.323362	0.001841	5.243475	31.18258

D. Lutein Comparison - BELLY vs COLLAR by species

contrast	**species**	**estimate**	**SE**	**df**	**t.ratio**	**p.value**	**lower.CI**	**upper.CI**
Belly - Collar	*M. vitellinus*	-0.09275	0.044681	30	-2.07588	0.046573	-0.184	-0.0015
Belly - Collar	Hybrid	-0.06467	0.044681	30	-1.44745	0.15814	-0.15592	0.026577
Belly - Collar	*M. aurantiacus*	-0.30473	0.044681	30	-6.82011	1.45E-07	-0.39598	-0.21348

E. Lutein effect on reflectance color components from pavo

Dependent variable	**Independent variable**	**estimate**	**SE**	**lower.CI**	**upper.CI**	**p.value**
Yellow saturation (S1Yellow)	Lutein	0.07937	0.025494	0.02533	0.1334	6.69E-03
UV saturation (S1UV)	Lutein	-0.105	0.031868	-0.17256	-0.03745	0.00457
Carotenoid chroma (S1carotchroma)	Lutein	0.14257	0.0664	0.00181	0.283323	0.0474
mean brightness (b2meanbright)	Lutein	-2.87	6.977	-17.6612	11.92124	0.686
Peak Hue (H1peakwavhue)	Lutein	-15.60	13.658	-44.5541	13.35418	0.27

Chapter 2: Copepod coloration

Supplemental Figure 2.1

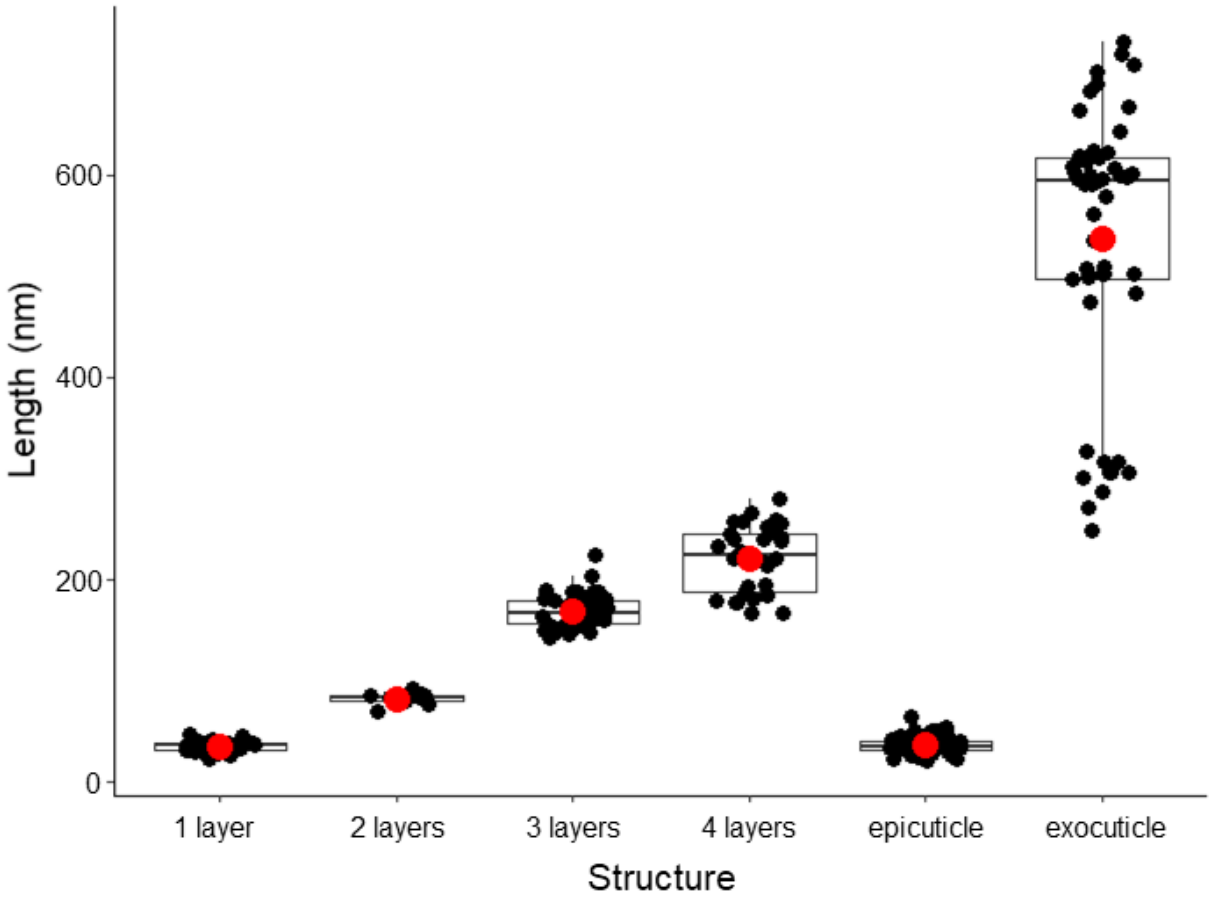

A summary of the thickness (nm) of each feature of the copepod exoskeleton measured using Image J. The numbers one – four refer to the number of air layers present in the exoskeleton, and the measurements associated with each one.

Supplemental Figure 2.2

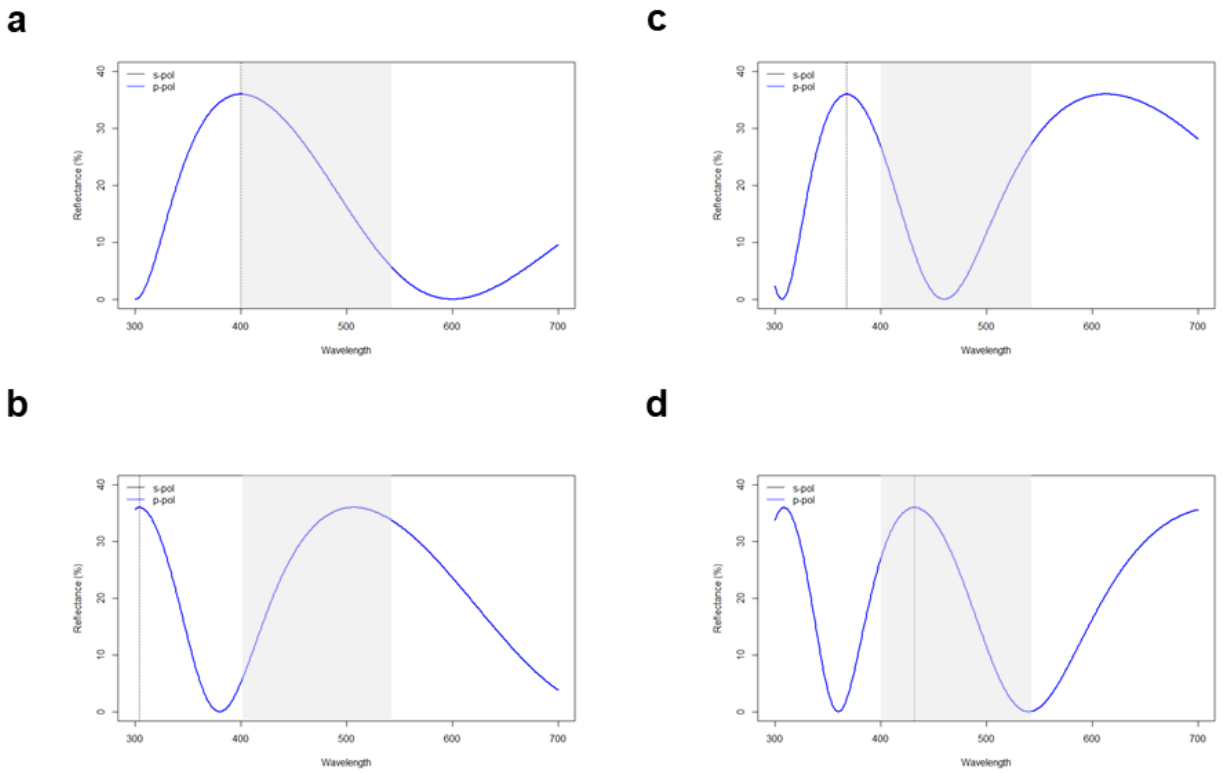

Predicted peak reflectance given (**a**) five air layers, (**b**) six air layers, (**c**) seven air layers, and (**d**) eight air layers.

Supplemental Figure 2.3

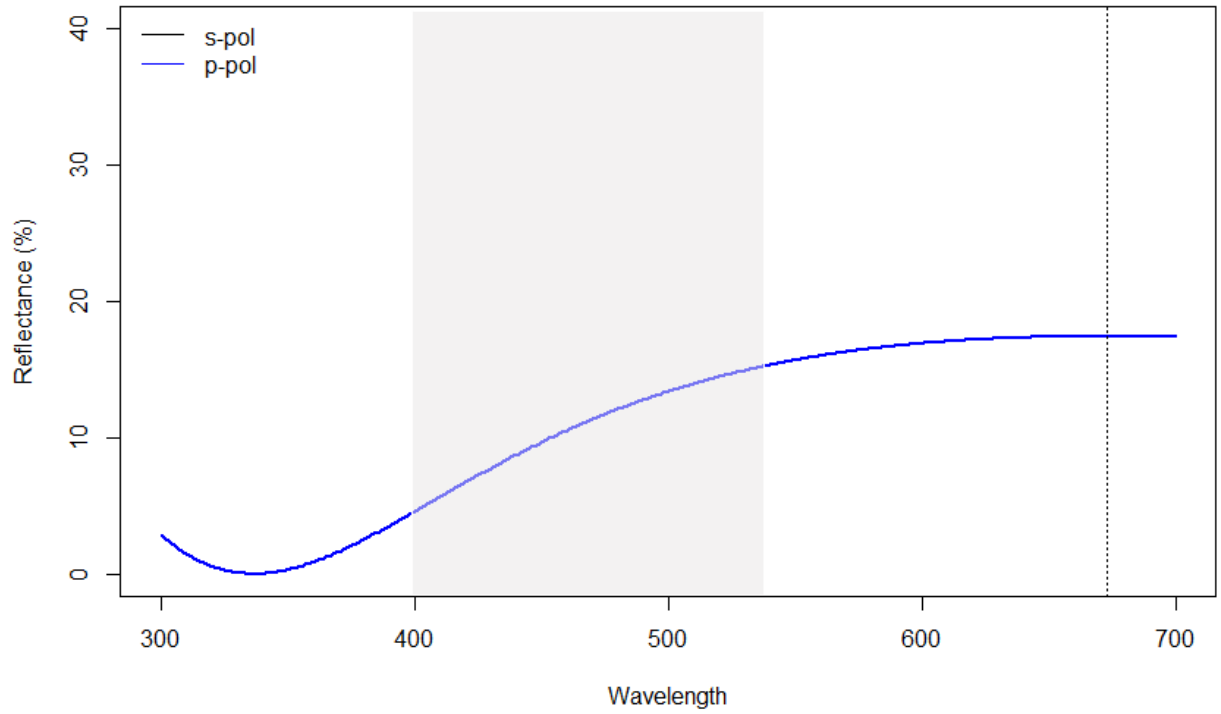

Predicted peak reflectance when changing the refractive index of chitin from 2.0 to a more conservative estimate of 1.56. This reduces overall brightness but does not impact the predicted hue.

Supplemental Figure 2.4

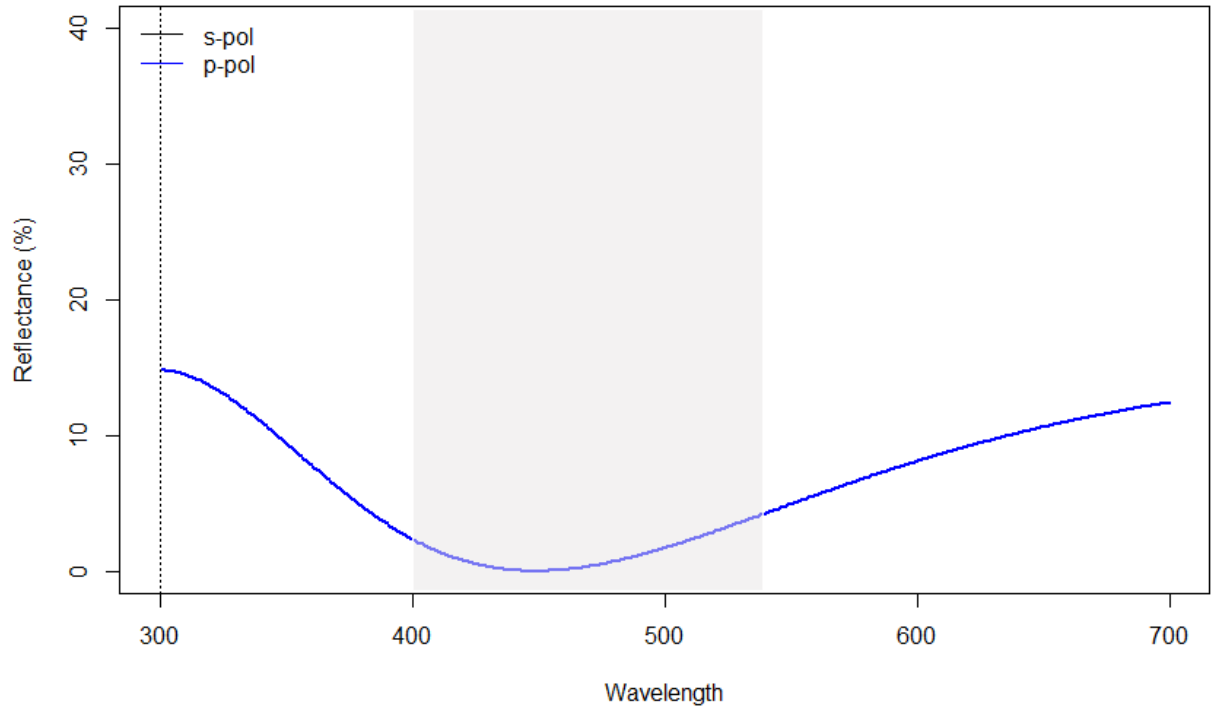

Predicted peak reflectance when changing the refractive index of the air layers from 1 to 1.333 to simulate the possibility that they could be filled with a liquid. This reduces overall brightness but once again does not impact the predicted hue.

Supplemental Figure 2.5

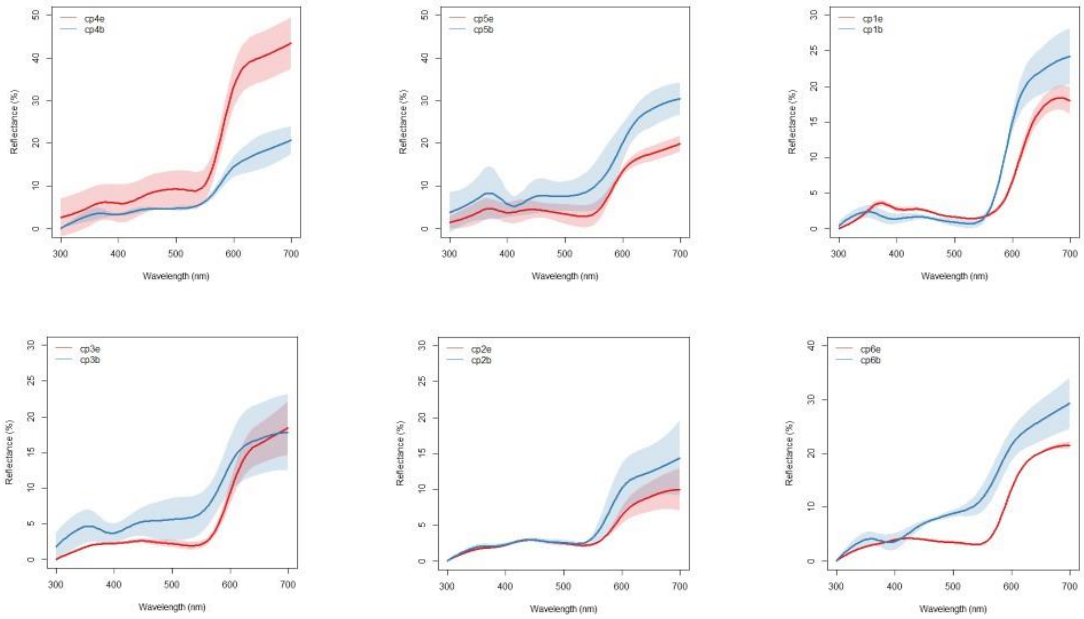

Observed microspectrophotometry reflectance of six copepod individuals. Three measurements from the eyespot and body were averaged to produce the spectra and shaded variance. The blue lines represent reflectance spectra obtained from the body, and the red lines represent reflectance spectra from the eyespot.

Chapter 3: Painted Bunting coloration

Supplemental Figure 3.1:

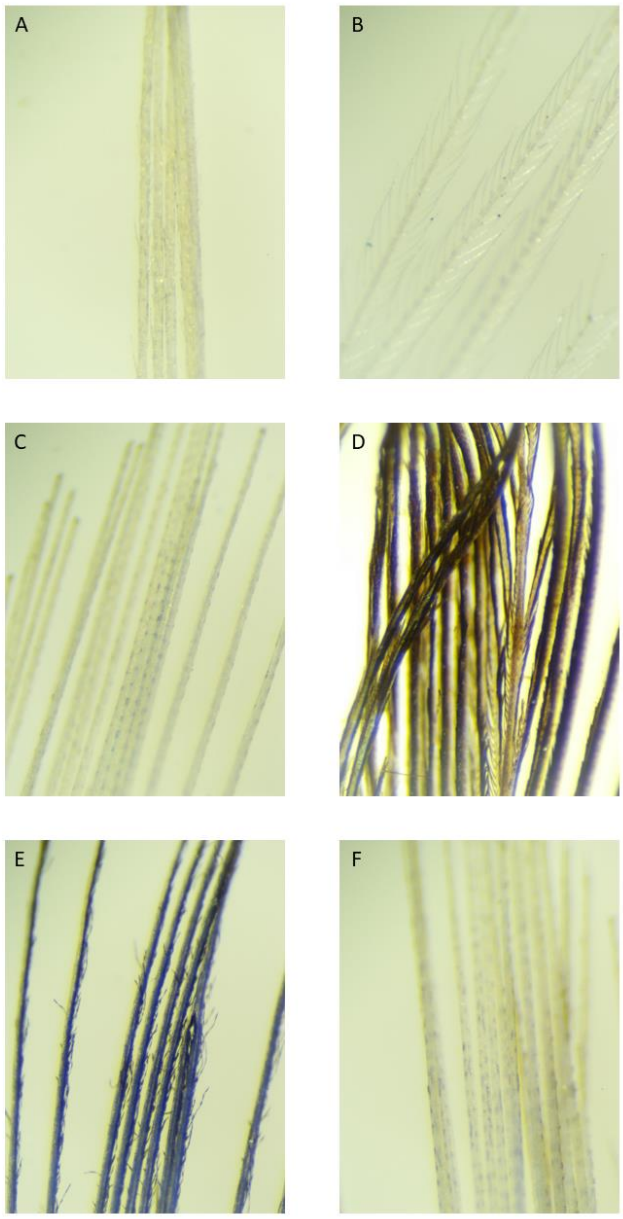

Light microscopy of A) red, B) orange, C) yellow-green, D) green, E) blue-violet, and F) purple male Painted Bunting feathers after pigment extraction.

Supplemental Figure 3.2:

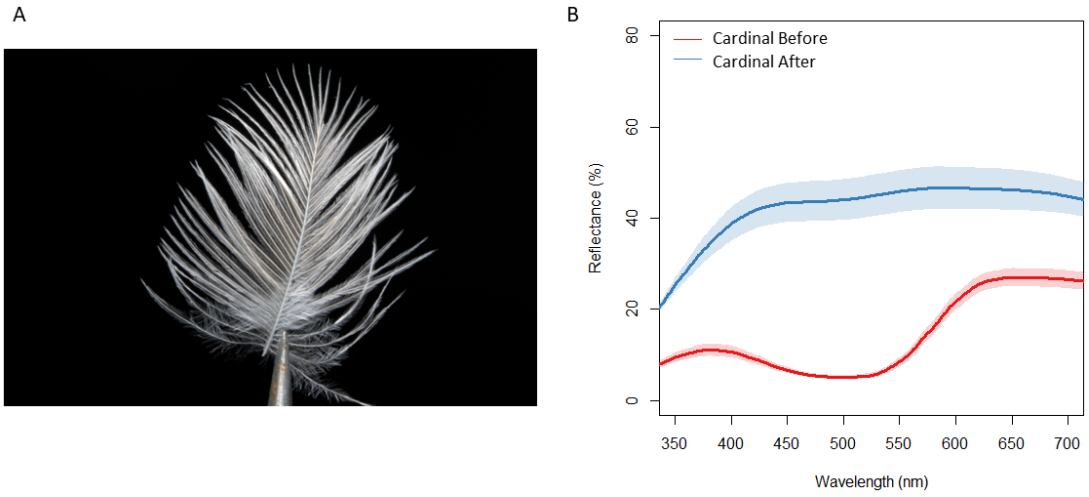

Photograph of A) a nearly white Northern Cardinal feather after pigment extraction and B) UV-vis reflectance spectroscopy of the Northern Cardinal feathers before and after pigment extraction.

Supplemental Figure 3.3:

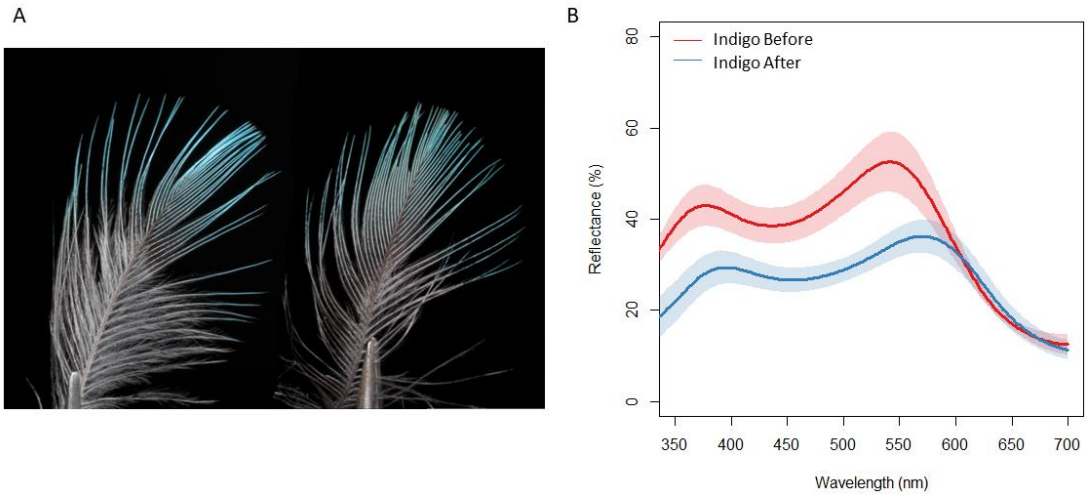

Photograph of A) an Indigo Bunting feather before and after pigment extraction and B) UV-vis reflectance spectroscopy of the feathers.

Chapter 4: Vulture Color

Supplemental Figure 4.1:

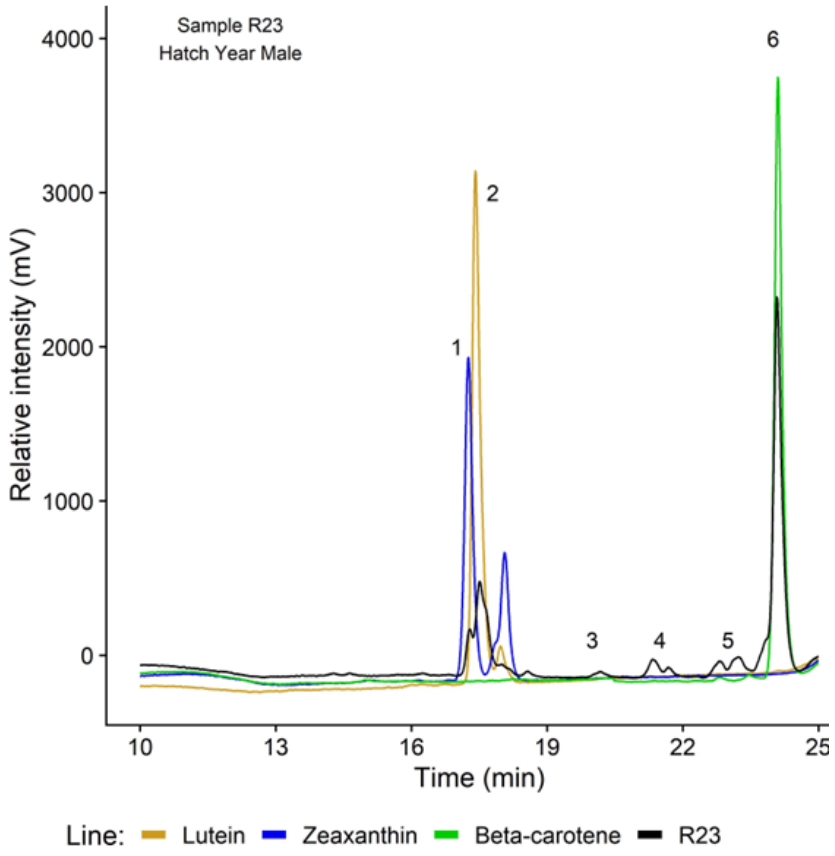

HPLC chromatogram from a single Turkey Vulture skin sample (R23 Hatch Year Male) showing the six carotenoids detected, their relative intensity (mV), and retention time (min) compared to carotenoid standards.

Supplemental Figure 4.2:

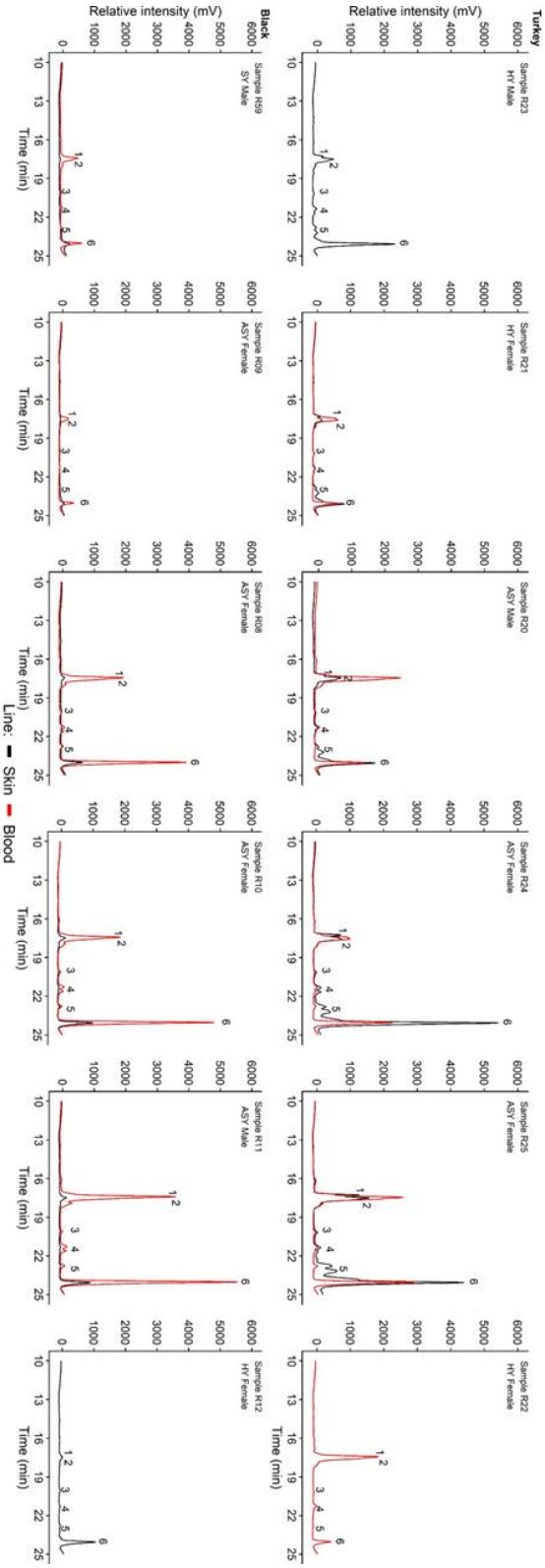

Individual HPLC chromatograms for each individual Turkey Vulture and Black Vulture sampled in the study. Black lines indicate skin samples and red lines indicate blood samples.

Supplemental Figure 4.3:

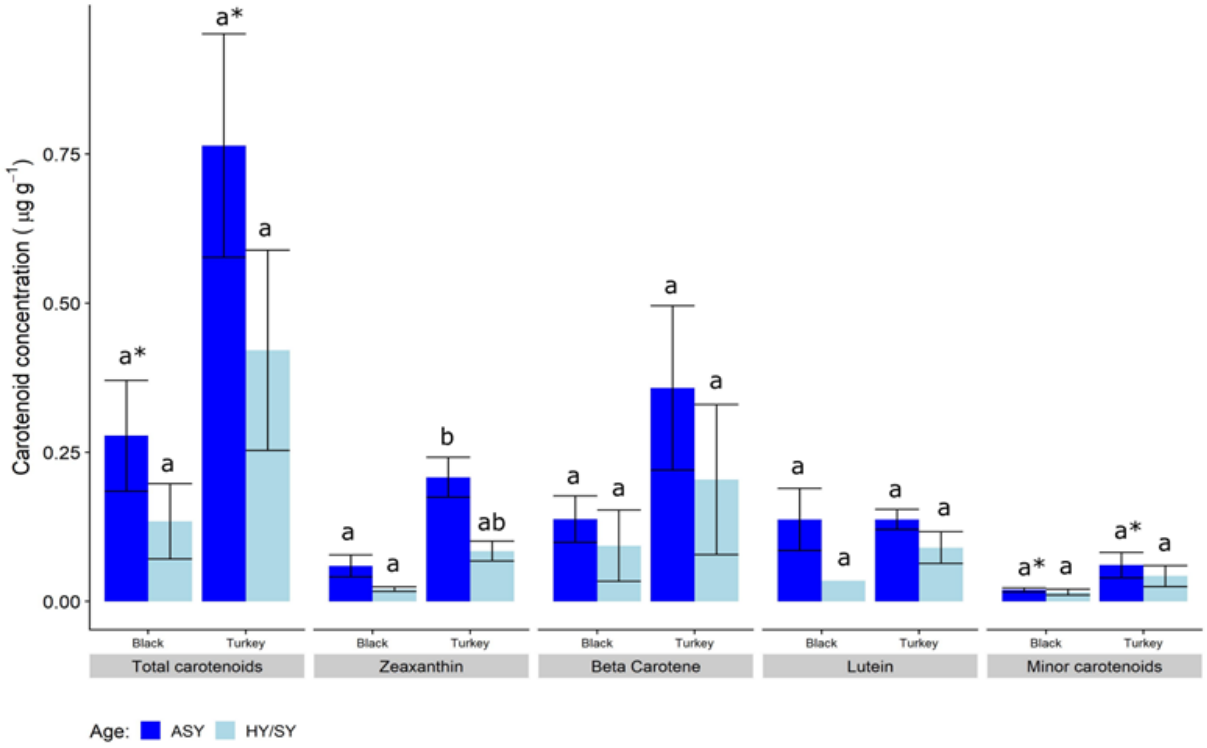

Carotenoid concentrations per age group, standardized by tissue mass. ASY = after second year, HY/SY = second year or younger.

Supplemental Figure 4.4:

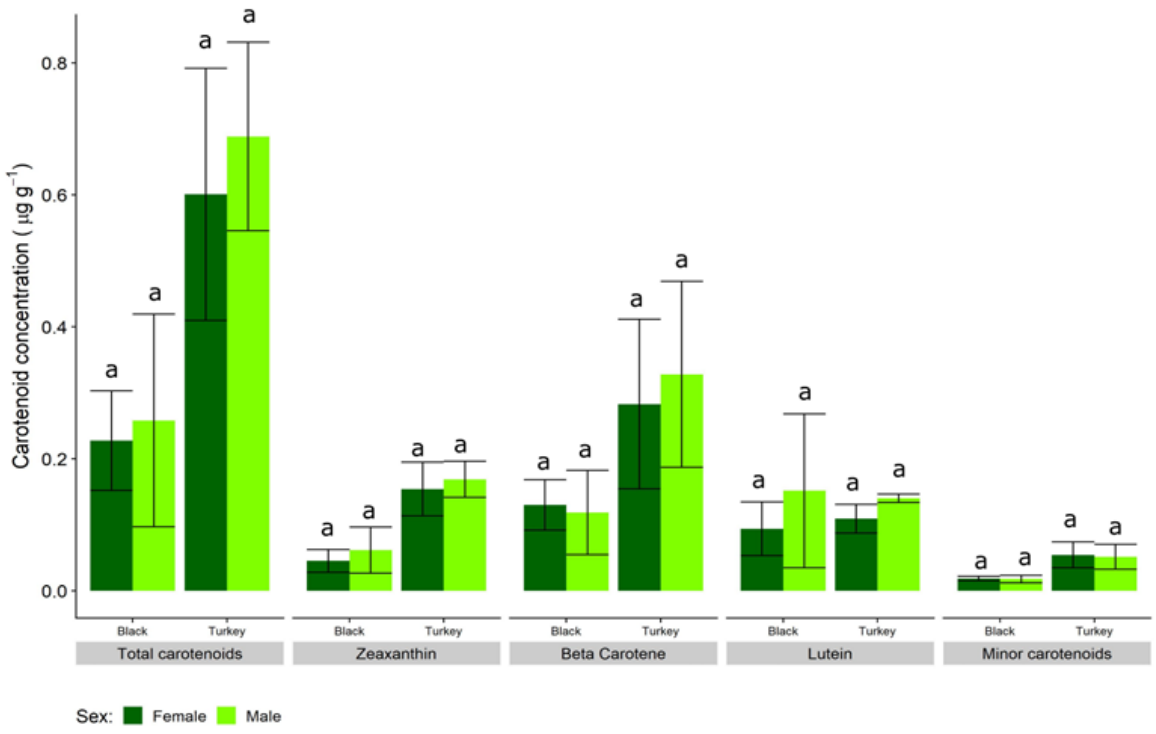

Carotenoid concentrations per sex, standardized by tissue mass.